



TECHNISCHE UNIVERSITÄT MÜNCHEN
FAKULTÄT FÜR MEDIZIN

Abteilung für Diagnostische und Interventionelle Neuroradiologie

**Development and Validation of MR-based
Quantitative Biomarkers for Detection of
Pathological Changes in Skeletal Muscle Tissue
of Patients with Neuromuscular Diseases**

Sarah Joanna Schläger

Vollständiger Abdruck der von der Fakultät für Medizin der
Technischen Universität München zur Erlangung des akademischen
Grades eines

Doktors der Medizinischen Wissenschaft (Dr. med. sci.)

genehmigten Dissertation.

Vorsitzender: Prof. Dr. Jürgen Schlegel
Prüfer der Dissertation: 1. apl. Prof. Dr. Jan St. Kirschke
2. Prof. Dr. Dimitrios Karampinos
3. apl. Prof. Dr. Marcus Deschauer

Die Dissertation wurde am 12.08.2020 bei der Technischen Universität München eingereicht und durch die Fakultät für Medizin am 17.02.2021 angenommen.

Abstract

During the last decades magnetic resonance imaging (MRI) has become the imaging modality of choice and an important tool in the diagnostic workup of patients with neuromuscular diseases (NMD). This broadly defined group of rare and heterogenous disorders presents with different symptoms, disease severity and ways of progression. As the main pathological changes in the muscle tissue of patients with NMD are muscle atrophy or hypertrophy, fatty infiltration and oedematous alterations next to remaining healthy muscle tissue, MRI offering high soft tissue contrast is a perfect tool for diagnostics in these diseases.

In the clinical routine, mainly qualitative imaging techniques are used in order to get insights into the pathological involvement patterns, narrow differential diagnosis for genetic testing, guide appropriate muscles for biopsy and monitor disease progression as well as therapy effectiveness. Due to the subjective character of assessment based on qualitative imaging recently a lot of effort has been invested in order to develop quantitative magnetic resonance (MR) techniques revealing robust MR biomarkers. Thereby, proton density fat fraction (PDFF) and T_2 water (T_{2w}) are currently seen as valuable biomarkers to objectively determine fatty infiltration and oedematous changes. While PDFF is a rather stable parameter based on chemical shift encoding-based water-fat MRI, T_{2w} reflecting the water mobility of the tissue is highly sensitive to changes in the muscle microenvironment for example influenced by the amount of daily exercise. However, particularly T_{2w} is of high interest currently being seen as a maker for "disease activity" and therefore as a predictor for disease progression and therapy effectiveness.

In the first journal publication magnetic resonance spectroscopy (MRS) is used to gain deeper insights into T_{2w} as a MR biomarker. In the work T_{2w} was determined in regions of higher fatty infiltration often being present in heterogeneously affected muscles of patients with NMD. Thereby, MRS offers the possibility to chemically selectively determine the T_2 relaxation time of water in the muscle tissue. It was shown that T_{2w} is decreased with increasing fat content which has to be considered when interpreting T_{2w} measurements especially in the presence of fat. Additionally, the findings suggest that it is crucial to take partial volume effects into account when the region of interest includes healthy, fatty and oedematous muscle tissue.

Besides the clean determination of T_{2w} using MRS, this technique can not deliver spatial resolution. Therefore, the second journal publication investigates the performance of a novel T_{2w} mapping technique based on a T_2 -prepared 3D turbo spin echo (TSE) sequence with spectral adiabatic inversion recovery (SPAIR) fat suppression. This method not only offers the possibility of T_{2w} quantification directly at the acquisition side without the need for further simulations, but also has the advantage of relatively minor B1 and B0 sensitivity. The purpose of this work was to investigate whether the T_2 -prepared

Abstract

3D TSE sequence with SPAIR enables the determination of robust and reliable T_{2w} values in the presence of fat. Therefore Bloch simulations theoretically reflecting the signal behavior of water and fat and in vivo measurements in patients with NMD compared to the reference standard MRS and the standard T_2 mapping sequence 2D multi echo spin echo (MESE) were performed. The work shows that the T_2 -prepared 3D TSE with SPAIR is a good alternative for T_{2w} mapping in NMD.

The results of the present dissertation are based on a large-scale MR study in patients with various acquired and hereditary NMD. The study enabled the further evaluation of the important MR biomarker T_{2w} and the investigation of the T_2 -prepared 3D TSE, as a promising T_{2w} mapping technique. The provided insights into T_{2w} will be further considered when interpreting its value as an MR biomarker. The T_{2w} mapping technique T_2 -prepared 3D TSE is and will be further applied in research studies and effort is being made to implement the technique in the clinical routine of patients with NMD.

List of Included Journal Publications

The present dissertation is based on the following two first-authored journal publications.

- [JP-I] **S. Schlaeger**, D. Weidlich, E. Klupp, F. Montagnese, M. Deschauer, B. Schoser, S. Bublitz, S. Ruschke, C. Zimmer, E. J. Rummeny, J. S. Kirschke, and D. C. Karampinos. “Decreased water T2 in fatty infiltrated skeletal muscles of patients with neuromuscular diseases”. In: *NMR in Biomedicine* 32.8 (2019), e4111.
- [JP-II] **S. Schlaeger**, D. Weidlich, E. Klupp, F. Montagnese, M. Deschauer, B. Schoser, S. Bublitz, S. Ruschke, C. Zimmer, E. J. Rummeny, J. S. Kirschke, and D. C. Karampinos. “Water T2 Mapping in Fatty Infiltrated Thigh Muscles of Patients With Neuromuscular Diseases Using a T2-Prepared 3D Turbo Spin Echo With SPAIR”. In: *Journal of Magnetic Resonance Imaging* 51.6 (2020), pp. 1727–1736.

The above two journal publications are referred to as JP-I and JP-II, respectively. The journal publications can be found in chapter 6.

List of Related Publications

The author contributed also to the following subject-related first-authored journal publications (ordered by year of appearance):

- [J1] **S. Schlaeger**, F. Freitag, E. Klupp, M. Dieckmeyer, D. Weidlich, S. Inhuber, M. Deschauer, B. Schoser, S. Bublitz, F. Montagnese, C. Zimmer, E. J. Rummeny, D. C. Karampinos, J. S. Kirschke, and T. Baum. “Thigh muscle segmentation of chemical shift encoding-based water-fat magnetic resonance images: The reference database MyoSegmenTUM”. In: *PloS one* 13.6 (2018), e0198200.
- [J2] **S. Schlaeger**, E. Klupp, D. Weidlich, B. Cervantes, S. C. Foreman, M. Deschauer, B. Schoser, C. Katemann, H. Kooijman, E. J. Rummeny, C. Zimmer, J. S. Kirschke, and D. C. Karampinos. “T2-Weighted Dixon Turbo Spin Echo for Accelerated Simultaneous Grading of Whole-Body Skeletal Muscle Fat Infiltration and Edema in Patients With Neuromuscular Diseases”. In: *J Comput Assist Tomogr* 42.4 (2018), pp. 574–579.
- [J3] **S. Schlaeger**, S. Inhuber, A. Rohrmeier, M. Dieckmeyer, F. Freitag, E. Klupp, D. Weidlich, G. Feuerriegel, F. Kreuzpointner, A. Schwirtz, E. J. Rummeny, C. Zimmer, J. S. Kirschke, D. C. Karampinos, and T. Baum. “Association of paraspinal muscle water-fat MRI-based measurements with isometric strength measurements”. In: *Eur Radiol* 29.2 (2019), pp. 599–608.

The author contributed also to the following subject-related co-authored journal publications (ordered by year of appearance):

- [J4] E. Klupp, D. Weidlich, **S. Schlaeger**, T. Baum, B. Cervantes, M. Deschauer, H. Kooijman, E. J. Rummeny, C. Zimmer, J. S. Kirschke, and D. C. Karampinos. “B1-insensitive T2 mapping of healthy thigh muscles using a T2-prepared 3D TSE sequence”. In: *PloS one* 12.2 (2017), e0171337.
- [J5] D. Weidlich, **S. Schlaeger**, H. Kooijman, P. Bornert, J. S. Kirschke, E. J. Rummeny, A. Haase, and D. C. Karampinos. “T2 mapping with magnetization-prepared 3D TSE based on a modified BIR-4 T2 preparation”. In: *NMR Biomed* 30.11 (2017), e3773.
- [J6] N. Sollmann, M. Dieckmeyer, **S. Schlaeger**, A. Rohrmeier, J. Syvaeri, M. N. Diefenbach, D. Weidlich, S. Ruschke, E. Klupp, D. Franz, E. J. Rummeny, C. Zimmer, J. S. Kirschke, D. C. Karampinos, and T. Baum. “Associations Between Lumbar Vertebral Bone Marrow and Paraspinal Muscle Fat Compositions—An Investigation by Chemical Shift Encoding-Based Water-Fat MRI”. In: *Frontiers in endocrinology* 9 (2018), p. 563.

List of Related Publications

- [J7] E. Burian, A. Rohrmeier, **S. Schlaeger**, M. Dieckmeyer, M. N. Diefenbach, J. Syväri, E. Klupp, D. Weidlich, C. Zimmer, E. J. Rummeny, D. C. Karampinos, J. S. Kirschke, and T. Baum. “Lumbar muscle and vertebral bodies segmentation of chemical shift encoding-based water-fat MRI: the reference database MyoSegmenTUM spine”. In: *BMC Musculoskeletal Disorders* 20.1 (2019), p. 152.
- [J8] L. Schlaffke, R. Rehmann, M. Rohm, L. A. M. Otto, A. de Luca, J. Burakiewicz, C. Baligand, J. Monte, C. den Harder, M. T. Hooijmans, A. Nederveen, **S. Schlaeger**, D. Weidlich, D. C. Karampinos, A. Stouge, M. Vaeggemose, M. G. D’Angelo, F. Arrigoni, H. E. Kan, and M. Froeling. “Multi-center evaluation of stability and reproducibility of quantitative MRI measures in healthy calf muscles”. In: *NMR Biomed* 32.9 (2019), e4119.
- [J9] E. Klupp, B. Cervantes, **S. Schlaeger**, S. Inhuber, F. Kreuzpointner, A. Schwirtz, A. Rohrmeier, M. Dieckmeyer, D. M. Hedderich, M. N. Diefenbach, F. Freitag, E. J. Rummeny, C. Zimmer, J. S. Kirschke, D. C. Karampinos, and T. Baum. “Paraspinal Muscle DTI Metrics Predict Muscle Strength”. In: *J Magn Reson Imaging* 50.3 (2019), pp. 816–823.
- [J10] S. Inhuber, N. Sollmann, **S. Schlaeger**, M. Dieckmeyer, E. Burian, C. Kohlmeyer, D. C. Karampinos, J. S. Kirschke, T. Baum, F. Kreuzpointner, and A. Schwirtz. “Associations of thigh muscle fat infiltration with isometric strength measurements based on chemical shift encoding-based water-fat magnetic resonance imaging”. In: *European Radiology Experimental* 3.1 (2019), p. 45.
- [J11] E. Burian, S. Inhuber, **S. Schlaeger**, M. Dieckmeyer, E. Klupp, D. Franz, D. Weidlich, N. Sollmann, M. Löffler, A. Schwirtz, E. J. Rummeny, C. Zimmer, J. S. Kirschke, D. C. Karampinos, and T. Baum. “Association of thigh and paraspinal muscle composition in young adults using chemical shift encoding-based water-fat MRI”. In: *Quantitative Imaging in Medicine and Surgery* 10.1 (2020), p. 128.
- [J12] M. Dieckmeyer, F. Zoffl, L. Grundl, S. Inhuber, **S. Schlaeger**, E. Burian, C. Zimmer, J. S. Kirschke, D. C. Karampinos, T. Baum, and N. Sollmann. “Association of quadriceps muscle, gluteal muscle, and femoral bone marrow composition using chemical shift encoding-based water-fat MRI: a preliminary study in healthy young volunteers”. In: *European Radiology Experimental* 4.1 (2020), pp. 1–8.

List of Related Publications

The author contributed also to the following subject-related first-authored conference abstracts (ordered by year of appearance):

- [C1] **S. Schläger**, E. Klupp, D. Weidlich, S. Bublitz, F. Montagnese, C. Zimmer, M. Deschauer, B. Schoser, D. C. Karampinos, and J. S. Kirschke. “Vergleich von T2W STIR und Dixon FFE mit T2W Dixon anhand von Rating-Skalen für ödematöse und fettige Veränderungen in der Oberschenkelmuskulatur von Patienten mit neuromuskulären Erkrankungen”. In: *23. Kongress des Wissenschaftlichen Beirates der Deutschen Gesellschaft für Muskelkranke e.V.* (oral presentation). Munich, Germany, 2017.
- [C2] **S. Schlaeger**, E. Klupp, D. Weidlich, B. Cervantes, M. Deschauer, B. Schoser, S. Bublitz, F. Montagnese, C. Katemann, H. Kooijman, E. J. Rummeny, C. Zimmer, J. S. Kirschke, and D. C. Karampinos. “T2-weighted Dixon TSE for accelerated simultaneous grading of whole body skeletal muscle fat infiltration and edema in patients with neuromuscular diseases”. In: *Proceedings 25. Annual Meeting International Society for Magnetic Resonance in Medicine.* (electronic poster). USA, Hawaii, Honolulu, 2017, p. 5011.
- [C3] **S. Schläger**, D. Weidlich, E. Klupp, F. Montagnese, B. Schoser, S. Bublitz, M. Deschauer, C. Zimmer, D. C. Karampinos, and J. S. Kirschke. “Robuste Ödemquantifizierung bei Patienten mit neuromuskulären Erkrankungen mittels einer neuen T2mapping-Sequenz”. In: *Proceedings of 52. Jahrestagung der Deutschen Gesellschaft für Neuroradiologie e. V.* (oral presentation). Cologne, Germany, 2017.
- [C4] **S. Schlaeger**, D. Weidlich, E. Klupp, M. Deschauer, B. Schoser, S. Bublitz, F. Montagnese, E. J. Rummeny, C. Zimmer, J. S. Kirschke, and D. C. Karampinos. “Water T2 mapping of the fatty infiltrated thigh musculature using a T2-prepared 3D TSE sequence combined with SPAIR”. In: *Imaging in Neuromuscular Disease.* (traditional poster). Berlin, Germany, 2017.
- [C5] **S. Schlaeger**, D. Weidlich, E. Klupp, F. Montagnese, M. Deschauer, B. Schoser, S. Bublitz, C. Zimmer, E. J. Rummeny, J. S. Kirschke, and D. C. Karampinos. “Water T2 mapping in fatty infiltrated thigh muscles of patients with neuromuscular diseases using a T2-prepared 3D TSE with SPAIR”. In: *Proceedings 26. Annual Meeting International Society for Magnetic Resonance in Medicine.* (oral presentation, ISMRM Merit Award **Magna Cum Laude**). Paris, France, 2018, p. 0815.
- [C6] **S. Schlaeger**, D. Weidlich, E. Klupp, F. Montagnese, M. Deschauer, B. Schoser, S. Bublitz, C. Zimmer, E. J. Rummeny, J. S. Kirschke, and D. C. Karampinos. “Decreasing Water T2 based on multi-TE single-voxel MRS in fatty infiltrated skeletal muscles of patients with neuromuscular diseases”. In: *Proceedings 26. Annual Meeting International Society for Magnetic Resonance in Medicine.* (electronic poster). Paris, France, 2018, p. 5059.

List of Related Publications

The author contributed also to the following subject-related co-authored conference abstracts (ordered by year of appearance):

- [C7] E. Klupp, B. Cervantes, **S. Schlaeger**, S. Inhuber, F. Kreuzpointer, M. Dieckmeyer, F. Freitag, E. J. Rummeny, C. Zimmer, J. S. Kirschke, D. C. Karampinos, and T. Baum. “Relationship of paraspinal muscle DTI metrics to isometric strength measurements”. In: *Proceedings 26. Annual Meeting International Society for Magnetic Resonance in Medicine*. (power pitch). Paris, France, 2018, p. 0329.
- [C8] D. Weidlich, M. Diefenbach, **S. Schlaeger**, A. Hock, S. Ruschke, and D. C. Karampinos. “In-vivo water T2 mapping in tissues containing water and fat using a T2-prepared 3D Dixon TSE sequence and a pre-calibrated fat spectrum model”. In: *Proceedings 26. Annual Meeting International Society for Magnetic Resonance in Medicine*. (electronic poster). Paris, France, 2018, p. 4223.
- [C9] T. Baum, **S. Schlaeger**, S. Inhuber, F. Kreuzpointer, M. Dickmeyer, F. Freitag, E. Klupp, B. Cervantes, A. Schwirtz, J. S. Kirschke, and D. C. Karampinos. “Association of thigh muscle fat infiltration with isometric strength measurements based on chemical shift encoding-based water–fat MRI”. In: *Proceedings 26. Annual Meeting International Society for Magnetic Resonance in Medicine*. (electronic poster). Paris, France, 2018, p. 5080.
- [C10] N. Sollmann, M. Dieckmeyer, **S. Schlaeger**, R. Rohrmeier, J. Syvaeri, M. N. Diefenbach, D. Weidlich, S. Ruschke, E. Klupp, D. Franz, E. J. Rummeny, C. Zimmer, J. S. Kirschke, D. C. Karampinos, and T. Baum. “Associations between lumbar vertebral bone marrow and paraspinal muscle fat compositions—an investigation by chemical shift encoding-based water-fat MRI”. In: *Proceedings of 4th International Meeting on Bone Marrow Adiposity*. (oral presentation). Lille, France, 2018.
- [C11] M. Löffler, **S. Schlaeger**, S. Inhuber, M. Dieckmeyer, D. Weidlich, A. Schwirtz, E. J. Rummeny, C. Zimmer, J. S. Kirschke, D. C. Karampinos, and T. Baum. “Regional thigh muscle composition based on chemical shift encoding-based water-fat MRI and its association with muscle strength”. In: *Proceedings 27. Annual Meeting International Society for Magnetic Resonance in Medicine*. (electronic poster). Montreal, Canada, 2019, p. 1261.

Contents

Abstract	I
List of Included Journal Publications	III
List of Related Publications	IV
1 Introduction	1
1.1 Scientific and Clinical Relevance	2
1.2 Thesis Purpose	3
1.3 Thesis Structure	3
2 Neuromuscular Diseases	5
3 Skeletal Muscle Tissue	7
3.1 Anatomy and Physiology of Healthy Skeletal Muscle Tissue	7
3.2 Pathological Changes in Diseased Skeletal Muscle Tissue	9
3.2.1 Atrophy and Hypertrophy	10
3.2.2 Fatty Infiltration	10
3.2.3 Oedematous Alterations	11
4 Magnetic Resonance Measurements in Neuromuscular Diseases	13
4.1 Excursus: Relaxation	14
4.2 Excursus: Chemical Shift	15
4.3 Qualitative MR Measurements	16
4.3.1 T_1 -Weighted and T_2 -Weighted Imaging	16
4.3.2 Semi-quantitative Rating	18
4.4 Quantitative MR Measurements	22
4.4.1 The Quantitative Biomarker Proton Density Fat Fraction	22
4.4.2 The Quantitative Biomarker T_2 Water	23
4.4.3 Single-Voxel Proton Magnetic Resonance Spectroscopy	24
4.4.4 Chemical Shift Encoding-Based Water-Fat Imaging	26
4.4.5 T_2 Water Mapping	29
5 Compliance with Ethical Standards	33

Contents

6	Journal Publications	34
6.1	Journal Publication I: Decreased Water T_2 in Fatty Infiltrated Skeletal Muscles of Patients with Neuromuscular Diseases	34
6.1.1	Abstract	34
6.1.2	Authors Contribution	35
6.2	Journal Publication II: Water T_2 Mapping in Fatty Infiltrated Thigh Muscles of Patients With Neuromuscular Diseases Using a T_2 -Prepared 3D Turbo Spin Echo With SPAIR	46
6.2.1	Abstract	46
6.2.2	Authors Contribution	47
7	Discussion	58
7.1	Review of the Existing Literature	58
7.1.1	T_2 Water as a Biomarker in the Context of Skeletal Muscle Health	58
7.1.2	T_2 Water Quantification Based on Magnetic Resonance Spectroscopy	59
7.1.3	T_2 Water Quantification Based on Magnetic Resonance Imaging .	59
7.2	Present Work	60
7.2.1	Novelty	60
7.2.2	Impact	60
7.2.3	Limitations	61
7.3	Perspective	62
	Acknowledgements	64
	List of Symbols and Abbreviations	66
	List of Tables	68
	List of Figures	69
	Bibliography	71

1 Introduction

Neuromuscular imaging is subject to a constant development. In the 1980s and early 1990s computed tomography (CT) was introduced and used in the diagnostic workup of patients with inherited or acquired neuromuscular disorders while, during the past three decades, magnetic resonance imaging (MRI) emerged as the imaging modality of choice for various neuromuscular diseases (NMD). Increasing availability and persistent development of ever faster and more accurate acquisition techniques have been the key factors for this progress. Today, MRI has almost completely replaced CT and is next to ultrasonography increasingly relevant for diagnosis and therapy planning of patients with NMD. [1, 2, 3, 4, 5, 6]

Magnetic resonance (MR) basically shows image contrast due to specific behaviour of proton spins being bound in molecules such as water or fatty acids. Therefore, the imaging contrast of MR images represents a tissue inherent property. [7]

In the clinical setting of imaging in NMD, primarily qualitative imaging techniques are applied allowing a visual assessment of the muscle pathology. However, recently the development and implementation of quantitative MR techniques is wildly fostered. In course of the overall attempt towards quantitative imaging in modern radiology practice also in the field of NMD novel advanced techniques have been introduced [5, 6, 8].

The Quantitative Imaging Biomarkers Alliance (QIBA) of Radiological Society of North America (RSNA) has defined quantitative imaging and its advantages for modern evidence-based medicine as following:

“Quantitative imaging is the extraction of quantifiable features from medical images for the assessment of normal or the severity, degree of change, or status of a disease, injury, or chronic condition relative to normal. Quantitative imaging develops, standardizes and optimizes: anatomical, functional and molecular imaging acquisition protocols, data analyses, display methods, and reporting structures. These features permit the validation of accurately and precisely obtained image-derived metrics with anatomically and physiologically relevant parameters, including treatment response and outcome, and the use of such metrics in research and patient care.” [9]

In particular a lot of effort is being invested in order to forward the development of robust quantitative MR techniques such as magnetic resonance spectroscopy (MRS), chemical shift encoding-based water-fat imaging, T2 water (T_{2w}) mapping, perfusion MRI and diffusion MRI [5, 6] with the over all aim to advance them from mere research studies to the clinical practice in the workup of patients with NMD. Thereby, quantitative MR allows the extraction of MR biomarkers which characterize a tissue specific property and provide insights about disease severity, progression and therapy effectiveness [9, 8].

1.1 Scientific and Clinical Relevance

Due to its non-invasiveness, possibility for whole-body assessment and lack of radiation MRI has become an inevitable tool in the diagnostic workup of patients with NMD. The high soft tissue contrast enables assessment of pathologies in the muscle tissue such as atrophy or hypertrophy, fatty infiltration and oedematous alterations. Additional to the neurological examination, functional neurophysiological tests and laboratory results MRI is used to guide biopsies, narrow the differential diagnoses for subsequent genetic testing and monitor disease progression as well as therapy effectiveness. [3, 4, 5, 10, 6, 8, 11]

The traditionally used MRI techniques in the field of NMD are mainly T_1 -weighted sequences and T_2 -weighted sequences with additional fat suppression [4, 12, 13, 5, 14, 6]. Due to the assessment based on relative contrast a qualitative, subjective interpretation of the pathologies and therefore less accurate intra- and inter-rater agreement are common [15]. Additionally, the monitoring of disease progression or therapy success, mostly reflected through subtle changes in the imaging contrast, is challenging [8]. Despite the introduction of semi-quantitative rating scales with the attempt to render assessment of pathologies based on qualitative imaging more comparable [16, 4, 17, 14, 18], these techniques remain highly dependent on the reader's judgement. Therefore, a lot of effort is being invested in the establishment of objective, quantitative MR biomarkers in the field of NMD [5, 6, 8]: (i) proton density fat fraction (PDFF) as a biomarker for fatty infiltration [19, 20] and (ii) T_2 water (T_{2w}) as a biomarker for oedematous alterations [21, 22, 23, 24].

Chemical shift encoding-based water-fat MR measurements allow the extraction of PDFF, a rather stable tissue property representing the concentration of the MR visible lipid concentration in the tissue of interest [25, 20].

A far more dynamic and hence unstable biomarker is T_{2w} . It represents the water mobility in the muscle tissue and increases in a variety of circumstances with higher water content such as inflammation, necrosis, denervation or exercise. Currently, T_{2w} is being seen as a marker for "diseases activity" in the context of NMD and as a predictor for later degenerative changes such as fatty infiltration in the muscle tissue. Hence T_{2w} is a promising biomarker for early diagnosis and assessment of disease severity and progression as well as monitoring response to treatment. [26, 27, 28, 21, 10, 29, 6, 22, 24, 30, 8, 31]

However, the assessment of T_{2w} is difficult mainly because of two challenges. On the one hand, the variety of physiological and pathological circumstances leading to T_{2w} alterations [22, 8], renders a definite interpretation of the observed alterations challenging. On the other hand T_{2w} is technically difficult to determine using MR imaging sequences. The measurement of T_{2w} is sensitive to B1 and B0 inhomogeneities that lead to an inaccurate application of radio frequency (RF) pulses [32, 33, 34, 35, 36, 10]. The longer T_2 of surrounding, unsuppressed fat leads to an overestimation of the T_{2w} value of the tissue [37, 38, 39, 40, 41, 22, 8, 31].

Thus, there is a high need for research on the behaviour of T_{2w} in different diseases, progression states, muscles and surrounding micro environmental conditions [8] and on

imaging techniques providing a robust T_{2w} quantification. This is important, so that a correct interpretation of T_{2w} values in the context of NMD can be achieved and T_{2w} can be precisely used as a biomarker.

As patients with NMD typically show fatty infiltration next to healthy or oedematous muscle tissue [31], particularly the behaviour of T_{2w} in the presence of surrounding fat is of high relevance. As fatty infiltration is next to field inhomogeneities a main confounding effect for a robust T_{2w} quantification imaging technique, T_{2w} mapping techniques that are insensitive to all of these confounding effects are needed. However, both problems have not been sufficiently solved yet.

1.2 Thesis Purpose

The present work represents a valuable contribution to bridge the gap from research to the clinical application of T_{2w} as a diagnostic parameter in NMD. To archive this, the behaviour of the biomarker T_{2w} was evaluated in the presence of fatty infiltration which is a common pathology in the skeletal muscles of patients with NMD. More specifically, the purpose of the present work was twofold:

- (i) Understanding the physical behaviour of the biomarker T_{2w} in skeletal muscles with different degrees of fatty infiltration is crucial for a further clinical application in the field of NMD. Therefore, the purpose of this study part was to assess T_{2w} in a large-scale study using the reference standard measurement technique MRS, to reveal details about the behaviour of T_{2w} in the proximity of fat.
- (ii) To determine T_{2w} as a reliable biomarker in the context of NMD the underlying sequence needs to be robust towards field inhomogeneities and fat in the surrounding tissue as confounding factors. The recently presented T_2 -prepared 3D turbo spin echo (TSE) sequence with spectral adiabatic inversion recovery (SPAIR) fat suppression potentially provides quantitative information in a clinically feasible scan time with relatively low sensitivity to field inhomogeneities [42, 43]. In this study part the performance of the T_2 -prepared 3D TSE with SPAIR was analysed in the presence of fatty infiltrations.

Summarizing, the present dissertation contributes to the overall attempt of a clinical implementation of quantitative imaging techniques in the field of NMD.

1.3 Thesis Structure

In the present cumulative dissertation, the clinical and technical background of the two embedded journal publications are described. Furthermore, the dissertation gives an overview of the literature and discusses the findings of the journal publications in this context.

1 Introduction

Chapter 2 gives an overview of NMD, their clinical presentation, treatment options and the common diagnostic workflow in the clinical routine. Chapter 3 offers insights into anatomy and physiology of healthy skeletal muscle tissue and typical histopathological findings in diseased muscle tissue with concentration on those being of interest for neuromuscular imaging. A summarization of MRI in NMD is being provided in chapter 4 dealing with qualitative and quantitative techniques as well as going into detail about the MR biomarkers PDFF and T_{2w} . In chapter 6 the two embedded journal publications are presented highlighting the author's contribution to the work, respectively. At the end in chapter 7, a brief review of the existing literature as well as a discussion of the two journal publications concentrating on novelty, impact, limitations and perspectives of the present work are given.

2 Neuromuscular Diseases

NMD represent a relatively rare, heterogeneous and broad group of hereditary or acquired disorders with malfunction of the muscle tissue itself, or pathologies of the neuromuscular junctions, the muscle-innervating nerves or the anterior horns of the spinal cord [44, 45, 46]. According to a classification by Walton et al. approximately 800 different NMD are known [47]. A rough classification distinguishes between

- (i) muscular dystrophies, showing progressive, genetically determined degeneration of muscle fibres,
- (ii) congenital myopathies with innate muscle weakness and limited muscle function,
- (iii) myotonic disorders and periodic paralysis due to ion channel defects,
- (iv) inflammatory myopathies with subacute or chronic muscle weakness due to inflammatory alterations of the muscle tissue,
- (v) metabolic myopathies due to enzyme deficiencies,
- (vi) mitochondrial diseases with defects in the muscles' mitochondria,
- (vii) myopathies in the course of endocrinological disorders,
- (viii) toxic myopathies due to e. g. medication or alcohol,
- (ix) neuromuscular junction diseases with defect signal transmission between nerves and muscles,
- (x) spinal muscular atrophy with degeneration of anterior horn cells of the spinal cord and motor cranial nerves, and
- (xi) amyotrophic lateral sclerosis and other motor neuron diseases, in which first and/or second motor neurons are affected,
- (xii) neuropathies, with affection of peripheral nerve fibres [48].

Usually, periodic or permanent muscle weakness or premature muscle fatigue are the most prominent symptoms, however patients present to clinics with a variety of symptoms including myalgia, myotonia, muscle spasm, cramps, fasciculations, muscle atrophy, hypertrophy or pseudo hypertrophy, muscular hypotonia, myoglobinuria and/or cardiac involvement. Numbness or paraesthesia are present when the peripheral sensitive nerves

are affected. Thereby on the one hand, different NMD differ on clinical symptoms, patterns of involvement and additional findings such as specific laboratory results. On the other hand, heterogeneous disease pathologies might show a rather similar clinical presentation. [48]

Time of disease onset differs wildly between different disorders and could be between at birth and late adulthood. Also, severity of affection and progression vary tremendously from one disease to another eventually leading to e.g. loss of ambulation or respiratory failure. [49]

Nowadays treatments for inflammatory diseases of the muscle tissue, the nerves and the neuromuscular junctions are established in the clinical routine. Also for several hereditary disorders drugs targeting the underlying pathology are already existing or currently being developed and evaluated in large-scale drug studies, such as enzyme replacement, antisense oligonucleotide or gene replacement therapy. Additionally, supportive treatment such as physiotherapy, ergotherapy, speech therapy and respiratory support are helping to increase the patients' quality of live substantially. [50, 51, 52, 53, 54, 55, 56, 57, 58, 59, 60, 61, 62, 63]

In order to offer appropriate and effective therapy an exact classification of the underlying NMD is crucial and specific diagnostics have to be performed. The complex diagnostic process in NMD has been mainly driven by neurological examination to determine the clinical phenotype, neurophysiological assessments and laboratory tests in order to narrow the underlying pathology as well as to plan further diagnostic tests such as diagnostic muscle biopsies and genetic analysis [48]. In recent years, latter gained increasing importance in the diagnostic pathway of hereditary NMD passing mere muscle biopsies as basis for a diagnosis. The discovery of various new genetic abnormalities associated with inherited NMD enabled new insights into the underlying pathologies and helped further understanding of these heterogeneous disorders as well as forwarding new therapies. [5, 8].

However, genetic mutation analysis still remains complex and requires narrowing of the differential diagnosis in order to enable determination of the clinically relevant pathogenic changes. Furthermore, accurate information about diseases progression and response to treatment is needed and still lacking in most scenarios [24].

That is why neuromuscular imaging is becoming increasingly important as a tool for describing the pattern and degree of muscle involvement and nowadays muscle imaging techniques are a fixed component in the clinical routine of patients with NMD. Thereby, neuromuscular imaging is supposed to confine the complex range of differential diagnoses, to support the clinical diagnosis, to guide interventional procedures such as muscle biopsies, to focus genetic analysis, and to monitor disease progression as well as therapy effectiveness. [5, 8]

3 Skeletal Muscle Tissue

Regardless of the underlying pathophysiology most NMD show an affection of the muscle tissue leading to symptoms of impaired muscle function and/or muscle pain. In order to understand the pathophysiological processes behind the clinical symptoms and the appearance of muscle tissue in imaging of NMD a profound knowledge of the healthy skeletal muscle anatomy as well as of characteristic histopathological changes in the muscle tissue related to NMD are inevitable.

3.1 Anatomy and Physiology of Healthy Skeletal Muscle Tissue

Muscle tissue enables active contraction. Two types of muscle tissue, striated and smooth muscle tissue, can be distinguished in the human body. In contrast to smooth muscle tissue representing the basis of the intestines and vessels, striated muscle tissue of the skeletal muscles and the heart exhibits repeating functional units called sarcomeres. Skeletal muscle consists of muscle fibres, supplying blood vessels, innervating nerves, and connective tissue. A muscle fibre is a large cell, structured as a syncytium with multiple nucleoli arranged close to the cell membrane, termed sarcolemma. The sarcolemma forms several invaginations into the muscle cell enabling an efficient signal transduction. The muscle cell itself contains cytoplasm, termed sarcoplasm, regular cellular structures such as mitochondria and nucleoli as well as functional units called myofibrils. The myofibrils are composed of the myofilaments actin (thin) and myosin (thick) (Fig. 3.1). The interaction of latter is crucial for the active muscle contraction and their regular alignment as units termed sarcomeres causes the striated, alternating dark and bright appearance of skeletal muscle tissue under the light microscope (Fig. 3.2). [48, 64]

Skeletal muscle is wrapped in fascia and subjacent epimysium both made out of connective tissue. Connected with the epimysium is the perimysium which is infiltrating the muscle and forming connective tissue bundles. The individual muscle fibre is surrounded by endomysium a thin layer of connective tissue. This organization is crucial for the structural integrity during contraction. (Fig. 3.3) [48, 64]

As skeletal muscle tissue has to fulfil different requirements in order to allow appropriate contraction, in general two muscle fibre types with different functionalities are known. Due to differences on the cellular level one can distinguish between slow-twitch (type I) fibres enabling slow, long lasting contractions and fast-twitch (type II) fibres enabling short, powerful contractions. Every skeletal muscle consists of type I and type II fibres, respectively. [48]

Several hundred muscle fibres are innervated by one motor neuron originating from the spine forming a so-called motor unit. The strength of contraction is being controlled by the amount of recruited motor units. [48]

3 Skeletal Muscle Tissue

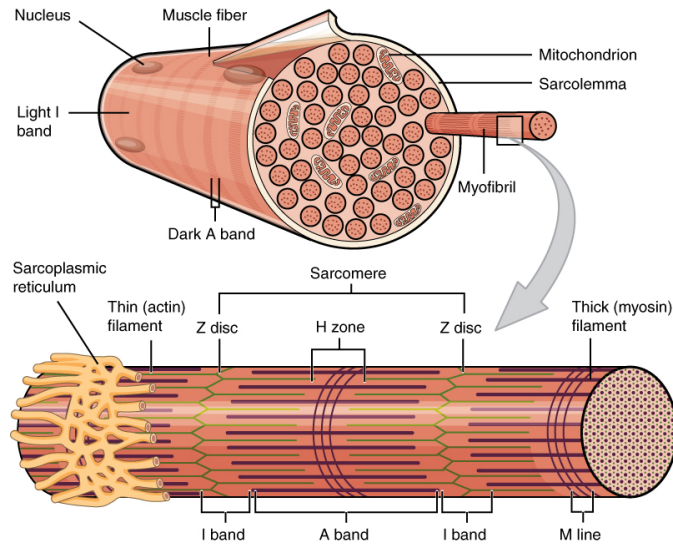


Figure 3.1: A single muscle fibre consists of several myofibrils composed of actin and myosin which are forming a functional unit. Figure according to [64].

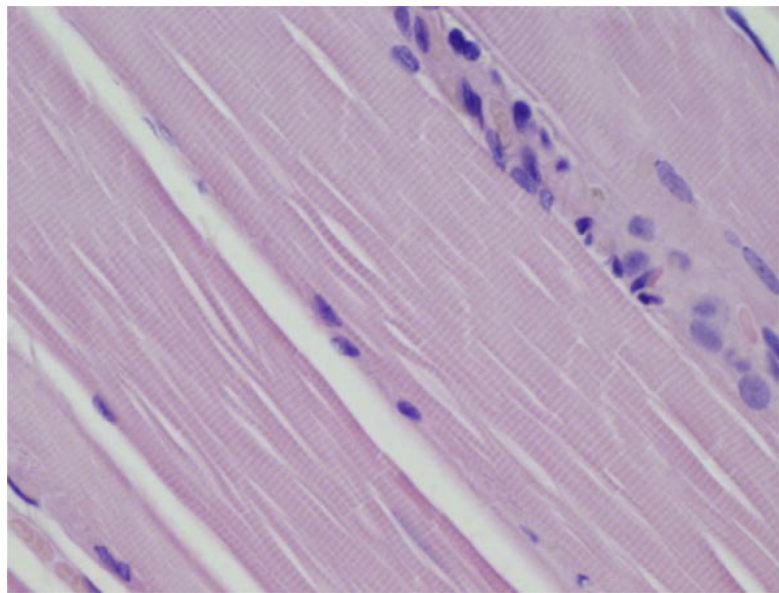


Figure 3.2: Histological assessment of healthy skeletal muscle tissue with nucleoli arranged near the sarcolemma. The typical striated appearance is clearly visible. Hematoxylin and eosin stain. Figure according to Joyce et al. [65].

Individual skeletal muscles differ with regard to their function, but also with regard to their vulnerability towards pathogenic influences. That is the reason why different NMD

3 Skeletal Muscle Tissue

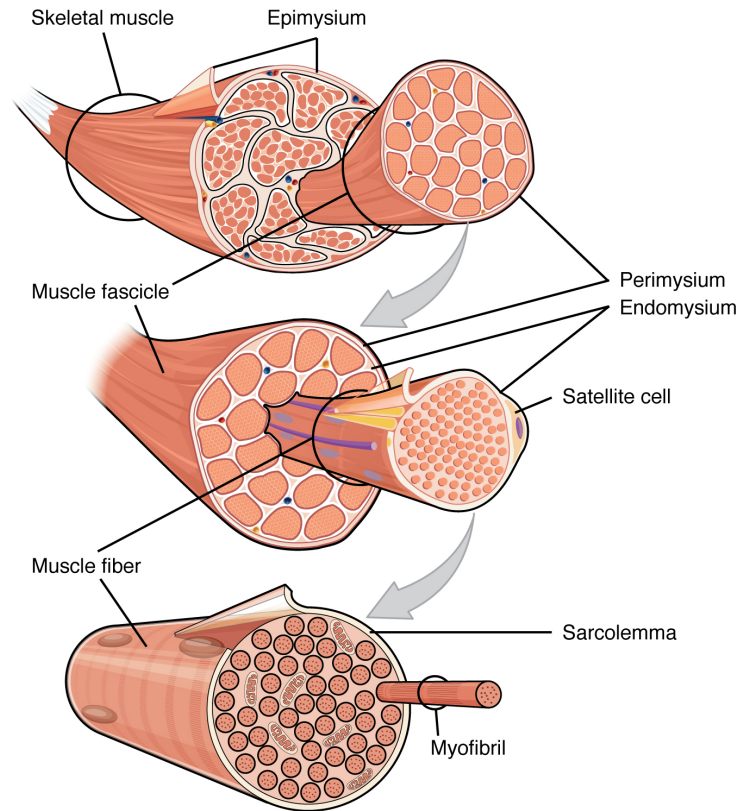


Figure 3.3: The three connective tissue layers epimysium, perimysium and endomysium organize skeletal muscles by structuring them in muscle fascicles and muscle fibres. Figure according to [64].

show different, however often disease characteristic patterns of involvement, respectively. [48]

3.2 Pathological Changes in Diseased Skeletal Muscle Tissue

Histopathological examination gives insights into structural changes of diseased muscle tissue. Thereby a similar histopathological finding can occur due to different underlying pathophysiologies. Several findings might be indicative for a specific disease. However, usually only the combined interpretation of various different histopathological findings helps to guide diagnosis, referred to as myopathological syndrome. Different histopathological changes of the muscle tissue in patients with NMD are known: (i) characteristic structural changes of the muscle fibres themselves such as atrophy, hypertrophy, muscle fibre type grouping, abnormal nucleus arrangement, necrosis, and numerous others, (ii) fatty infiltration, (iii) endomysial fibrosis (iv) oedematous alterations and affection of intramuscular blood vessels, and (v) changes of nerve-related structures. The combi-

nation of specific pathologies of the muscle architecture are indicative for a myopathic, myositic or neurogenic syndrome, respectively. [48]

Furthermore, it is important to be aware of the dynamic character of striated muscle tissue, being influenced not only by pathological changes but also by physiological factors such as exercise, age and gender [66].

Atrophy or hypertrophy, fatty infiltration and oedematous alterations are currently among the pathologies of utmost interest for neuromuscular imaging. Therefore, they are discussed in more detail in the following.

3.2.1 Atrophy and Hypertrophy

Atrophy and hypertrophy can either affect only single muscle fibres or have influence on the whole muscle volume (Fig. 3.4) [48, 6]. Atrophy and hypertrophy can be assessed by routinely performed imaging techniques.

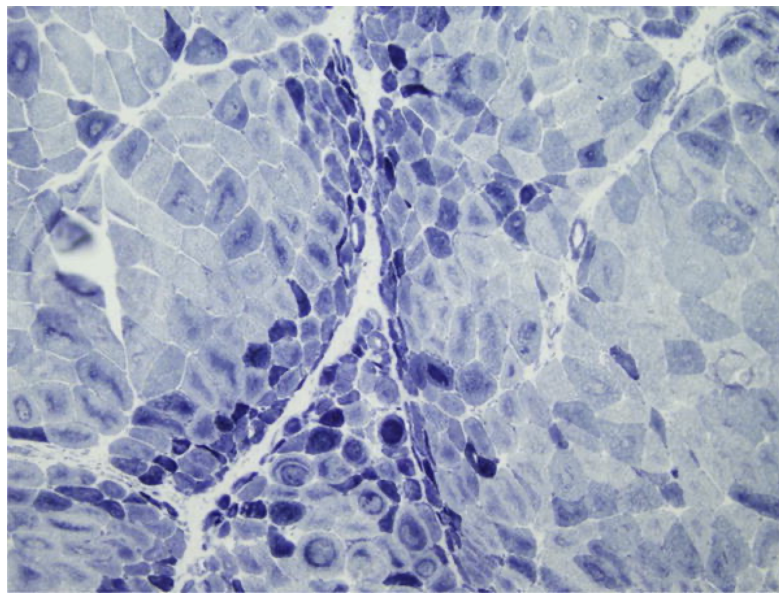


Figure 3.4: Histopathological assessment of a dermatomyositis patient's muscle biopsy. The disease characteristic atrophy of the muscle fibres at the periphery of fascicles (perifascicular) is prominent. Nicotinamide adenine dinucleotide stain. Figure according to Joyce et al. [65].

3.2.2 Fatty Infiltration

In advanced disease stages the NMD patients' muscles typically show a significant increase of interstitial fat content up to replacement of the whole functional muscle tissue by fat (Fig. 3.5). In general, fatty infiltration of muscle tissue occurs in various conditions such as ageing, muscle inactivity, disuse, as side effect of e. g. steroid medication,

and in NMD. It can either occur locally or diffusively. Imaging of the patients' muscles enables the determination of a fatty infiltration involvement pattern which is fairly specific for the underlying disease and therefore can narrow the differential diagnosis in the field of NMD. While fatty infiltration in elderly people occurs rather symmetrically and homogeneously in almost all skeletal muscles, in patients with NMD it is more heterogeneous and usually different muscle groups are involved. [6]

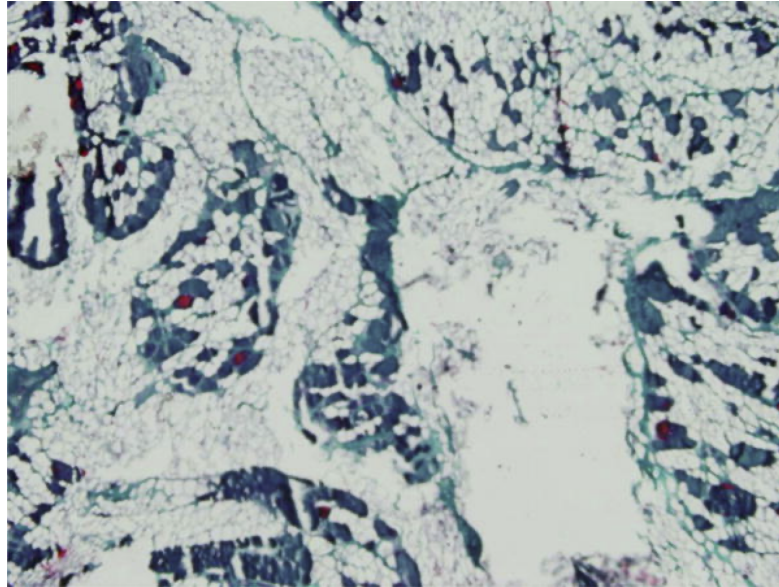


Figure 3.5: Histopathological assessment of an end stage muscle showing an almost complete replacement of muscle fibres by fatty infiltration. Figure according to Joyce et al. [65].

Fatty infiltration is often accompanied by muscle atrophy. Recent research raised the suspicion that fatty infiltration might inversely correlate with muscle strength [67, 68]. The amount of functional muscle tissue without fatty infiltration is an indicator for remaining muscle strength [69].

3.2.3 Oedematous Alterations

An increase of extra- and/or intracellular water content, referred to as oedematous alterations, might occur focally in a single muscle or diffusively involving different muscle groups, as in rhabdomyolysis. Several different, rather unspecific circumstances lead to an increase of muscle water content such as inflammation, necrosis, dystrophic cell lesions, denervation, or tumours. Physiologically, muscle oedema might also be present after exercise of moderate to high intensity. In patients with NMD exercise might even enhance pre-existing oedematous alterations. Currently, muscle oedema is seen as the imaging correlate to histopathological loss of muscle fibre integrity accompanied by in-

3 Skeletal Muscle Tissue

creased water content and invasion of inflammatory cells (Fig. 3.6). That is the reason why muscle oedema is currently being understood as the first pathological manifestation and therefore as an early imaging sign before degeneration of muscle fibres with subsequent replacement by fat and connective tissue. Muscles showing oedema in imaging are preferably chosen as biopsy sides in order to obtain tissue with active disease, which might enable an early diagnosis and hence prompt therapeutic intervention. [70, 5, 6, 22, 8]

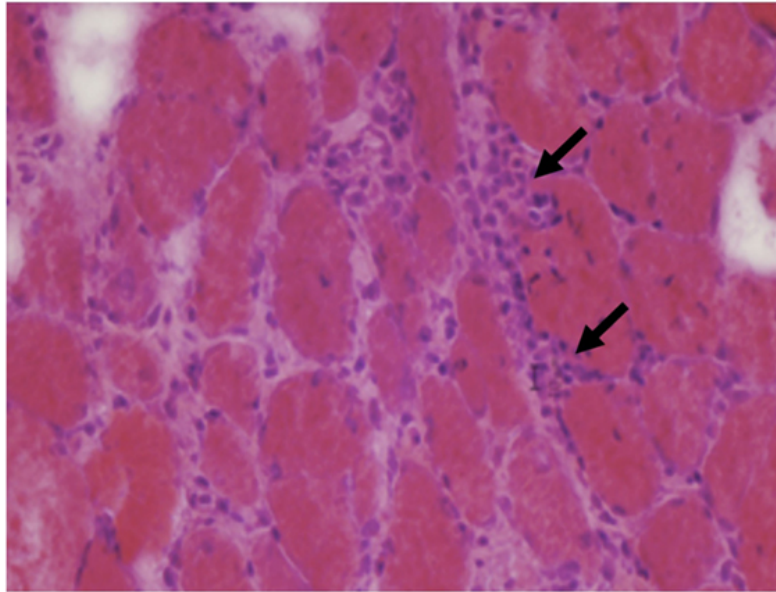


Figure 3.6: Histopathological assessment of a polymyositis patient's muscle biopsy. Endomysial inflammatory cells (arrow) are prominent. Hematoxylin and eosin stain. Figure according to [71].

4 Magnetic Resonance Measurements in Neuromuscular Diseases

MR measurements provide a high soft tissue contrast in various anatomies of the human body. As the main morphological changes in diseased muscle tissue of patients with NMD are mainly muscle atrophy or hypertrophy, fatty infiltration and oedematous alterations, MR measurements are a valuable diagnostic tool in this field. MRI enables excellent assessment of skeletal muscles regarding their shape, volume and tissue architecture. Signal intensity and hence brightness of different tissue types on MR images, referred to as MR image contrast, originate from differences in spin behaviour of protons in fat and water molecules. Specific MR sequences are sensitive to the fat content or to changes in the hydration level of the tissue. Consequently, these MR techniques are appropriate for assessment of fatty infiltration and oedematous changes of skeletal muscle tissue. Also because of its non-invasive character and the possibility of whole-body imaging, MRI is a valuable diagnostic tool in the clinical assessment of NMD next to the neurological examination, neurophysiological assessments, laboratory results, and genetic analysis. [3, 4, 5, 6, 8]

Routinely, MR sequences in muscle imaging in NMD are performed in the axial plane. Thereby, especially whole-body imaging enables detection of pathologies of muscles in unusual and therefore unexpected locations and allows an almost complete description of the muscle involvement pattern. The lack of ionising radiation renders MR techniques particularly interesting for the examination of children or for longitudinal imaging studies with multiple acquisitions. Additional advantages of MR measurements are the possibility of high-resolution imaging and multi-parametric tissue analysis with different contrast techniques. [5, 6]

MRI can help to describe pattern and degree of muscle involvement, focus appropriate genetic analysis, to determine muscle biopsy sides and to monitor disease progression and response to treatment. Therefore, MR techniques are widely used in patients with suspected and proven neuromuscular disorders [10, 4, 5, 11, 6, 8, 3].

In general, MR techniques for imaging of NMD can be subdivided into on the one hand conventional qualitative imaging techniques (section 4.3) which are routinely used in clinics and on the other hand quantitative measurement techniques (section 4.4). Qualitative techniques provide so-called weighted images and the image contrast of tissues and pathologies can be visually assessed by the reader. Whereas, quantitative techniques try to determine tissue parameters and therefore are more objective and potentially more accurate than qualitative sequences. Quantitative techniques offer new insights into pathological changes of the muscle tissue by providing absolute biomarkers for pathological changes. Hence, development of quantitative MR measurement tech-

niques has been brought forward during the last years. Quantitative MR methods are currently mainly used in research studies, however their clinical implementation is highly desirable and being forwarded. [5, 6, 8]

4.1 Excursus: Relaxation

Crucial for understanding the following sections 4.3 and 4.4 and the described MR signal behaviour of sequences are the terms T_1 and T_2 relaxation time.

Thereby the T_1 relaxation time, also called spin-lattice (longitudinal) relaxation, is a tissue specific parameter indicating the time proton spins need to return from the transverse magnetization plane to their starting magnetization on the longitudinal axis after excitation. The realignment to the longitudinal direction is caused by interactions of the spins with surrounding tissue, the lattice. Whereas the T_2 relaxation time, also called spin-spin (transverse) relaxation, is a tissue property for the loss of phase coherence in the transverse plane due to interactions between neighbouring spins. These interactions are due to slightly different precessional frequencies of the spins leading to slightly different magnetic fields that the neighbouring spins are experiencing, respectively. Both relaxation parameters influence the amount of MR signal present in a specific sequence and consequently influence the signal contrast. In general, T_2 is shorter than T_1 . Table 4.1 gives an overview of T_1 and T_2 relaxation times of skeletal muscle tissue and fat at main magnetic field strengths of 1.5 T and 3 T. [7]

Tissue	T_1 [ms]		T_2 [ms]	
	1.5 T	3 T	1.5 T	3 T
Muscle	1075	898	33	29
Fat	200	382	-	68

Table 4.1: T_1 and T_2 relaxation times of skeletal muscle tissue and fat at 1.5 T and 3 T [7].

As skeletal muscle tissue has a high water content and water and fat have very different T_1 relaxation times, T_1 -weighted contrast sequences can be used to distinguish between healthy muscle tissue and fatty infiltration. The parameter T_2 is sensitive to the amount of water in skeletal muscle and is therefore a desirable parameter to investigate oedema indicating an increased water content. However, for an accurate assessment of T_2 the specially designed sequence has to be insensitive to the relaxation parameter T_1 and to fatty infiltration to obtain an unaffected measure of the hydration state of the tissue. For example, this can be realized by long repetition times in a spin echo acquisition and fat suppression techniques.

4.2 Excursus: Chemical Shift

Crucial for understanding in particular the sections 4.4.1, 4.4.3 and 4.4.4 is the term chemical shift.

Protons in the water molecule and protons with different chemical microenvironments in triglyceride molecules experience slightly different magnetic field strengths due to differing electron clouds and therefore different chemical shielding. This leads to differing resonance frequencies of the protons in different molecules such as water or triglycerides, referred to as chemical shift. In large molecules as triglycerides, the chemical shift can lead to a complex MR frequency spectrum with different peaks corresponding to different locations of the protons. In less complex molecules as water only one frequency peak is present. Based on the frequency spectrum consequently different molecules can be distinguished in a MR experiment, hence a decomposition of different protons based on the chemical shift is possible. The chemical shift in the resonance frequency is mostly expressed as a fraction of the main resonance frequency in parts per million (ppm).

4.3 Qualitative MR Measurements

The routinely in clinics performed MR imaging techniques in the diagnostic workup of patients with NMD enable a qualitative assessment of the patients' muscle pathologies fatty infiltration and oedematous alterations [4, 12, 13, 5, 14, 6].

4.3.1 T_1 -Weighted and T_2 -Weighted Imaging

Fatty infiltration is evaluated based on T_1 -weighted imaging [4, 5, 6]. In this case, the contrast is obtained by the difference in T_1 relaxation time between muscle tissue and fat [7]. Oedematous alterations are assessed with T_2 -weighted imaging with fat suppression techniques such as short tau inversion recovery (STIR) [12, 13, 5, 14, 6]. In this case the contrast is obtained by the difference in T_2 relaxation time between healthy and oedematous skeletal muscle tissue without the confounding factor of fatty infiltration [7].

In order to generate images with bright fat signal T_1 -weighted sequences are used (Fig. 4.1). In the applied sequences the inherent T_1 relaxation time is inversely related to the brightness of the tissue on the image. Fat having a short T_1 relaxation time appears brighter on T_1 -weighted images than water with a longer T_1 relaxation time. Due to short repetition times (TR), the T_1 -weighted images can be rapidly acquired. [4, 5, 6, 7]

In order to depict oedematous alterations of the muscle tissue, representing increased fluid content of intracellular or extracellular water, T_2 -weighted TSE sequences with STIR can be used (Fig. 4.1). The T_2 -weighting leads to a qualitatively brighter appearance of tissue with inherently longer T_2 relaxation time than of tissue with short T_2 . As oedematous muscle tissue has a higher water content than healthy muscle tissue, the increasing water content leads to a longer T_2 relaxation time. Because fat also has a long T_2 relaxation time and is most of the time simultaneously present in patients with NMD, a robust suppression of fat is additionally needed for correct assessment of oedematous changes. In qualitative skeletal muscle imaging STIR is a widespread technique for fat suppression due to its insensitivity to field inhomogeneities leading to a homogenous suppression of the fat signal. STIR uses an inversion recovery pulse to invert water and fat. Due to the inherently shorter T_1 relaxation, the fat signal recovers fast after the inversion pulse. The acquisition of the T_2 -weighted imaging starts exactly when the fat signal is nulled and is therefore acquired without influence of the fat signal. However, it has to be paid attention to the fact, that every tissue within the range of the same T_1 relaxation time as fat will be attenuated during signal acquisition. Furthermore, different fat peaks have differing T_1 relaxation times, hence a complete suppression of the whole fat spectrum is challenging. The appropriate inversion recovery time (TI) depends on the T_1 relaxation time of the tissue to be suppressed. Other fat suppression techniques use spectral information for suppression of the fat signal for example spectral adiabatic inversion recovery (SPAIR). However, the spectrally resolved suppression of different fat peaks is sensitive to B_0 errors and not suppressing the olefinic fat peak which is in proximity to the water peak. Hyperintensities on T_2 -weighted STIR images

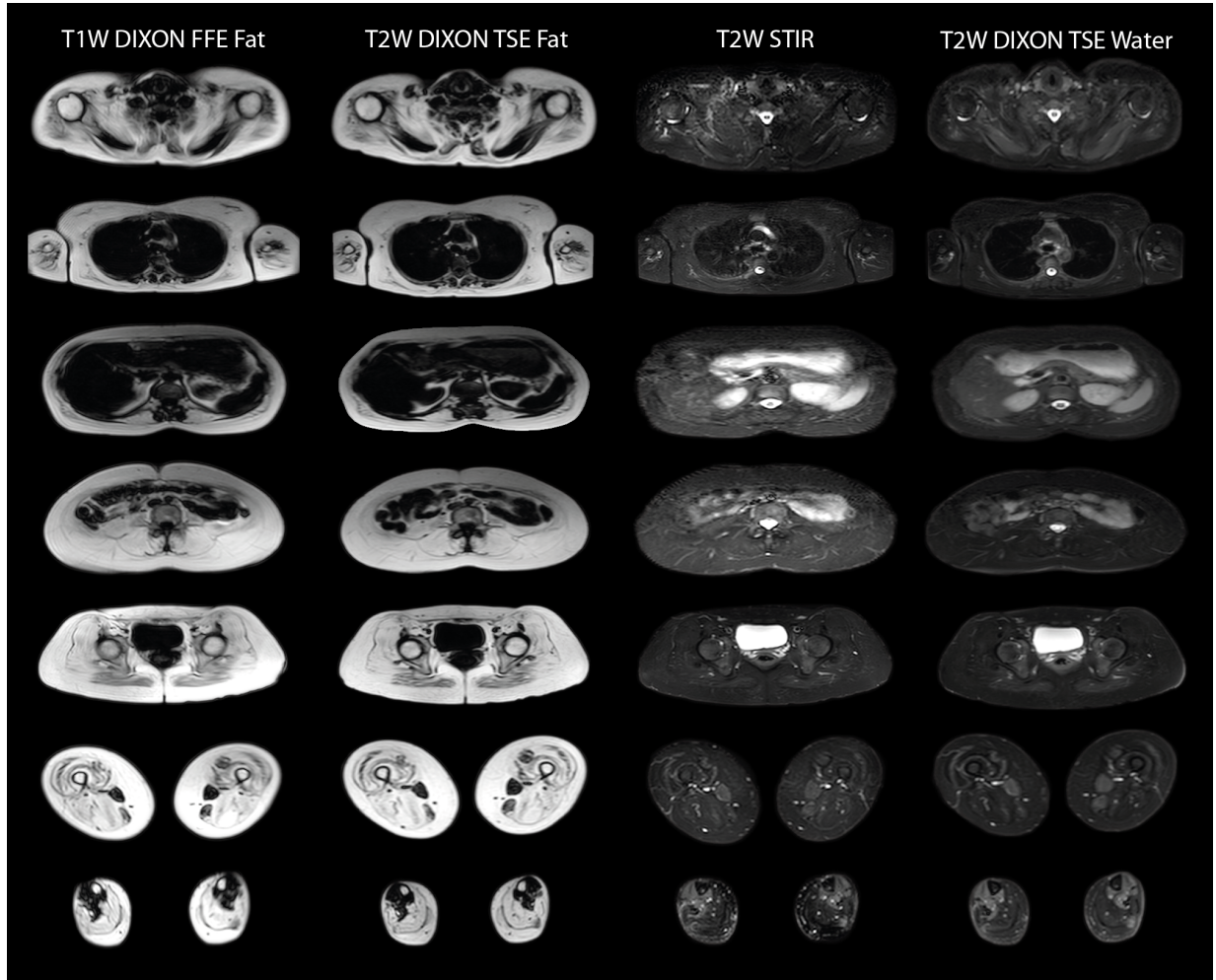


Figure 4.1: Representative whole-body T_1 -weighted and T_2 -weighted sequences with fat suppression in a severely affected patient with limb girdle muscular dystrophy type 2A (LGMD2A). Figure according to Schlaeger et al. [15].

are seen as an indicator for higher water content of the tissue and therefore for oedema in the muscle tissue. The T_2 -weighting of TSE sequences requires long scan time as the T_2 -weighting requires long echo times (TE) and a low influence of T_1 requires long TR. [72, 12, 13, 5, 14, 6, 41, 7]

Combing the assessment of fatty infiltration and oedematous alterations in one single imaging sequence can be achieved by a T_2 -weighted Dixon TSE sequence (Fig. 4.1) [15]. As basis for the fat and water contrast this sequence utilizes the Dixon technique, a chemical-shift imaging method proposed by Dixon which enables the calculation of separated fat and water images [73]. In this specific sequence, which is combining T_2 -weighting and Dixon, T_2 -weighted fat images (to assess fatty infiltration) and T_2 -

weighted water images (to assess oedematous changes) are obtained. The underlying mechanism of chemical shift imaging is explained in more detail in section 4.2. The simultaneous assessment of the two pathological changes yields several advantages such as a more time efficient scanning procedure which is particularly of interest in a whole-body assessment, the especially to motion more robust fat separation based on the Dixon technique compared to fat suppression using STIR and the simultaneous acquisition of water and fat images which facilitates the implementation of automatic ways of muscle segmentation due to the co-registered water and fat images [15].

4.3.2 Semi-quantitative Rating

In order to enable a more comparable assessment of pathological changes based on qualitative imaging several semi-quantitative visual rating scales for fatty infiltration and oedematous changes have been established.

Mercuri et al. [4], Kornblum et al. [16], and Fischer et al. [17] developed slightly different rating scales which can be used in order to visually rate the degree of fatty infiltration in a single muscle. Table 4.2 gives an overview of the respective rating scales.

Also for assessment of muscle oedema several rating scales have been introduced and are used in clinical and research set ups. Table 4.3 presents exemplary rating scales for oedematous alterations by Morrow et al. [18] and Poliachik et al. [14].

Grade	Mercuri et al.	Kornblum et al.	Fischer et al.
0		Normal appearance	Normal appearance
1	Normal appearance	Discrete moth-eaten appearance with sporadic T ₁ hyperintense areas	Mild: traces of increased signal intensity on the T ₁ -weighted MRI sequences
2	Mild involvement: Early moth-eaten appearance with scattered small areas of increased signal or with numerous discrete areas of increased signal with beginning confluence, comprising < 30 % of the volumen of the individual muscle	(a) Moderate moth-eaten appearance with numerous scattered T ₁ hyperintense areas (b) Late moth-eaten appearance with numerous confluent T ₁ hyperintense areas	Moderate: increased T ₁ -weighted signal intensity with beginning confluence in < 50 % of the muscle
3	Moderate involvement: Late moth-eaten appearance with numerous discrete areas of increased signal with beginning confluence, comprising 30 - 60 % of the volume of the individual muscle	Complete fatty degeneration, replacement of muscle by connective tissue and fat	Severe: increased T ₁ -weighted signal intensity with beginning confluence in > 50 % of the muscle
4	Severe involvement: Washed-out appearance, fuzzy appearance due to confluent areas of increased signal, or an end-stage appearance, with muscle replaced by increased-density connective tissue and fat, and only a rim of fascia and neurovascular structures		End-stage appearance, entire muscle replaced by increased-density connective tissue and fat

Table 4.2: Semi-quantitative scales for a visual rating of fatty infiltration in affected muscles published by Mercuri et al. [4], Kronblum et al. [16], and Fischer et al. [17].

Grade	Morrow et al.	Poliachik et al.
0	Absence of intramuscular hyperintensity on STIR images	
1	Mild intramuscular hyperintensity on STIR images	Myoedema absent
2	Definite intramuscular hyperintensity on STIR images	Slight, interfascicular myoedema
3		Slight, interfascicular, segmental myoedema of individual muscle
4		Slight, interfascicular, global myoedema of individual muscle
5		Moderate, interfascicular, segmental myoedema of individual muscle
6		Moderate, interfascicular, global myoedema of individual muscle

Table 4.3: Semi-quantitative scales for a visual rating of oedematous alterations in affected muscles published by Morrow et al. [18] and Poliachik et al. [14].

Rating scales enable a more objective and inter-/intra-rater comparable assessment of the pathological changes compared to mere subjective description of the muscle tissue architecture and can for example be used in order to create heatmaps in which each rating score is depicted with an appropriate colour intensity, respectively [74]. Such heatmaps enable a fast overview of the patients' muscle involvement pattern (Figure 4.2).

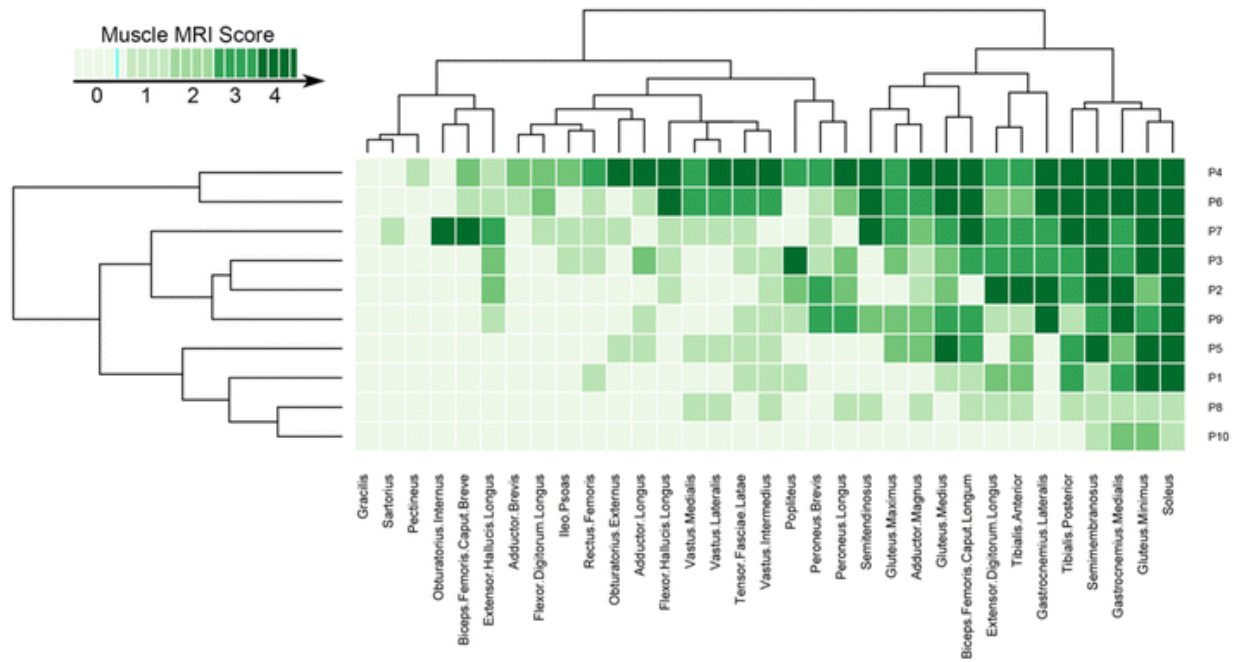


Figure 4.2: Representative heatmap visualizing the lower limb muscle involvement in patients with neutral lipid storage disease (NLSD). For the scheme the five-point Fischer et al. scale for fatty infiltration was used [17]. Figure according to Garibaldi et al. [74].

Still, assessment of muscle pathology using semi-quantitative rating scales remains dependent on the reader’s judgement. Therefore, it remains challenging to compare among different acquisition times, centres, scanners and readers. The ratings can be prone to artefacts in the acquisition and only represent a rough classification of the pathologies. Additionally, an automated assessment based on semi-quantitative rating is challenging as it requires quite some manual input. Quantitative imaging techniques promise to overcome these disadvantages.

4.4 Quantitative MR Measurements

In addition to qualitative imaging sequences, recently a lot of effort is being invested in the development of quantitative MR techniques in the field of NMD [75, 76, 77, 78, 5, 6, 8]. Particularly in the age of evidence based medicine, robust, objective biomarkers, independently assessable from the patient’s collaboration are essential [49].

Hence the move towards quantitative methods leads to more profound diagnosis and treatment decisions. Biomarkers based on quantitative MR techniques allow detection of subtle changes which is crucial for an early diagnosis and start of therapy intervention as well as the basis for longitudinal research studies. [79, 80, 81, 82, 83, 84, 85, 8]

In contrast to qualitative MR techniques where the signal intensity is a relative parameter and prone to confounding effects, quantitative MR measurements generate absolute values representing a tissue property.

Quantitative MR techniques allow the definition of MR biomarkers. In order to render a biomarker useful for the application in clinics it has to measure a clinically relevant quantity. A biomarker has to be accurate, precise, robust, and reproducible. Sufficient accuracy ensures, that the biomarker predicts the quantity it is supposed to measure, thus the results match with the reference standard. Precision describes the inter- and intra-patient repeatability of the biomarker. A robust biomarker is insensitive to changes in the acquisition setup. Last but not least biomarker measurements should be reproducible, hence independent from different scanner platforms, acquisition days, field strengths, operators and readers. A biomarker fulfilling all these requirements enables assessment of pathological changes for therapy monitoring, longitudinal studies and allows patients to bring results from earlier examinations with a different setup or even from another hospital. Thus the definition of standardized biomarkers and the development of quantitative techniques to determine these biomarkers are critical for research and clinical use. Biomarkers allow a precise comparison to other quantitative clinical measurements such as muscle strength, laboratory results or functional scores. [20]

In the following the quantitative MR biomarkers PDFF representing fatty infiltration (section 4.4.1) and T_{2w} representing oedematous alterations (section 4.4.2) are being described. Additionally, the MR acquisition technique single-voxel ^1H MRS (section 4.4.3) as well as the imaging techniques chemical shift encoding-based water-fat MRI (section 4.4.4) and T_{2w} mapping (section 4.4.5) are being explained in more detail. Figure 4.3 shows representative PDFF and T_{2w} maps.

4.4.1 The Quantitative Biomarker Proton Density Fat Fraction

PDFF is the MR biomarker for tissue fat concentration which is broadly accepted and recommended in the MR community. It is defined as the ratio of density of mobile protons from triglycerides and the total density of protons from mobile triglycerides and mobile water. Triglycerides, that are composed of three fatty acids esterified with glycerol, constitute the major building block of human fat tissue. The underlying principle for quantifying PDFF with MRI and MRS is the chemical shift between the resonance frequencies of water protons and protons in the triglyceride molecule with different

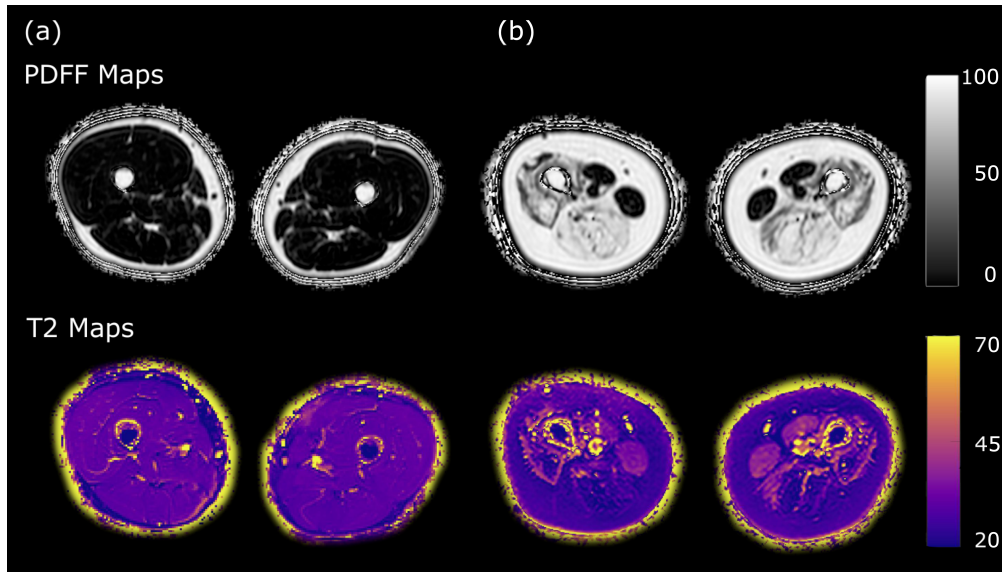


Figure 4.3: Representative MR images showing PDFF and T_{2w} values based on maps in a healthy volunteer (a) and a patient with Becker muscular dystrophy (b).

chemical environments (section 4.2). The measurement of PDFF is rather insensitive to changes in acquisition parameters, different scanner platforms or manufacturers and field strength inhomogeneities due to its unconfounded and fundamental tissue property character. This means a significant advantage over measurements of signal intensity ratios of fat and water based on conventional in/out of phase imaging with lacking correction for confounding factors. PDFF accurately and precisely reflects the fat ratio in various tissue types and therefore is a robust and reliable biomarker. In the muscle tissue of NMD patients, PDFF is a measure for the amount of fatty infiltration. Apparent PDFF is a marker for the physiological functionality of the muscle tissue as PDFF is inversely correlating with muscle strength. However, it is important to state, that due to MR invisible molecules with short T_2 relaxation times PDFF is not a measure for the mass fat fraction determined in standard biochemical assays. The fully automated calculation pipeline of PDFF maps based on MR methods from which the PDFF value of a voxel can directly be extracted render PDFF an easy applicable and convenient biomarker in the clinical setting. In JP-I and JP-II PDFF is calculated using single-voxel ^1H MRS in various patients with NMD. [86, 87, 25, 88, 89, 20, 49, 67, 15, 68]

4.4.2 The Quantitative Biomarker T_2 Water

In contrast, T_{2w} , representing the water mobility in the muscle tissue, is a rather un-specific biomarker being affected by a variety of circumstances such as: inflammation, necrosis, dystrophic cell lesions, denervation, and tumour, as well as exercise of moderate to high intensity.

A way to determine T_2 is by using a spin echo sequence with a 90° RF pulse followed by a train of 180° refocusing pulses. The mono-exponential signal decay allows the calculation of T_2 by using the following equation:

$$S(t) = M_0 \exp\left(\frac{-t}{T_2}\right) \quad (4.4.1)$$

where S is the signal amplitude, M_0 is the net magnetization and t is the overall time from the excitation to the measured echo.

In the context of skeletal muscle tissue, the thereby calculated T_2 is a non-chemically specific parameter, incorporating the mixed muscle T_2 relaxation time without separating between water and fat tissue, therefore referred to as global T_2 . As T_2 of fat is usually longer than T_2 of water and especially in patients with NMD healthy muscle, oedema and fat are often simultaneously present, the amount of fatty infiltration has a crucial influence on the global T_2 calculation resulting in a longer global T_2 with increasing fat content. Hence, it is crucial to measure T_2 without the influencing factor of fat, referred to as T_{2w} , in order to determine a clinically important MR biomarker. The chemically specific biomarker T_{2w} is currently seen as a marker for "disease activity" in patients with NMD as it is not only reflecting the intensity of the underlying pathology but also responding rapidly to acute and already subtle changes of the muscle microenvironment. T_{2w} , sensitive to the proportion of free fluid present, is affected by early changes in the muscle integrity potentially preceding later fatty infiltration and is therefore of immense value to longitudinal research on determination of the interplay between change in T_{2w} and change in fatty infiltration in NMD. When using MRS, the confounding influence of fatty infiltration is eliminated because of the possibility for a chemically specific determination of the water signal. That is why MRS can be seen as a reference standard for T_{2w} determination. [70, 37, 38, 90, 26, 27, 28, 21, 10, 29, 6, 91, 22, 92, 93, 24, 94, 30, 8, 31, 7]

JP-I shows by using stimulated echo acquisition mode (STEAM) MRS that chemically specific T_{2w} is decreased with increasing fat fraction, an important aspect which has to be considered in future interpretations of T_{2w} measurements. In order to distinguish between global T_2 and T_{2w} also in imaging techniques an accurate and robust separation or suppression of the fat signal is essential. In recent years, a lot of effort has been invested in the development of novel T_{2w} mapping techniques for a fat insensitive T_{2w} determination. Section 4.4.5 gives deeper insights into current T_2 mapping techniques and their advantages and disadvantages. In JP-II a novel T_{2w} mapping technique, the T_2 -prepared 3D TSE with SPAIR fat suppression is investigated with regard to its T_{2w} quantification robustness in muscles with fatty infiltration.

4.4.3 Single-Voxel Proton Magnetic Resonance Spectroscopy

In vivo single-voxel ^1H MRS provides insights into the underlying chemical structure of tissue composition in a clearly defined volume of interest, referred to as a voxel. Therefore, this technique is seen as the reference standard for metabolite quantification in (musculoskeletal) MR [95, 96, 97, 98, 41, 99].

Based on the chemical shift and therefore different resonance frequencies (section 4.2) different metabolites can be independently quantified and their relative concentration based on the area of each peak in the spectrum can be calculated. Two different techniques are routinely used for single-voxel ^1H spectroscopy: STEAM and point-resolved spectroscopy (PRESS). STEAM uses three sequential 90° excitation pulses, each applied together with a slice-selective gradient in one of the three directions x, y, and z, respectively. Whereas PRESS requires one 90° excitation pulse followed by two 180° refocusing pulses also with appropriate slice-selective gradients. PRESS being based on a spin echo sequence delivers a better signal-to-noise ratio (SNR) than STEAM, whereas STEAM allows rather short echo times and is less prone to j-coupling effects. Therefore, which technique is used, depends on the specific tissue of interest and question. Applying the Fourier transformation on the acquired raw data and several additional processing steps such as zero filling, apodization and phase correction produces a high quality spectrum. [7]

Figure 4.4 shows a representative STEAM spectrum.

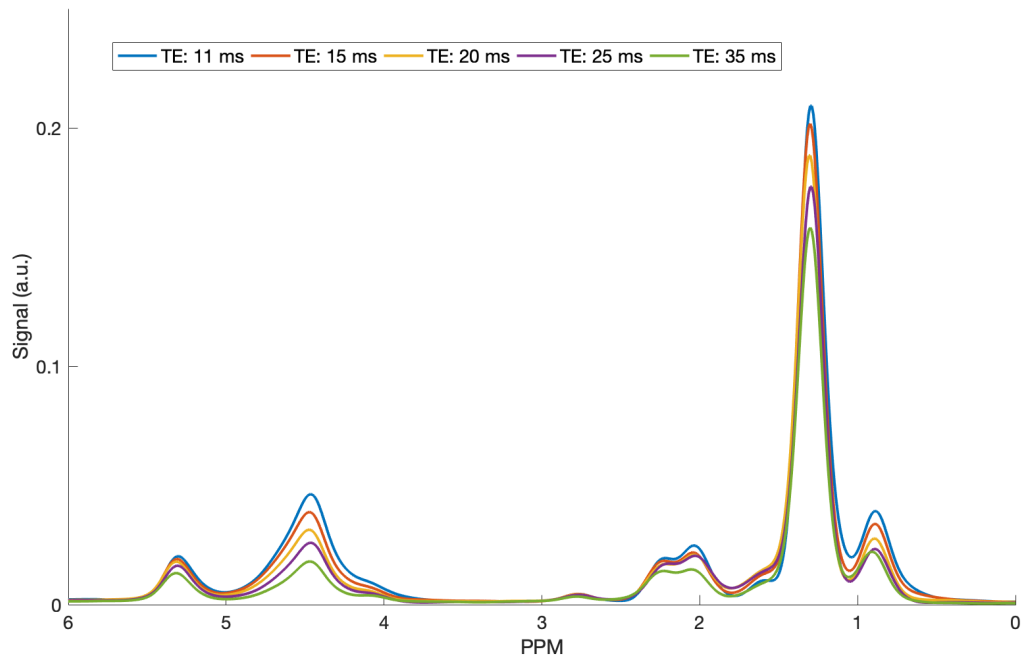


Figure 4.4: Representative multi-TE single-voxel ^1H STEAM spectrum in the highly fatty infiltrated muscle tissue of a patient with distal myopathy.

Critical for high-quality assessment of MRS are the correct determination of the voxel location, appropriate shimming and voxel dimensions. The voxel has to incorporate the tissue of interest which requires adequate imaging scans for planning before the MRS

acquisition. Good shimming produces readable spectra with narrow line widths. Smaller voxels are good for shimming, however, show the disadvantage of lower SNR. [7]

Representative voxel location planning on T₂-weighted Dixon TSE water and fat images with corresponding STEAM spectra is shown in Figure 4.5 from JP-I.

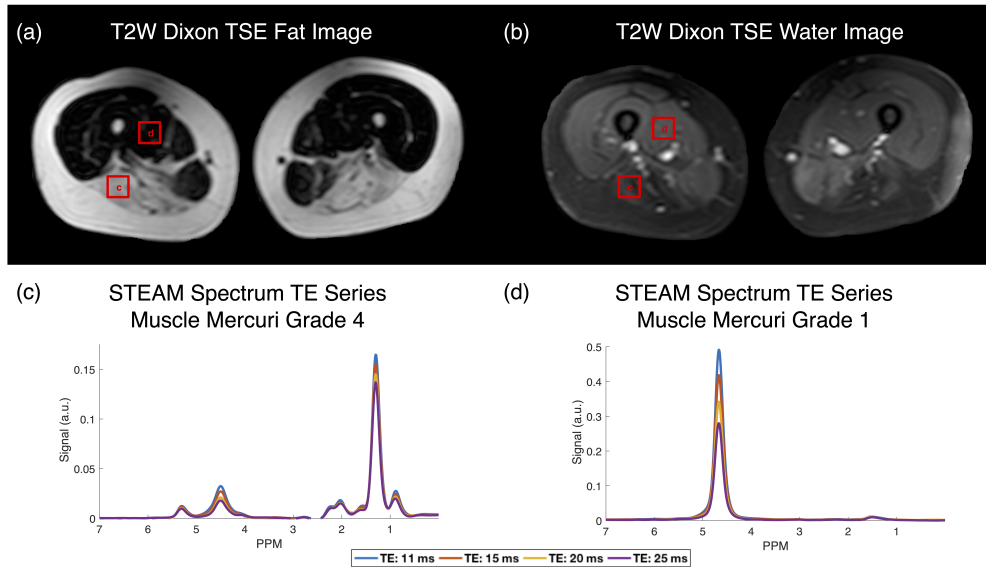


Figure 4.5: Voxel location planning based on a T₂-weighted Dixon TSE fat image (a) and on a T₂-weighted Dixon TSE water image (b). (c) represents a voxel location in a region with highly fatty infiltrated muscle tissue with the corresponding STEAM spectrum, (d) represents a voxel location in a region with healthy muscle tissue with the corresponding STEAM spectrum. Figure according to JP-I.

Although single-voxel ¹H MRS allows robust quantification of water and fat, without mutual confounding effects, this technique lacks spatial resolution. Especially for an accurate assessment of the patients' muscle tissue in the context of NMD knowledge about the spatial distribution of pathological changes is essential. Additionally, MRS requires complex post processing routines and therefore does not enable a straightforward interpretation of the results and in general, images are easier to interpret for the reader compared to a spectrum. Chemical shift encoding-based water-fat MRI and T_{2w} mapping are promising techniques for a spatially resolving quantification of fatty infiltration and oedematous alterations.

4.4.4 Chemical Shift Encoding-Based Water-Fat Imaging

Fat quantification based on routinely performed T₁-weighted sequences always requires reference measurements as the determined signal intensity is not an absolute quantity for the tissue fat content. An additional disadvantage for robust fat quantification using T₁-

weighted sequences is their sensitivity to B1 and B0 inhomogeneities. Furthermore, the absolute value for the obtained fat fraction can strongly depend on the chosen acquisition parameters. [40, 100]

Therefore, quantitative determination of fat content, referred to as PDFF measurements, are nowadays routinely based on an alternative technique called chemical shift encoding-based water-fat imaging [20]. The underlying principle are the different resonance frequencies, referred to as chemical shift (section 4.2) of the water peak and the fat peaks. Due to their different resonance frequencies, the metabolites accumulate different amount of phase after the excitation pulse and consequently the signal for different echo times of a mixture of metabolites is modulated. The modulation of the signal can be rather complex, when the underlying frequency spectrum is complex.

In a simplified scenario, originally investigated by Dixon [73], only the main fat peak (methylene, at 1.3 ppm) and the water peak is considered. The complex signal behaviour of water and fat thereby reduces to a mixture of these two metabolites with distinct resonance frequencies. Due to the different resonance frequencies of water and methylene, they process with slightly different speeds and accumulate different amount of phase. When the resonance frequencies are known, the angle between the two magnetization vectors is a function of the acquisition echo time.

When the two vectors point in the opposite direction, it is referred to as out of phase and the total signal is the difference between the two components. When the vectors form an angle of 0° , it is referred to as in phase, and their signals add up. Figure 4.6 shows representative out of phase and in phase images of the lower leg.

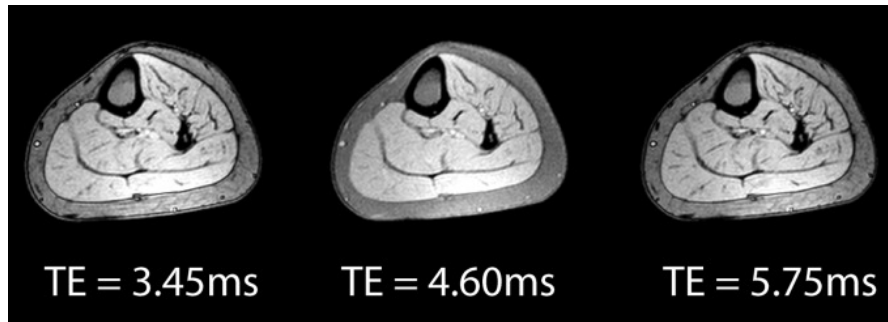


Figure 4.6: Magnitude signal of a healthy lower leg muscle with a gradient echo sequence with out of phase (TE = 3.45 ms and 5.75 ms) and in phase (TE = 4.60 ms) TEs. In the out of phase images, there is no signal at the water-fat boundaries. Figure according to Burakiewicz et al. [49].

In the very simple case only assuming two components, no field inhomogeneities, no additional phase errors and a perfectly defined angle between the two vectors, the total signals during out of phase (S_{OP}) and in phase (S_{IP}) can be used for quantification of

the fat signal with help of the following equations:

$$S_{IP} = (S_w + S_f) \quad (4.4.2)$$

$$S_{OP} = (S_w - S_f) \quad (4.4.3)$$

where S_w is the water signal and S_f is the fat signal.

Hence the separated water and fat signal can be calculated using equation 4.4.4 and 4.4.5:

$$S_{IP} + S_{OP} = (S_w + S_f) + (S_w - S_f) = 2S_w \quad (4.4.4)$$

$$S_{IP} - S_{OP} = (S_w + S_f) - (S_w - S_f) = 2S_f \quad (4.4.5)$$

Subsequently the fat fraction (FF) in each voxel can be calculated by equation 4.4.6:

$$FF = \frac{S_f}{S_f + S_w} \quad (4.4.6)$$

Summarising, the presented technique requires two acquired echoes at distinct time points and is therefore called two point Dixon approach. With this technique the fat fraction can be determined, however potentially the water and fat signal can be interchanged. This circumstance is called water-fat swap or water-fat ambiguity. If the water-fat determination is performed on complex data, this water-fat ambiguity can be avoided. [6, 49, 7]

B0 inhomogeneities, routinely present in MR scanning, lead to an additional angle of the signal and consequently to quantification errors. An additional echo can be acquired (leading now to a three point Dixon sequence) and enables B0 inhomogeneity corrections, hence renders the sequences rather insensitive to field inhomogeneities [101].

In order to turn PDFF into an accurate, precise, robust and reproducible biomarker as described in section 4.4.1, Dixon sequences with three or more echoes as well as long TR and low flip angle for minimizing the T_1 -weighting are used. Additionally, multi-spectral modelling of fat and T_2^* correction are implemented in the PDFF calculation pipeline. After all, for example in liver tissue chemical shift encoding-based water-fat imaging enables a reproducibility co-efficient of less than 0.5 % for PDFF determination. [49, 6]

The acquisition of echoes not only when water and fat are in or out of phase but form different angles to one another, combined with an iterative algorithm for water and fat separation known as iterative decomposition of water and fat with echo asymmetry and least-squares estimation (IDEAL), improves SNR and robustness of PDFF even further [102, 103].

4.4.5 T_2 Water Mapping

Traditionally performed T_2 -weighted sequences are designed in order to indicate T_2 -weighted contrast showing muscle tissue mid-intense and water and fat with a brighter appearance. The voxel signal intensity based on T_2 -weighted sequences can be compared to the surrounding tissue offering a relative signal estimation rather than an absolute T_2 quantification. Especially, when all the investigated skeletal muscles of a patient show oedematous alterations it is challenging to assess the level of muscle affection using weighted images [104].

Quantitative T_2 water mapping techniques try to provide robust, absolute T_{2w} values of the tissue of interest. Thereby, the main challenges especially in the imaging of NMD are quantification errors due to transmit B1 or B0 field inhomogeneities and the presence of fat. [70, 34, 37, 38, 39, 90, 35, 40, 21, 36, 10, 14, 29, 6, 22, 23, 41, 24, 8, 31]

In principle, images with different amount of T_2 -weighting need to be acquired and quantitative T_2 maps can be obtained in a subsequent step assuming an exponential signal decay in each voxel. The T_2 -weighted raw images can be achieved by measuring spin echoes with increasing echo times, by measuring the echoes after multiple refocusing pulses or by applying a T_2 -preparation module [105] before the excitation pulse followed by a spin echo or gradient echo readout.

The simplest way for T_2 determination is by acquiring the T_2 -weighted raw data based on a single spin echo sequence containing one 90° and one 180° refocusing pulse with increasing echo times [106]. As only one k-space line is acquired per repetition time this technique is very slow with the additional risk of quantification errors due to diffusion and involuntary subject motion during the long acquisition time. The application of several 180° refocusing pulses after the excitation as in MESE sequences gives the advantage of acquiring all the T_2 -weighted data for one k-space line after only one excitation [34, 33]. The MESE approach is consequently faster, but can suffer from unwanted magnetization pathways that do not follow a pure T_2 relaxation [34, 36, 10]. These so-called stimulated echoes lead to T_2 quantification errors due to additional influence of T_1 relaxation on the magnetization decay. In order to minimize the formation of stimulated echoes an exact application of the excitation and refocusing pulses is crucial what renders the MESE technique particularly sensitive to B1 and B0 inhomogeneities. Several approaches have been published to overcome sensitivity of MESE to field inhomogeneities such as acquiring an additional B1 map and subsequently excluding voxels from the T2 map with high B1 errors [107, 41]. Other approaches model the signal decay using Bloch [108] or extended phase graph (EPG) formulations [109, 36, 31]. In these approaches the magnetization evolution is simulated including simulated echoes. Consequently, by comparing the simulated signal to the measured signal the influence of stimulated echoes can be deducted. Another approach, the so called double-echo-steady-state (DESS) sequence uses the free induction decay (FID) signal and the echo signal for T_2 quantification [110].

In contrast, a T_2 -preparation module used for T_2 quantification can be applied before the data readout module which can either be a spin echo [42] or a gradient echo sequence [111, 112, 113]. In principle, a T_2 -preparation module consist of a 90° pulse, one or multiple refocusing elements and a -90° pulse. Different T_2 -weightings can be achieved

by varying the spacing between the RF pulses (varying the gaps) or by introducing more RF pulses. Both designs alter the time of the magnetization in the transverse plane and therefore lead to different T_2 -weightings. If such a T_2 -preparation is used for T_2 mapping, only the T_2 -preparation and not the readout needs to be insensitive to inhomogeneities. That can be achieved because the T_2 -weighting is decoupled from the data acquisition in such a case. To reach a high insensitivity towards B1 inhomogeneities, adiabatic pulses can be utilized for the T_2 -preparation. Klupp et al. [42] proposed to use an adiabatic B1 insensitive rotation-4 (BIR-4) pulse with gaps combined with a 3D TSE readout, referred to as T_2 -prepared 3D TSE. Figure 4.7 shows the pulse sequence diagram of the T_2 -prepared 3D TSE with SPAIR sequence.

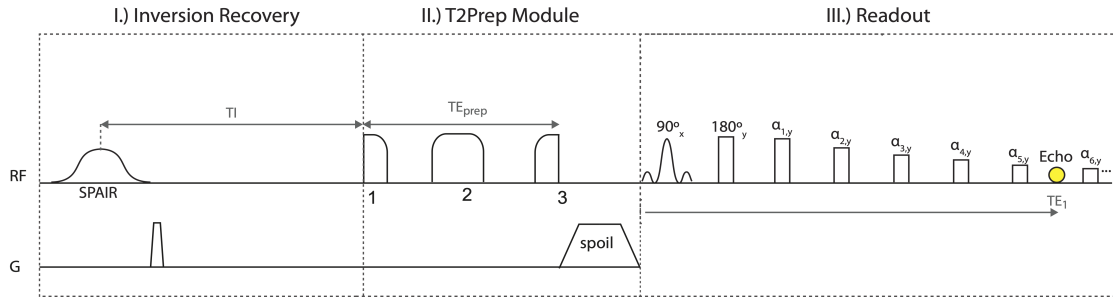


Figure 4.7: Pulse sequence diagram of the T_2 -prepared 3D TSE with SPAIR sequence. The RF pulses of the T_2 -preparation module with spacing in between and the flip angle modulation of the 3D TSE readout are illustrated.

This pulse design offers a T_2 -weighting that is insensitive towards a wide range of B1 inhomogeneities [42] and mildly affected by B0 inhomogeneities [43]. Figure 4.8 shows that a stable T_2 quantification is possible for B1 varying between 60 % and 70 % and for B0 offsets between -60 Hz and 60 Hz, which is the typical range for thigh muscle imaging at 3 T.

Additional to that, the 3D TSE readout offers the possibility to acquire high resolution 3D datasets. The TSE readout utilizes a varying flip angle modulation train to increase the echo train length and therefore accelerate the acquisition. This enables a SNR efficient acquisition of a 3D dataset enabling the visualization of smaller objects and multiplanar reconstruction. A simple mono-exponential fitting of the signal decay in each voxel subsequently allows T_2 quantification. Figure 4.9 shows the signal decay in a region of interest.

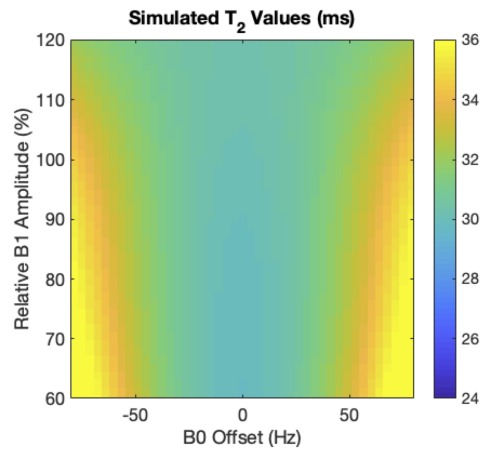


Figure 4.8: Simulation results of the sensitivity of T_2 quantification based on the T_2 -prepared 3D TSE to B1 and B0 errors. Figure according to Klupp et al. [42].

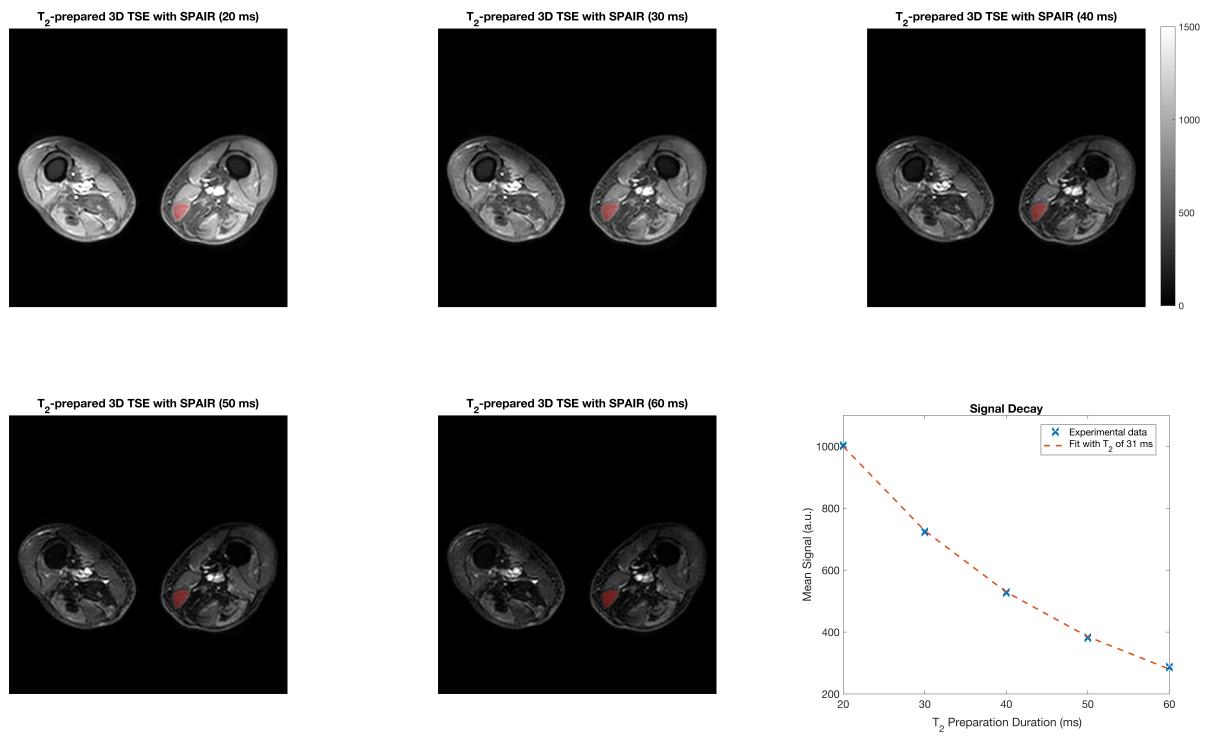


Figure 4.9: Raw T_2 -weighted images based on the T_2 -prepared 3D TSE sequence with SPAIR of the thigh region in a patient with Pompe disease. The bottom right corner shows the signal decay for the indicated region of interest in gracilis muscle for different T_2 -preparation durations of 20, 30, 40, 50 and 60 ms with corresponding mono-exponential fitting.

If the tissue only included water components, the measured T_2 and T_{2w} would be equivalent. However, in the context of NMD a non-negligible amount of fat might be present in the skeletal muscle tissue. As explained in section 4.4.2 it is absolutely crucial to correct for the influence of the fat signal on the T_{2w} determination particularly in the context of NMD.

During the last years various approaches have been published in order to suppress or separate the fat signal from the water signal for robust T_{2w} quantification. For example the application of the EPG formulation on MESE data does not only allow to overcome errors because of field inhomogeneities but also when incorporating additional information such as the appropriate fat spectrum and T_2 of the different fat peaks to get rid of the influence of the fat signal [31]. However, this approach does not suppress or separate the fat signal directly on the acquisition side, requires large computational power and is highly dependent on the appropriate parameter input. Another approach uses the chemical shift between water and fat for fat separation (please refer to section 4.2 for more details). For example, the Dixon approach can be combined with a MESE sequence [114]. However, this approach is prone to field inhomogeneities resulting in a less robust chemical shift separation and especially in regions with high fat content has its difficulties due to the relatively low water signal [41]. Also the approach of applying a multi exponential fitting model incorporating the signal decay of the water and the fat signal, respectively, leads to a separation of these components, however has its difficulties in regions with moderate to high fatty infiltration [41].

In JP-II the T_2 -prepared 3D TSE sequence combined with SPAIR [72] for fat suppression was investigated in its T_{2w} quantification performance in fatty infiltrated thigh muscles of patients with NMD. Thereby SPAIR reduces the total energy of the fat signal and with the appropriate timing between SPAIR and the T_2 -preparation module the influence of the fat signal on the readout can be largely reduced. However, the mechanism of the fat suppression as well as the performance of the fat suppression in highly fatty infiltrated muscles has so far been purely understood. Based on simulations and in vivo measurements the work in JP-II shows that the combination of SPAIR and the T_2 -preparation module leads to a partial signal cancellation of the fat signal. This allows an accurate T_{2w} determination correlating highly with T_{2w} measurements based on MRS even in the presence of higher fat content. In this approach, T_{2w} mapping with negligible influence of fatty infiltration is possible without additional modelling of fat signal behaviour.

5 Compliance with Ethical Standards

All investigations performed in the studies involving human participants were in accordance with the ethical standards of the institution and national research committee as well as the 1964 Helsinki declaration and its later amendments or comparable ethical standards. All participants included in the studies gave written informed consent.

6 Journal Publications

6.1 Journal Publication I: Decreased Water T_2 in Fatty Infiltrated Skeletal Muscles of Patients with Neuromuscular Diseases

The publication entitled *Decreased Water T_2 in Fatty Infiltrated Skeletal Muscles of Patients with Neuromuscular Diseases* was published in NMD in Biomedicine (ISSN: 0952-3480, DOI: 10.1002/nbm.4111). The manuscript was authored by Sarah Schlaeger, Dominik Weidlich, Elisabeth Klupp, Federica Montagnese, Marcus Deschauer, Benedikt Schoser, Sarah Bublitz, Stefan Ruschke, Claus Zimmer, Ernst J. Rummeny, Jan S. Kirschke, and Dimitrios C. Karampinos.

6.1.1 Abstract

Quantitative imaging techniques are emerging in the field of magnetic resonance imaging of neuromuscular diseases (NMD). T_2 of water (T_{2w}) is considered an important imaging marker to assess acute and chronic alterations of the muscle fibers, being generally interpreted as an indicator for “disease activity” in the muscle tissue. To validate the accuracy and robustness of quantitative imaging methods, ^1H magnetic resonance spectroscopy (MRS) can be used as a gold standard.

The purpose of the present work was to investigate T_{2w} of remaining muscle tissue in regions of higher proton density fat fraction (PDFF) in 40 patients with defined NMD using multi-TE single-voxel ^1H MRS. Patients underwent MR measurements on a 3 T system to perform a multi-TE single-voxel stimulated echo acquisition method (STEAM) MRS (TE = 11/15/20/25(/35) ms) in regions of healthy, edematous and fatty thigh muscle tissue. Muscle regions for MRS were selected based on T_2 -weighted water and fat images of a two-echo 2D Dixon TSE.

MRS results were confined to regions with qualitatively defined remaining muscle tissue without edema and high fat content, based on visual grading of the imaging data. The results showed decreased T_{2w} values with increasing PDFF with $R^2 = 0.45$ ($p < 10^{-3}$) (linear fit) and with $R^2 = 0.51$ (exponential fit).



The observed dependence of T_{2w} on PDFF should be considered when using T_{2w} as a marker in NMD imaging and when performing single-voxel MRS for T_{2w} in regions enclosing edematous, nonedematous and fatty infiltrated muscle tissue.

6.1.2 Authors Contribution

The author performed the MR measurements of the study patients with NMD on a 3 T Philips scanner as well as the post-processing, quantification and analysis of the MRS data using MATLAB. Additionally, the author reviewed the existing literature and kept up to date about novel scientific developments in the field through conferences and workshops. In collaboration with the co-authors, the author designed the MRI protocol and performed the recruitment of the patients, adapted the existing MRS post-processing frame-work using MATLAB, analysed and interpreted the data, and drafted the publication manuscript.

RESEARCH ARTICLE

Decreased water T_2 in fatty infiltrated skeletal muscles of patients with neuromuscular diseases

Sarah Schlaeger^{1,2}  | Dominik Weidlich¹  | Elisabeth Klupp² | Federica Montagnese³ | Marcus Deschauer⁴ | Benedikt Schoser³ | Sarah Bublitz⁴ | Stefan Ruschke¹ | Claus Zimmer² | Ernst J. Rummeny¹ | Jan S. Kirschke² | Dimitrios C. Karampinos¹

¹ Department of Diagnostic and Interventional Radiology, Technical University of Munich, Munich, Germany

² Department of Diagnostic and Interventional of Neuroradiology, Technical University of Munich, Munich, Germany

³ Friedrich-Baur-Institut, Department of Neurology, Ludwig-Maximilians-University, Munich, Germany

⁴ Department of Neurology, Technical University of Munich, Munich, Germany

Correspondence

Sarah Schlaeger, Department of Diagnostic and Interventional Radiology, Klinikum rechts der Isar, Ismaninger Str. 22, 81675 Munich, Germany.
Email: sarah.schlaeger@tum.de

Funding information

Philips Healthcare; German Society for Muscle Diseases

Quantitative imaging techniques are emerging in the field of magnetic resonance imaging of neuromuscular diseases (NMD). T_2 of water (T_{2w}) is considered an important imaging marker to assess acute and chronic alterations of the muscle fibers, being generally interpreted as an indicator for “disease activity” in the muscle tissue. To validate the accuracy and robustness of quantitative imaging methods, ^1H magnetic resonance spectroscopy (MRS) can be used as a gold standard.

The purpose of the present work was to investigate T_{2w} of remaining muscle tissue in regions of higher proton density fat fraction (PDFF) in 40 patients with defined NMD using multi-TE single-voxel ^1H MRS. Patients underwent MR measurements on a 3 T system to perform a multi-TE single-voxel stimulated echo acquisition method (STEAM) MRS (TE = 11/15/20/25(/35) ms) in regions of healthy, edematous and fatty thigh muscle tissue. Muscle regions for MRS were selected based on T_2 -weighted water and fat images of a two-echo 2D Dixon TSE.

MRS results were confined to regions with qualitatively defined remaining muscle tissue without edema and high fat content, based on visual grading of the imaging data. The results showed decreased T_{2w} values with increasing PDFF with $R^2 = 0.45$ ($p < 10^{-3}$) (linear fit) and with $R^2 = 0.51$ (exponential fit).

The observed dependence of T_{2w} on PDFF should be considered when using T_{2w} as a marker in NMD imaging and when performing single-voxel MRS for T_{2w} in regions enclosing edematous, nonedematous and fatty infiltrated muscle tissue.

KEYWORDS

fatty infiltration, imaging marker, MRS, NMD, PDFF, quantitative imaging techniques, skeletal muscle, T_2 of water

Abbreviations used: ALS, amyotrophic lateral sclerosis; CNM, centronuclear myopathy; DM2, myotonic dystrophy type 2; EPG, extended phase graph; FSHD, facioscapulohumeral muscular dystrophy; GRASE, gradient and spin echo; IBM, inclusion body myositis; LGMD2A, limb girdle muscular dystrophy type 2A; LGMD2I, limb girdle muscular dystrophy type 2I; LGMD2L, limb girdle muscular dystrophy type 2L; MESE, multi-echo spin-echo; MRI, magnetic resonance imaging; MRS, magnetic resonance spectroscopy; NMD, neuromuscular diseases; PDFF, proton density fat fraction; STEAM, stimulated echo acquisition method; T_{2f} , T_2 of fat; T_{2w} , T_2 of water; TSE, turbo spin-echo; VOI, volume of interest

1 | INTRODUCTION

Magnetic resonance imaging (MRI) is emerging as a diagnostic and monitoring tool for patients with neuromuscular diseases (NMD).¹ Qualitative imaging routinely based on T_1 -weighted sequences and T_2 -weighted short tau inversion recovery (STIR) sequences enables assessment of three main, often simultaneously present, tissue compartments: healthy, edematous and fatty muscle tissue.² In order to classify and assess the extent of edematous muscular alterations as well as fatty infiltration, semi-quantitative rating scales are commonly used.^{3,4} As semi-quantitative rating is highly reader-dependent and cannot easily track small changes, research efforts have expanded aiming to develop robust methods for quantitative imaging such as chemical shift encoding-based water-fat imaging⁵⁻⁷ or T_2 mapping.⁸

In order to quantify edematous muscle alterations, research efforts have concentrated on T_2 alterations of muscle tissue, since the spin-spin relaxation of muscle water is generally interpreted as an indicator for "disease activity" in muscle tissue.⁸ Thereby a precise differentiation between muscle global T_2 and muscle water T_2 (T_{2w}) is important to prevent misinterpretation.^{9,10} Muscle global T_2 refers to the mono-exponential, nonchemically selective T_2 decay in muscle tissue without fat suppression, spectrally selective excitation of water or modeling of the signal decay of a water-fat mixture.^{8,10} Therefore, muscle global T_2 measures relaxation properties of its two main components, water and fat, and depends on the muscle-fat composition as lipids have a longer T_2 than skeletal muscle fibers.^{9,10} On the contrary, T_{2w} being independent from the influence of fat tissue is a marker for water mobility in the muscle tissue and therefore reflects the T_2 relaxation of the tissue, including contributions from extracellular matrix, blood and muscle fibers.¹⁰ T_{2w} assesses the alteration of the muscle itself by the pathological process.⁹ The water mobility increases in a variety of circumstances such as inflammation, denervation or exercise. A pathological change in T_{2w} is commonly seen as a marker for "disease activity" in the muscle tissue.^{8,10-12}

Therefore, a lot of effort is being made to reliably determine muscle T_{2w} . Robust determination of muscle T_{2w} requires the complete suppression of the energy of all nonwater signal components. Several approaches have been proposed to suppress the fat signal or separate the water from the fat signal via the chemical shift difference between water and fat. Existing techniques include the acquisition of 2D multi-echo spin-echo (MESE) combined with Dixon water-fat separation¹³⁻¹⁵ and the processing of 2D-MESE data using a multi-exponential T_2 decay model without¹⁶⁻¹⁹ and with the extended phase graph (EPG) formalism^{8,20} to additionally remove the effects of B1-inhomogeneities. Water-fat separation has also been combined with a 2D radial gradient and spin echo (GRASE) sequence to acquire T_{2w} maps in regions affected by motion.²¹

¹H magnetic resonance spectroscopy (MRS) can be used as the gold standard for accurate quantification of T_{2w} as it permits resolution of the spectral complexity of fat in fatty infiltrated muscles.¹⁶ Single-voxel MRS lacks the spatial information of spatially resolved T_2 -mapping techniques, but, when performed at multiple echo times (TEs), it can also be used to reliably determine T_{2w} in regions of higher fat fraction. Previous work mainly based on imaging sequences has concentrated on T_{2w} elevation as a marker for "disease activity" in regions of low to moderate fatty infiltration.^{8,22} The work by Arrigoni et al. is one of the few studies reporting a decreased T_{2w} in areas of high PDFF in subjects with LGMD based on quantitative imaging sequences.²³ However, there still needs to be more investigation of how T_{2w} behaves at muscle regions with higher PDFF using the gold standard MRS in various NMD and in a larger number of patients.

Therefore, the purpose of this study was to investigate T_{2w} based on multi-TE single-voxel ¹H MRS in fatty infiltrated skeletal muscles of patients affected by different NMD.

2 | METHODS

2.1 | Subjects

40 patients (27 females and 13 males; age: 48 ± 16.5 years) with acquired and hereditary NMD were recruited (Table 1). These included: myotonic dystrophy type 2 (DM2) ($n = 6$), limb girdle muscular dystrophy type 2A (LGMD2A) ($n = 5$), centronuclear myopathy (CNM) ($n = 1$), inflammatory myopathy ($n = 1$), Lamin A/C myopathy ($n = 1$), inclusion body myositis (IBM) ($n = 2$), facioscapulohumeral muscular dystrophy (FSHD) ($n = 1$), limb girdle muscular dystrophy type 2I (LGMD2I) ($n = 2$), dermatomyositis ($n = 2$), Bethlem myopathy ($n = 1$), amyotrophic lateral sclerosis (ALS) ($n = 1$), polymyositis ($n = 2$), Pompe disease ($n = 3$), hypokalemic periodic paralysis ($n = 1$), distal myopathy ($n = 2$), myositis triggered by infection ($n = 1$), overlap myositis ($n = 1$), myofibrillar myopathy ($n = 1$), limb girdle muscular dystrophy type 2L (LGMD2L) ($n = 1$), rhabdomyolysis ($n = 1$), and unclassified myopathy ($n = 4$). Diagnosis was based on muscle biopsies and/or genetic testing. The study was approved by the local institutional Committee on Human Research. All patients gave written informed consent.

2.2 | MR measurements

Patients were scanned on a 3 T system (Ingenia, Philips Healthcare, Best, The Netherlands) using the whole-body coil, the built-in 12-channel posterior coil and a 16-channel anterior coil placed on top of the hip and thigh region. Subjects were positioned in a head-first supine position. A whole body two-echo T_2 -weighted 2D Dixon TSE sequence was performed in five stacks: TR/TE/ Δ TE = 3725/100/1.0 ms, FOV = 330 x 450 x 306 mm³, acquisition voxel size = 2.5 x 2.7 x 6.0 mm³, slices = 26, slice gap = 6 mm, TSE factor = 45, averages = 2. A multi-TE single voxel STEAM

TABLE 1 Patient ID, age, gender and disease

Patient ID	Age, years	Gender	Disease
P001	63	Female	Myotonic dystrophy type 2
P002	54	Female	Myotonic dystrophy type 2
P003	47	Female	Limb girdle muscular dystrophy type 2A
P004	34	Female	Myotonic dystrophy type 2
P005	49	Female	Limb girdle muscular dystrophy type 2A
P006	30	Female	Limb girdle muscular dystrophy type 2I
P007	26	Male	Limb girdle muscular dystrophy type 2A
P008	61	Female	Myotonic dystrophy type 2
P009	52	Male	Myotonic dystrophy type 2
P010	45	Male	Centronuclear myopathy
P011	52	Female	Limb girdle muscular dystrophy type 2A
P012	61	Male	Unclassified myopathy
P013	34	Female	Unclassified myopathy
P014	50	Female	Unclassified myopathy
P015	45	Female	Limb girdle muscular dystrophy type 2A
P016	19	Female	Inflammatory myopathy
P017	20	Female	Lamin A/C myopathy
P018	77	Male	Inclusion body myositis
P019	22	Female	Facioscapulohumeral muscular dystrophy
P020	66	Female	Myotonic dystrophy type 2
P021	25	Female	Limb girdle muscular dystrophy type 2I
P022	39	Male	Unclassified myopathy
P023	36	Female	Dermatomyositis
P024	26	Female	Rhabdomyolysis
P025	49	Female	Bethlem myopathy
P026	55	Male	Amyotrophic lateral sclerosis
P027	57	Male	Polymyositis
P028	76	Female	Pompe disease
P029	84	Male	Pompe disease
P030	70	Male	Hypokalemic periodic paralysis
P031	34	Female	Distal myopathy
P032	61	Female	Polymyositis
P033	48	Male	Pompe disease
P034	36	Female	Myositis triggered by infection
P035	44	Female	Overlap myositis
P036	73	Female	Myofibrillar myopathy
P037	69	Female	Inclusion body myositis
P038	41	Male	Dermatomyositis
P039	49	Female	Distal myopathy
P040	48	Male	Limb girdle muscular dystrophy type 2L

MRS (TR/TM = 6000/16 ms, VOI = 15 x 15 x 15 mm³, 8 averages per TE) was performed at four/five echo times (TE = 11/15/20/25/(35) ms) in the patient's healthy, edematous and fatty thigh muscles. The thigh muscles were selected based on the T₂-weighted water and fat images, respectively, and varied depending on the patient's disease and muscle affection. Therefore, in 12 patients, MRS voxels were placed in two different muscle regions with a fat fraction difference of greater than 30% to perform an intra-patient analysis.

2.3 | Postprocessing

Water-fat separation of the T_2 -weighted two-echo 2D Dixon TSE images was performed online using the vendor's mDixon algorithm.²⁴ The processing of the MRS data was performed with in-house software and included zero order phasing, Gaussian apodization and frequency alignment of single acquisitions. Peak area quantification was performed considering eight to ten fat peaks (depending on the fat fraction and therefore visibility of smaller fat peaks)²⁵ and jointly incorporating the measurement of all four/five TEs into a peak-specific T_2 decay signal model.²⁶ Fitting was constrained with a common fat T_2 (T_{2f}) for all fat peaks. Based on the fat and water T_2 as well as the fat peak amplitudes, the proton density fat fraction (PDFF) can be calculated. The MRS quantification was eventually utilized to extract both PDFF and T_{2w} .

2.4 | Grading

The muscle tissue in the volume of interest (VOI) was rated based on the 2D Dixon TSE T_2 -weighted fat- and water-separated images by one reader using the Mercuri and the Morrow grading scales.²⁷ Severity of fatty infiltration was assessed via the four-point Mercuri grading scale with score 1 for muscles with normal appearance, score 2 for muscles with mild fatty infiltration (less than 30% of the volume of the original muscle), score 3 for muscles with moderate fatty infiltration (30 to 60% of the volume of the original muscles), and score 4 for muscles with severe fatty infiltration (greater than 60% of the volume of the original muscle).³ To rate intramuscular hyperintensities indicating edema, a three-point scale by Morrow et al was used with score 0 for absence of intramuscular hyperintensity, score 1 for mild hyperintensity, and score 2 for definite intramuscular hyperintensity.⁴ MRS performed in regions with Morrow Grade 1 or 2 indicating edematous changes were excluded to concentrate on the effect of fatty infiltration on T_{2w} of remaining healthy muscle tissue.

2.5 | Statistical analysis

Statistical analysis was performed using Matlab (Mathworks, Natick, MA, USA). Correlation analysis was based on R^2 for a linear fit and for an exponential fit to test if there is an overall trend in the dataset. Additionally, a group analysis of two PDFF regimes was performed. MRS voxels were divided into a low PDFF regime (PDFF < 60%) and a high PDFF regime (PDFF > 60%). A cut-off level of 60% was selected based on visual inspection of the data distribution. The T_{2w} values in the two PDFF regimes were compared using a boxplot analysis and a student t-test.

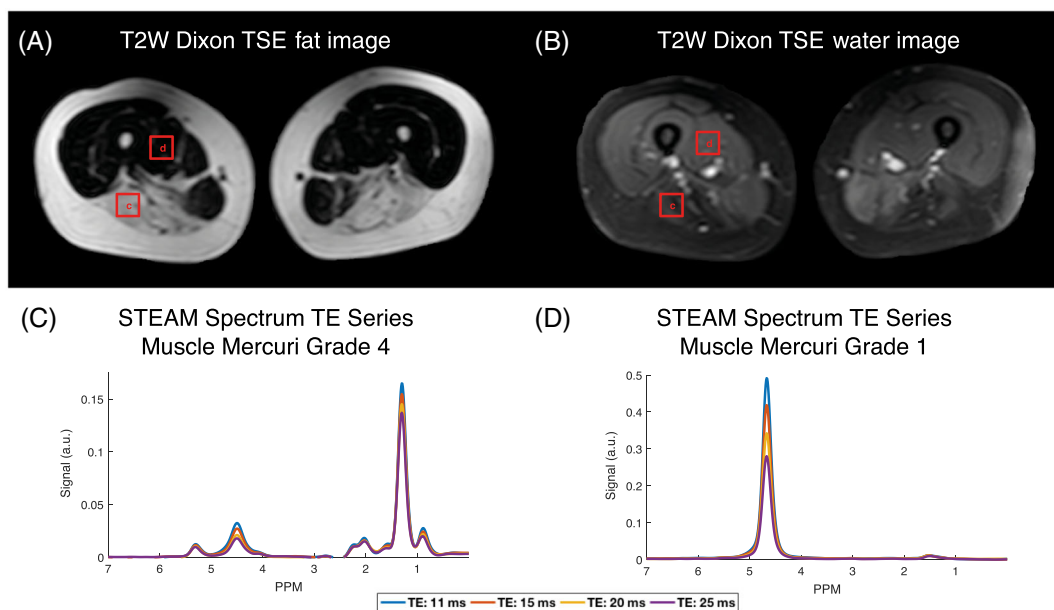


FIGURE 1 Representative spectroscopy voxel locations with corresponding spectra in a muscle with Mercuri Grade 4 (C) and a muscle with Mercuri Grade 1 (D) based on the T_2 -weighted Dixon TSE fat image (A) in a patient with limb girdle muscular dystrophy type 2A (LGMD2A). Both muscles with Morrow Grade 0 based on the T_2 -weighted Dixon TSE water image (B). (C) and (D) show the corresponding STEAM MRS TE-series

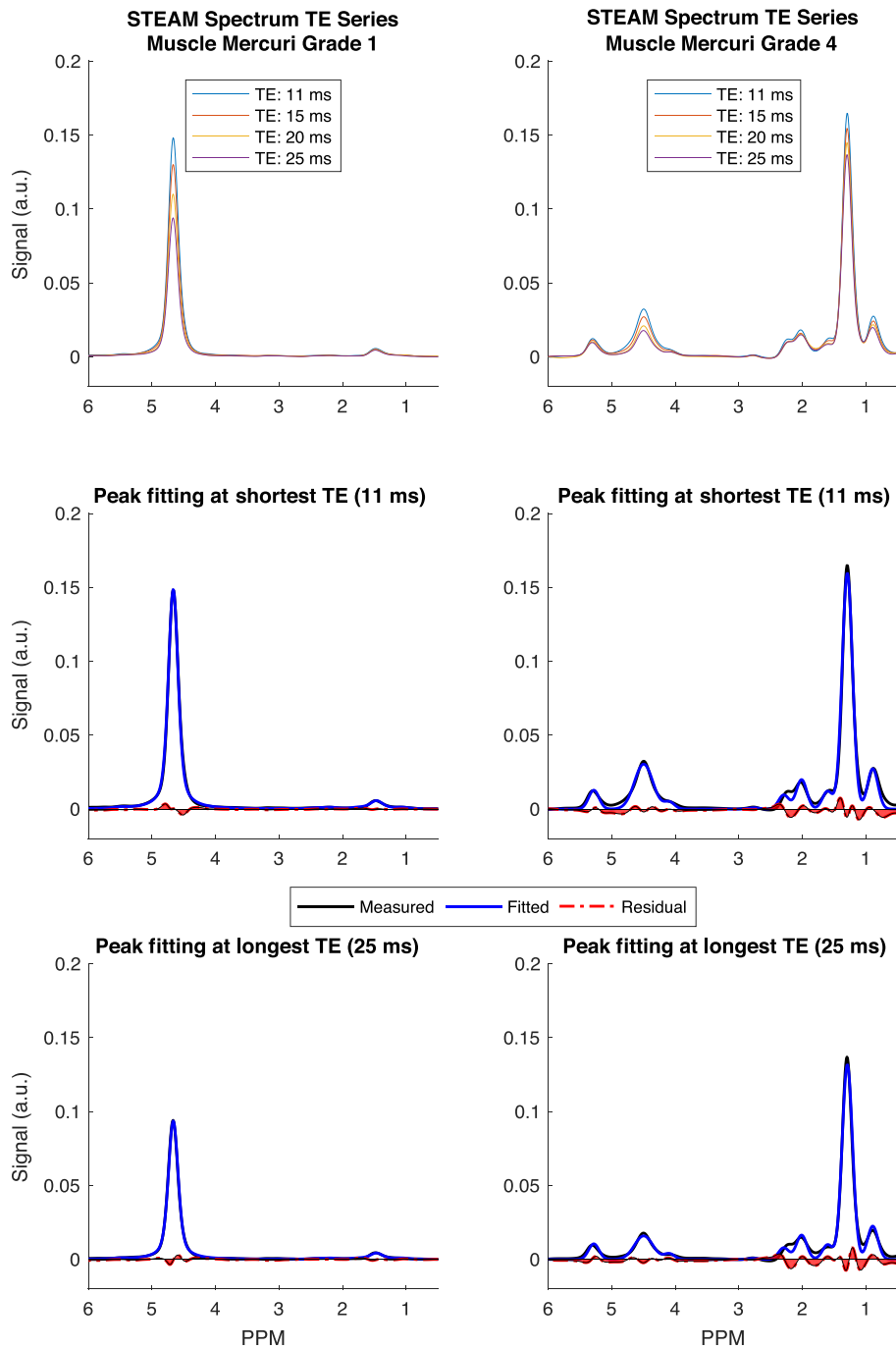


FIGURE 2 Peak fitting of multi-TE single-voxel STEAM spectra in Mercuri Grade 1 and Mercuri Grade 4 voxel locations. Negligible residuals detectable in both example spectra

3 | RESULTS

Figure 1 shows representative spectra and voxel locations in muscles graded with Mercuri Grade 1 and Mercuri Grade 4 based on T_2 -weighted Dixon TSE fat images in a patient with LGMD2A. Both regions were graded with Morrow Grade 0 on the T_2 -weighted Dixon water image. Figure 2 shows representative MRS peak fitting results for two regions with different Mercuri grading and thus different fat fraction. The applied fitting was reliable in regions with low fatty infiltration (Mercuri Grade 1) as well as in regions with high fatty infiltration (Mercuri Grade 4) having minimal residuals, especially in the spectral region around the water peak.

The correlation of T_{2w} and PDFF based on multi-TE single-voxel MRS performed in 40 patients with different NMD is shown in Figure 3A. Different NMD groups are shown with different symbols and colors. T_{2w} versus the PDFF showed a negative correlation between the two parameters with $R^2 = 0.45$ ($p < 10^{-3}$) (linear fit) and with $R^2 = 0.51$ (exponential fit). Figure 3B shows the correlation of T_{2w} and PDFF using a linear fit

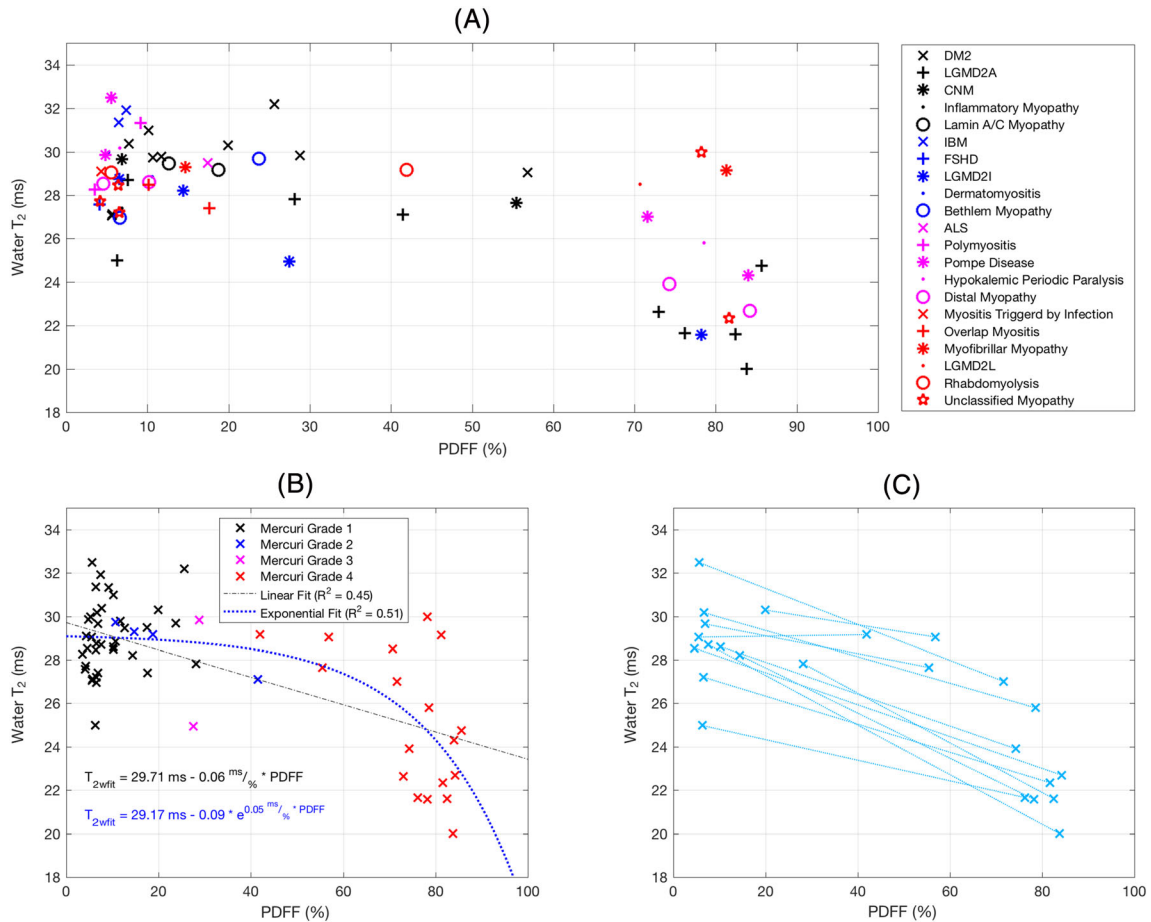


FIGURE 3 (A) Correlation of T_2 and PDFF based on multi-TE single-voxel MRS performed in 40 patients with different neuromuscular diseases. Different NMD groups are shown with different symbols and colors. (B) Correlation of T_2 and PDFF based on multi-TE single-voxel MRS performed in 40 patients with different neuromuscular diseases using a linear fit and an exponential fit. The different marker colors indicate the Mercuri grading of the investigated muscle region. T_2 decreased with increasing PDFF. (C) Correlation of T_2 and PDFF based on multi-TE single-voxel MRS in 12 patients. Spectra were measured in both a region with low and a region with high fat fraction. Measurements from the same patient are paired. T_2 also decreased with increasing PDFF when looking at an individual patient

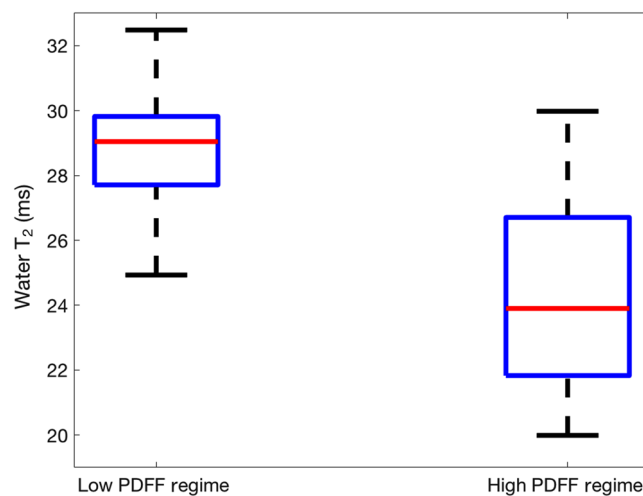


FIGURE 4 Boxplot analysis of T_2 values in a PDFF $<$ 60% regime (low PDFF regime) compared with a PDFF $>$ 60% regime (high PDFF regime). Difference between PDFF regimes is highly significant ($p < 10^{-5}$)

and an exponential fit, with different colors indicating Mercuri Grades 1 to 4. In Figure 3B, the qualitative Mercuri grading and the quantitative PDFF values do not fully agree but show a very similar trend for the acquired data. Figure 3C shows T_{2w} and PDFF, highlighting the decrease of T_{2w} with increasing PDFF, pairing the data from the muscles of the same patient in order to show the intra-patient behavior of T_{2w} . In 12 patients, spectra were measured in both a region with low and a region with high PDFF. For better clarity, only patients with an intra-patient PDFF difference of the two voxel locations of greater than 30% were included in the figure. When investigating the data from an individual patient, T_{2w} is decreased with increasing PDFF. Figure 4 shows the boxplot analysis of T_{2w} values in two PDFF regimes: PDFF < 60% and PDFF > 60%. The difference in T_{2w} values between the two groups is highly significant ($p < 10^{-5}$).

4 | DISCUSSION

The present study investigated T_{2w} based on multi-TE single-voxel ^1H MRS in fatty infiltrated skeletal muscles of patients affected by different NMD. It was shown that ^1H MRS-based T_{2w} is decreased with increasing ^1H MRS-based PDFF. The measurement of T_{2w} is currently considered as a marker of muscle "disease activity", as T_{2w} is a measurement of water mobility in the tissue. The water mobility increases in a variety of circumstances, being a nonspecific event, and is a parameter responding rapidly to changes in the microenvironment of the skeletal muscle fibers^{10,28}. Therefore, T_{2w} is seen as an important biomarker for acute or chronic changes in the muscle tissue.^{11,12} To the best of the authors' knowledge, ^1H MRS-based T_{2w} in muscle regions with PDFF greater than 60% has not been reported previously. The present results show that T_{2w} of remaining muscle tissue is decreased with increasing PDFF, especially in regions of fatty infiltration of greater than 60% PDFF.

The difference between T_{2w} values in a group with PDFF < 60% compared with a group with PDFF > 60% is highly significant. The cut-off value of 60% was selected based on the data reported in Figure 3. The observation based on the present work that T_{2w} is approximately stable up to a PDFF of 60%, and is abruptly decreased with a PDFF of greater than 60%, has important practical consequences, as it suggests that investigators do not have to consider any influence of fat content on the T_{2w} measurements up to PDFF values of 60%. Only if T_{2w} at regions with PDFF of greater than 60% is used then do correction or normalization factors have to be introduced.

Previous imaging studies have attempted to suppress or separate the effect of fat in order to measure T_{2w} instead of global T_2 in the context of NMD imaging.^{8,13-20} Many of these studies have investigated the relationship between T_{2w} and PDFF, aiming at a result where T_{2w} is not related to PDFF in order to validate the performance of the proposed methods in suppressing the effect of fat on the T_{2w} measurement. However, entirely suppressing the fat signal remains a challenging task, especially in regions with high PDFF. Single-voxel multi-TE MRS is instead the gold standard for measuring T_{2w} by directly quantifying the T_2 decay of the water peak, even in regions with high fat PDFF. Therefore, single-voxel multi-TE MRS would be the technique of choice for testing the quantitative fidelity of an imaging T_{2w} mapping method, especially in muscle regions with very high PDFF.

It was outside the scope of the present work to perform additional measurements beyond the employed single-voxel multi-TE MRS acquisition in order to provide a detailed explanation of the observed decrease of T_{2w} in muscle regions with high PDFF. However, some hypotheses are discussed below to explain the observed behavior of T_{2w} in muscle regions with high PDFF.

A first effect contributing to the observed dependence of T_{2w} on fat fraction might be related to exchange and the compartmentalization of the T_2 decay. The Zimmerman–Brittin model has been proposed to describe the relaxation processes in a spin system composed from a finite number of phases with each phase characterized by a single relaxation time.²⁹ Previous studies have shown that there is no exchange between lipids and water protons for either transverse or longitudinal relaxation, due to the hydrophobic character of large amounts of nonpolar lipids.³⁰ This means that if considerable amounts of fat are present in muscle, the observed dependence of T_{2w} on fat fraction cannot be explained by exchange effects between lipids and water. The observed dependence of T_{2w} on fat fraction could, however, be related to the multi-exponential nature of the water T_2 decay. Fat-infiltrated skeletal muscles might have a different multi-exponential water T_2 decay compared with healthy muscles, due to changes in the intracellular/extracellular space compartmentation and the tissue macromolecular content.³¹ It is also unclear how muscle disorganization affects the obtained T_2 water value because small but significant elevations of water T_2 were reported in animal studies. However, the reported changes in water T_2 were smaller than the changes described in the present work.⁹ In addition, fibrosis has to be specifically mentioned as a possible physiological explanation for decreased T_{2w} .^{23,32} Fibrosis means the replacement of skeletal muscle tissue by connective tissue, mainly collagen, which has a very short T_2 because of the tissue characterizing macromolecules.⁹ As the T_2 decay is a complex multi-exponential process, a sufficient amount of fibrosis might lead to a decreased measured T_{2w} . As fibrosis is a chronic change in muscle diseases and significant for the very last state of disease in muscle tissue, fibrosis will be more likely to be present in muscle with a higher fat content.

A second effect contributing to the observed dependence of T_{2w} on fat fraction might be the susceptibility differences between muscle water and fat. The expected signal loss in a spin-echo sequence due to the susceptibility difference between fatty deposits and the surrounding water in fatty infiltrated skeletal muscle depends on the microstructural properties of the fatty deposits. The effect of microscopic susceptibility deposits to the signal cannot be described by a general analytical solution. However, analytical solutions can be derived in the two limiting regimes of motional narrowing³³ and static dephasing.³⁴ The two regimes are determined based on the correlation time for diffusion with respect to the magnetic field inhomogeneities, $\tau = R^2/D$ (where R is the radius of the susceptibility perturbation and D is the diffusion coefficient of water) and the local Larmor

frequency shift δf produced by the susceptibility difference. The motional narrowing regime, holding when $\delta f \tau \ll 1$, is usually valid for small perturbations or rapid diffusion. In the motional narrowing regime, the protons sample the entire range of frequencies present in the VOI. The static dephasing regime, holding when $\delta f \tau \gg 1$, is usually valid for large perturbers or slow diffusion. In the static dephasing regime, the effects of diffusion are small and the signal is largely refocused in a spin-echo experiment. For spherical deposit of fat within skeletal muscle ($D = 1.7 \cdot 10^{-9} \text{ m}^2/\text{s}$) at $3 \text{ T } \delta f = 2/3 \gamma \delta \chi B_0 = 51 \text{ Hz}$ ³⁵, it can be shown that the static dephasing regime holds for $R > 20 \text{ } \mu\text{m}$ ($\delta f \tau > 10$) and the signal is refocused. However, for fat droplets with $R \approx 6 \text{ } \mu\text{m}$ ($\delta f \tau \approx 10$), the difference in magnetic susceptibility between the water and fat could induce a T_{2w} that reduces with fat fraction.³⁶ If fat accumulates as increasingly larger zones of lipid droplets (adipocytes), the hereby described effect on the water T_2 might be negligible. However, if the number and size of adipocytes randomly distributed in the muscle tissue is increasing, susceptibility effects could be a potential explanation of the decreasing water T_2 values.

Irrespective of the exact explanation for the observed dependence of T_{2w} on fat fraction, the present results have some important implications for the use of T_{2w} in NMD imaging. First, elevated T_{2w} is currently considered as a marker for a pathological process of muscle fibers themselves not being affected by surrounding fatty infiltration.⁹ However, the present results indicate that T_{2w} shows at least a mild dependence on the degree of the fatty infiltration, and this should be taken into consideration if studying T_{2w} in regions with high fat fractions. Second, due to the typical heterogeneity of fatty infiltrated muscles, the large MRS voxel could include edematous (with elevated T_{2w}) as well as remaining nonedematous (with reduced T_{2w}) muscle tissue. Thus, the two effects could compensate each other, and the overall T_{2w} of the remaining muscle might have a T_{2w} value similar to the T_{2w} in healthy muscle. The effect could be especially severe when the muscle tissue is highly infiltrated and heterogeneous. Therefore, there is a need for accurate and high resolution T_{2w} mapping using imaging in patients with NMD.

The present study has some limitations. First, subjects with different NMD at different disease stages were grouped and no disease-specific or stage-specific analysis of T_{2w} was performed. Additionally, when MRS at multiple voxel locations was acquired in the same patient, such measurements cannot be considered as independent in the subsequent statistical analysis. However, the observed dependence of T_{2w} on fat fraction was present in all disease types and disease stages. Due to the large heterogeneity of different diseases and expected physiological muscle T_{2w} differences between patients, we decided to use both a linear fit and an exponential fit to test for the overall trend in the heterogeneous dataset. Second, the employed single-voxel MRS sequence used only a few short TEs and could not therefore assess the presence of any multi-exponential decay for T_{2w} . Third, MRS peak area quantification was performed considering different numbers of fat peaks varying from eight to ten fat peaks depending on the fat fraction and therefore visibility of smaller fat peaks. However, the aim was to minimize the residual and therefore maximize the quality of the fitting. Furthermore, the limitation concerning the MRS peak area quantification only affects quantification of PDFF whereas T_{2w} quantification should not be affected. Fourth, a common T_2 was used for all fat peaks neglecting that different fat peaks have different T_2 s.¹⁶ However, the present work focuses on the behavior of the water peak and therefore using a common T_2 for all fat peaks has a minor impact on the reported results. The assumption of a common fat T_2 was mainly used to stabilize the fitting process by a reduction of fitting parameters.

5 | CONCLUSION

It is feasible to measure T_{2w} with single-voxel MRS in fatty infiltrated muscle tissue. The present study has shown that ^1H -MRS-based T_{2w} is decreased in fatty infiltrated muscle of patients with NMD. The observed dependence of T_{2w} on fat fraction should be considered when applying T_{2w} as a marker of "disease activity", currently seen as an important measurement to assess alterations in the muscle tissue of patients with NMD. Furthermore, when evaluating edematous changes single-voxel MRS could suffer from partial volume effects, especially when the voxel encloses edematous, nonedematous and fatty infiltrated muscle tissue. Therefore, there is a high need for accurate and high resolution T_{2w} mapping in patients with NMD as imaging could overcome the existing challenges that arise from the nonspatially resolved nature of single-voxel MRS.

ACKNOWLEDGEMENTS

The present work was supported by the German Society for Muscle Diseases and Philips Healthcare.

ORCID

Sarah Schlaeger  <https://orcid.org/0000-0002-2736-9225>

Dominik Weidlich  <https://orcid.org/0000-0001-7842-2682>

REFERENCES

1. Hollingsworth KG, de Sousa PL, Straub V, Carlier PG. Towards harmonization of protocols for MRI outcome measures in skeletal muscle studies: consensus recommendations from two TREAT-NMD NMR workshops, 2 May 2010, Stockholm, Sweden, 1–2 October 2009, Paris, France. *Neuromuscular Disord.* 2012;22:S54-S67.
2. Poliachik SL, Friedman SD, Carter GT, Parnell SE, Shaw DW. Skeletal muscle edema in muscular dystrophy: clinical and diagnostic implications. *Phys Med Rehabil Clin N Am.* 2012;23:107-122.

3. Mercuri E, Pichiecchio A, Allsop J, Messina S, Pane M, Muntoni F. Muscle MRI in inherited neuromuscular disorders: past, present, and future. *J Magn Reson Imaging*. 2007;25:433-440.
4. Morrow JM, Matthews E, Raja Rayan DL, et al. Muscle MRI reveals distinct abnormalities in genetically proven non-dystrophic myotonias. *Neuromuscul Disord*. 2013;23:637-646.
5. Karampinos DC, Yu H, Shimakawa A, Link TM, Majumdar S. T(1)-corrected fat quantification using chemical shift-based water/fat separation: application to skeletal muscle. *Magn Reson Med*. 2011;66:1312-1326.
6. Reeder SB, Hu HH, Sirlin CB. Proton density fat-fraction: a standardized MR-based biomarker of tissue fat concentration. *J Magn Reson Imaging*. 2012;36:1011-1014.
7. Burakiewicz J, Sinclair CDJ, Fischer D, Walter GA, Kan HE, Hollingsworth KG. Quantifying fat replacement of muscle by quantitative MRI in muscular dystrophy. *J Neurol*. 2017;264(10):2053-2067.
8. Marty B, Baudin PY, Reyngoudt H, et al. Simultaneous muscle water T2 and fat fraction mapping using transverse relaxometry with stimulated echo compensation. *NMR Biomed*. 2016;29:431-443.
9. Carlier PG, Marty B, Scheidegger O, et al. Skeletal Muscle Quantitative Nuclear Magnetic Resonance Imaging and Spectroscopy as an Outcome Measure for Clinical Trials. *J Neuromuscul Dis*. 2016;3:1-28.
10. Carlier PG. Global T2 versus water T2 in NMR imaging of fatty infiltrated muscles: Different methodology, different information and different implications. *Neuromuscul Disord*. 2014;24:390-392.
11. Arpan I, Forbes SC, Lott DJ, et al. T(2) mapping provides multiple approaches for the characterization of muscle involvement in neuromuscular diseases: a cross-sectional study of lower leg muscles in 5-15-year-old boys with Duchenne muscular dystrophy. *NMR Biomed*. 2013;26:320-328.
12. Wary C, Azzabou N, Giraudeau C, et al. Quantitative NMRI and NMRS identify augmented disease progression after loss of ambulation in forearms of boys with Duchenne muscular dystrophy. *NMR Biomed*. 2015;28:1150-1162.
13. Janiczek RL, Gambarota G, Sinclair CDJ, et al. Simultaneous T2 and lipid quantitation using IDEAL-CPMG. *Magn Reson Med*. 2011;66:1293-1302.
14. Mankodi A, Bishop CA, Auh S, Newbould RD, Fischbeck KH, Janiczek RL. Quantifying disease activity in fatty-infiltrated skeletal muscle by IDEAL-CPMG in Duchenne muscular dystrophy. *Neuromuscul Disord*. 2016;26:650-658.
15. Sinclair CD, Morrow JM, Janiczek RL, et al. Stability and sensitivity of water T2 obtained with IDEAL-CPMG in healthy and fat-infiltrated skeletal muscle. *NMR Biomed*. 2016;29:1800-1812.
16. Azzabou N, Loureiro de Sousa P, Caldas E, Carlier PG. Validation of a generic approach to muscle water T2 determination at 3 T in fat-infiltrated skeletal muscle. *J Magn Reson Imaging*. 2015;41:645-653.
17. Mankodi A, Azzabou N, Bulea T, et al. Skeletal muscle water T₂ as a biomarker of disease status and exercise effects in patients with Duchenne muscular dystrophy. *Neuromuscul Disord*. 2017;27:705-714.
18. Kan HE, Scheenen TW, Wohlgemuth M, et al. Quantitative MR imaging of individual muscle involvement in facioscapulohumeral muscular dystrophy. *Neuromuscul Disord*. 2009;19:357-362.
19. Yao L, Gai N. Fat-corrected T2 measurement as a marker of active muscle disease in inflammatory myopathy. *AJR Am J Roentgenol*. 2012;198:475-481.
20. Lebel RM, Wilman AH. Transverse relaxometry with stimulated echo compensation. *Magn Reson Med*. 2010;64:1005-1014.
21. Li Z, Graff C, Gmitro AF, et al. Rapid water and lipid imaging with T(2) mapping using a radial IDEAL-GRASE technique. *Magn Reson Med*. 2009;61:1415-1424.
22. Forbes SC, Willcocks RJ, Triplett WT, et al. Magnetic resonance imaging and spectroscopy assessment of lower extremity skeletal muscles in boys with Duchenne muscular dystrophy: a multicenter cross sectional study. *PLoS one*. 2014;9:e106435.
23. Arrigoni F, De Luca A, Velardo D, et al. Multiparametric quantitative MRI assessment of thigh muscles in limb-girdle muscular dystrophy 2A and 2B. *Muscle Nerve*. 2018;58:550-558.
24. Eggers H, Brendel B, Duijndam A, Herigault G. Dual-echo Dixon imaging with flexible choice of echo times. *Magn Reson Med*. 2011;65:96-107.
25. Ruschke S, Kienberger H, Baum T, et al. Diffusion-weighted stimulated echo acquisition mode (DW-STEAM) MR spectroscopy to measure fat unsaturation in regions with low proton-density fat fraction. *Magn Reson Med*. 2016;75:32-41.
26. Dieckmeyer M, Ruschke S, Cordes C, et al. The need for T(2) correction on MRS-based vertebral bone marrow fat quantification: implications for bone marrow fat fraction age dependence. *NMR Biomed*. 2015;28:432-439.
27. Schlaeger S, Klupp E, Weidlich D, et al. T2-weighted Dixon turbo spin echo for accelerated simultaneous grading of whole-body skeletal muscle fat infiltration and edema in patients with neuromuscular diseases. *J Comput Assist Tomogr*. 2018;42(4):574-579.
28. English AE, Joy ML, Henkelman RM. Pulsed NMR relaxometry of striated muscle fibers. *Magn Reson Med*. 1991;21:264-281.
29. Zimmerman JR, Brittin WE. Nuclear magnetic resonance studies in multiple phase systems: lifetime of a water molecule in an adsorbing phase on silica gel. *J Phys Chem*. 1957;61:1328-1333.
30. Fullerton GD, Cameron IL, Hunter K, Fullerton HJ. Proton magnetic resonance relaxation behavior of whole muscle with fatty inclusions. *Radiology*. 1985;155:727-730.
31. Saab G, Thompson RT, Marsh GD. Multicomponent T2 relaxation of in vivo skeletal muscle. *Magn Reson Med*. 1999;42:150-157.
32. C. A. Araujo E, Azzabou N, Vignaud A, Guillot G, Carlier PG. Quantitative ultrashort TE imaging of the short-T2 components in skeletal muscle using an extended echo-subtraction method. *Magn Reson Med*. 2017;78:997-1008.
33. Gillis P, Koenig SH. Transverse relaxation of solvent protons induced by magnetized spheres: application to ferritin, erythrocytes, and magnetite. *Magn Reson Med*. 1987;5:323-345.

34. Yablonskiy DA, Haacke EM. Theory of NMR signal behavior in magnetically inhomogeneous tissues: the static dephasing regime. *Magn Reson Med*. 1994;32:749-763.
35. Schenck JF. The role of magnetic susceptibility in magnetic resonance imaging: MRI magnetic compatibility of the first and second kinds. *Med Phys*. 1996;23:815-850.
36. Marciani L, Ramanathan C, Tyler DJ, et al. Fat emulsification measured using NMR transverse relaxation. *J Magn Reson*. 2001;153:1-6.

How to cite this article: Schlaeger S, Weidlich D, Klupp E, et al. Decreased water T_2 in fatty infiltrated skeletal muscles of patients with neuromuscular diseases. *NMR in Biomedicine*. 2019;e4111. <https://doi.org/10.1002/nbm.4111>

6.2 Journal Publication II: Water T_2 Mapping in Fatty Infiltrated Thigh Muscles of Patients With Neuromuscular Diseases Using a T_2 -Prepared 3D Turbo Spin Echo With SPAIR

The publication entitled *Water T_2 Mapping in Fatty Infiltrated Thigh Muscles of Patients With Neuromuscular Diseases Using a T_2 -Prepared 3D Turbo Spin Echo With SPAIR* was published in Journal of Magnetic Resonance Imaging (ISSN: 1053-1807, DOI: 10.1002/jmri.27032). The manuscript was authored by Sarah Schlaeger, Dominik Weidlich, Elisabeth Klupp, Federica Montagnese, Marcus Deschauer, Benedikt Schoser, Sarah Bublitz, Stefan Ruschke, Claus Zimmer, Ernst J. Rummeny, Jan S. Kirschke, and Dimitrios C. Karampinos.

6.2.1 Abstract

Background: Muscle water T_2 (T_{2w}) has been proposed as a biomarker to monitor disease activity and therapy effectiveness in patients with neuromuscular diseases (NMD). Multi-echo spin-echo (MESE) is known to be affected by fatty infiltration. A T_2 -prepared 3D turbo spin echo (TSE) is an alternative method for T_2 mapping, but has been only applied in healthy muscles.

Purpose: To examine the performance of T_2 -prepared 3D TSE in combination with spectral adiabatic inversion recovery (SPAIR) in measuring T_{2w} in fatty infiltrated muscles based on simulations and in vivo measurements in thigh muscles of patients with NMD.

Study Type: Prospective.

Subjects: One healthy volunteer, 34 NMD patients.

Field Strength/Sequence: T_2 -prepared stimulated echo acquisition mode (STEAM) magnetic resonance spectroscopy (MRS), SPAIR STEAM MRS, and SPAIR T_2 -prepared STEAM MRS were performed in the subcutaneous fat of a healthy volunteer's thigh. T_2 mapping based on SPAIR 2D MESE and SPAIR T_2 -prepared 3D TSE was performed in the NMD patients' thigh region. Multi-TE STEAM MRS was performed for measuring a reference T_{2w} at different thigh locations.

Assessment: The behavior of the fat spectrum in the SPAIR T_2 -prepared 3D TSE was simulated using Bloch simulations. The in vivo T_2 results of the imaging methods were compared to the in vivo T_{2w} MRS results.

Statistical Test: Pearson correlation coefficient with slope and intercept, relative error.

Results: The simulated T_2 for the SPAIR T_2 -prepared 3D TSE sequence remained constant within a relative error of not more than 4 % up to a fat fraction of 80 %. In vivo T_2 values of SPAIR T_2 -prepared 3D TSE were in good agreement with the T_{2w} values of STEAM MRS ($R = 0.86$; slope = 1.12; intercept = -1.41 ms). In vivo T_2 values of SPAIR 2D MESE showed large deviations from the T_{2w} values of STEAM MRS ($R = 0.14$; slope = 0.32; intercept = 38.83 ms).

Data Conclusion: The proposed SPAIR T_2 -prepared 3D TSE shows reduced sensitivity to fatty infiltration for T_{2w} mapping in the thigh muscles of NMD patients.

Level of Evidence: 1







Technical Efficacy: Stage 1

6.2.2 Authors Contribution

The author performed the MRI examinations of the study patients with NMD and the healthy volunteer on a 3 T Philips scanner as well as the post-processing, quantification and analysis of the MRS and T_{2w} mapping data using MATLAB. Furthermore, the author performed the simulations for the T_{2w} mapping sequence behaviour in regions with fatty infiltration. Additionally, the author reviewed the existing literature and kept up to date about novel scientific developments in the field through conferences and workshops. In collaboration with the co-authors, the author designed the MRI protocol and performed the recruitment of the patients, adapted the existing MRS post-processing frame-work and simulation pipeline using MATLAB, analysed and interpreted the data, and drafted the publication manuscript.



Water T_2 Mapping in Fatty Infiltrated Thigh Muscles of Patients With Neuromuscular Diseases Using a T_2 -Prepared 3D Turbo Spin Echo With SPAIR

Sarah Schlaeger,^{1,2*}  Dominik Weidlich, MSc,¹  Elisabeth Klupp, MD,²
Federica Montagnese, MD,³ Marcus Deschauer, MD,⁴ Benedikt Schooser, MD,³ 
Sarah Bublitz, MD,⁴ Stefan Ruschke, PhD,¹  Claus Zimmer, MD,² Ernst J. Rummeny, MD,¹
Jan S. Kirschke, MD,²  and Dimitrios C. Karampinos, PhD¹ 

Background: Muscle water T_2 (T_{2w}) has been proposed as a biomarker to monitor disease activity and therapy effectiveness in patients with neuromuscular diseases (NMD). Multi-echo spin-echo (MESE) is known to be affected by fatty infiltration. A T_2 -prepared 3D turbo spin echo (TSE) is an alternative method for T_2 mapping, but has been only applied in healthy muscles.

Purpose: To examine the performance of T_2 -prepared 3D TSE in combination with spectral adiabatic inversion recovery (SPAIR) in measuring T_{2w} in fatty infiltrated muscles based on simulations and in vivo measurements in thigh muscles of patients with NMD.

Study Type: Prospective.

Subjects: One healthy volunteer, 34 NMD patients.

Field Strength/Sequence: T_2 -prepared stimulated echo acquisition mode (STEAM) magnetic resonance spectroscopy (MRS), SPAIR STEAM MRS, and SPAIR T_2 -prepared STEAM MRS were performed in the subcutaneous fat of a healthy volunteer's thigh. T_2 mapping based on SPAIR 2D MESE and SPAIR T_2 -prepared 3D TSE was performed in the NMD patients' thigh region. Multi-TE STEAM MRS was performed for measuring a reference T_{2w} at different thigh locations.

Assessment: The behavior of the fat spectrum in the SPAIR T_2 -prepared 3D TSE was simulated using Bloch simulations. The in vivo T_2 results of the imaging methods were compared to the in vivo T_{2w} MRS results.

Statistical Tests: Pearson correlation coefficient with slope and intercept, relative error.

Results: The simulated T_2 for the SPAIR T_2 -prepared 3D TSE sequence remained constant within a relative error of not more than 4% up to a fat fraction of 80%. In vivo T_2 values of SPAIR T_2 -prepared 3D TSE were in good agreement with the T_{2w} values of STEAM MRS ($R = 0.86$; slope = 1.12; intercept = -1.41 ms). In vivo T_2 values of SPAIR 2D MESE showed large deviations from the T_{2w} values of STEAM MRS ($R = 0.14$; slope = 0.32; intercept = 38.83 ms).

Data Conclusion: The proposed SPAIR T_2 -prepared 3D TSE shows reduced sensitivity to fatty infiltration for T_{2w} mapping in the thigh muscles of NMD patients.

Level of Evidence: 1

Technical Efficacy: Stage 1

J. MAGN. RESON. IMAGING 2020;51:1727–1736.

View this article online at wileyonlinelibrary.com. DOI: 10.1002/jmri.27032

Received Sep 21, 2019, Accepted for publication Dec 5, 2019.

*Address reprint requests to: S.S., Department of Diagnostic and Interventional Neuroradiology, Klinikum rechts der Isar, Ismaninger Str. 22, 81675 Munich, Germany. E-mail: sarah.schlaeger@tum.de

Contract grant sponsor: German Society for Muscle Diseases; Contract grant sponsor: Philips Healthcare; Contract grant sponsor: European Research Council; Contract grant numbers: 677661-ProFatMRI and 637164-iBack.

From the ¹Department of Diagnostic and Interventional Radiology, School of Medicine, Technical University of Munich, Munich, Germany; ²Department of Diagnostic and Interventional Neuroradiology, School of Medicine, Technical University of Munich, Munich, Germany; ³Friedrich-Baur-Institut, Ludwig Maximilian University, Munich, Germany; and ⁴Department of Neurology, Technical University of Munich, Munich, Germany

This is an open access article under the terms of the Creative Commons Attribution License, which permits use, distribution and reproduction in any medium, provided the original work is properly cited.

MUSCLE WATER T_2 (T_{2w}) has been proposed as an important imaging marker for pathophysiological changes of skeletal muscle tissue.^{1,2} Muscle T_{2w} , in contrast to muscle global T_2 , reflects the chemically selective T_2 decay of the water component in the muscle tissue and is therefore considered an indicator for water mobility in the tissue.^{2,3} Water mobility in the muscle tissue is affected by several circumstances, such as inflammation, myocyte swelling, sarcoplasmic leakiness, cell necrosis, hydrostatic edema, denervation, or exercise of moderate to high intensity.^{1,2} Therefore, T_{2w} is a rather unspecific parameter, although responding rapidly to alterations in the muscle tissue and allowing assessment of acute as well as chronic changes.^{2,4-6} Due to its high sensitivity to alterations in the muscle fibers, T_{2w} has seen a growing consideration in the assessment of patients with neuromuscular diseases (NMD), where T_{2w} is currently considered a potential marker for diseases activity.^{1,2,4,5,7} T_{2w} has been proposed as an outcome measure to monitor muscle disease status and evaluate response to treatment.^{8,9}

The measurement of T_{2w} using quantitative magnetic resonance sequences allows objective, comparable, and precise assessment of even small changes in the muscle fiber composition.^{2,6} Single-voxel H^1 magnetic resonance spectroscopy (MRS) is considered the reference standard for robust quantification of muscle T_{2w} , as it determines the relative concentration of water and various metabolites and can also resolve the spectral complexity of fat.^{10,11} Therefore, single-voxel H^1 MRS enables a fat fraction independent quantification of T_{2w} .

In patients with NMD, pathological changes in the muscle tissue such as fatty and edematous alterations are often simultaneously present in a single muscle, affecting the muscle heterogeneously.¹ There is thus a need for techniques enabling robust and accurate spatially resolved T_{2w} quantification.¹² Thereby, especially the thigh musculature is a region of high interest for the application of quantitative imaging techniques, as it can be easily assessed with MRI due to its larger size compared to other body muscles and its relatively low B_1 and B_0 inhomogeneities.¹³ The thigh typically shows diagnostically important disease characteristic patterns of muscle involvement.^{14,15}

As analysis based on MRS does not contain any spatial information and spatially resolved chemical-shift imaging (CSI) can be time-consuming, prone to artifacts, and limited in spatial resolution,¹⁶ time-efficient quantitative imaging techniques for T_2 mapping are emerging. Several challenges need to be addressed for a robust quantitative T_{2w} determination. Transmit B_1 and B_0 inhomogeneities are a well-known source of errors for T_{2w} quantification, especially in the thigh.¹⁷⁻¹⁹ In the heterogeneously affected muscle tissue, the presence of fatty infiltration also affects T_{2w} estimation,^{1,20-22} as a complete fat suppression is challenging due to the

complexity of the fat spectrum with different chemical shift, T_1 and T_2 for each fat peak. Fatty infiltration and edematous changes both lead to increased T_2 values in the muscle tissue in most sequences. The effects of fatty infiltration and edematous changes on T_2 values cannot, in general, be thus distinguished.²³ Therefore, a reduction of the influence of fat on the T_{2w} determination is highly important in fatty infiltrated muscles.

Different T_2 mapping techniques have been developed to address the above challenges in robust muscle T_{2w} determination. 2D multi-echo spin echo (MESE) sequences have been traditionally used for muscle T_2 mapping, with known limitations, including the sensitivity to transmit B_1 inhomogeneities^{19,24} and the effect of fat on T_2 quantification. In order to remove the effects of transmit B_1 inhomogeneities, extended phase graph (EPG) techniques have been recently applied on 2D MESE data to model the occurrence of stimulated echoes in the decay of the signal.^{1,24} Techniques modeling the presence of fat based on Dixon MESE data²⁵ or based on MESE data combined with a multiexponential T_2 decay model without¹⁰ or with the phase graph formulation¹ have been proposed to remove the effect of fat. However, the robustness of the correct T_{2w} determination decreases at moderately high and high fat fractions due to small contribution of the remaining water component to the total signal.¹⁰

An alternative approach to reduce the effect of B_1 inhomogeneities directly during acquisition is the use of a T_2 -prepared 3D turbo spin echo (TSE) sequence consisting of an adiabatic BIR-4 radiofrequency (RF) pulse in the T_2 preparation and a 3D TSE readout combined with spectral adiabatic inversion recovery (SPAIR) fat suppression.^{13,26} The modified BIR-4 T_2 preparation is a method enabling accurate and precise T_2 mapping in the presence of large B_1 and B_0 offsets. It has been shown that the T_2 -prepared 3D TSE sequence allows B_1 -insensitive and reproducible thigh muscle T_2 mapping in a healthy cohort. However, it remains unknown how the T_2 quantification based on the SPAIR T_2 -prepared 3D TSE sequence is affected by the presence of fat.

The purpose of the present work was to investigate the performance of the T_2 -prepared 3D TSE combined with SPAIR fat suppression in measuring T_{2w} in fatty infiltrated muscles.

Materials and Methods

Theoretical Background

A T_2 -prepared 3D TSE sequence in combination with SPAIR for fat suppression was used as proposed by Klupp et al.¹³ The pulse sequence diagram is shown in Fig. 1a. The SPAIR T_2 -prepared 3D TSE consists of three main components: I) the SPAIR pulse, II) the adiabatic T_2 preparation module, and III) the 3D TSE readout.

SPECTRAL ADIABATIC INVERSION RECOVERY. A SPAIR pulse at the beginning of the sequence was used to invert the main

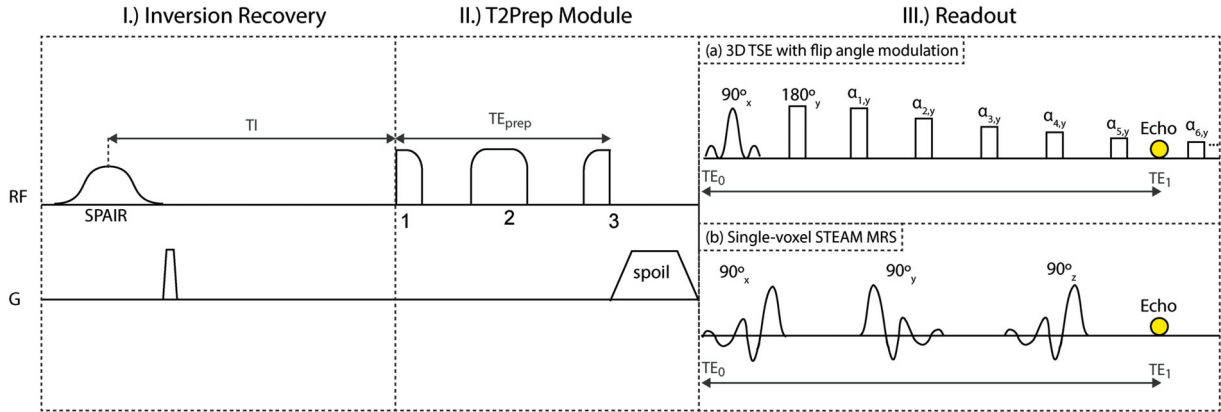


FIGURE 1: (a) Pulse sequence diagram of the SPAIR T₂-prepared 3D TSE including I) spectral adiabatic inversion recovery, II) T2Prep module, and III) 3D TSE with flip angle modulation readout and (b) pulse sequence diagram of the SPAIR T₂-prepared single-voxel STEAM MRS including I) spectral adiabatic inversion recovery, II) T2Prep module, and III) single-voxel STEAM MRS readout.

fat peaks (Fig. 1, I).²⁷ Traditionally, the energy of fat is reduced by nulling the main fat peak (methylene, at 1.3 ppm) at the beginning of the readout and reducing thereby the contribution of fat on the overall acquired signal. Keeping in mind that fat has multiple peaks with different T₁ relaxation times, SPAIR will not null all the fat peaks at once, rather than greatly reduce the total fat energy. Additionally, if off-resonance effects are neglected, SPAIR fat suppression does not affect the olefinic and glycerol fat peaks located in the spectral proximity to the water peak. After SPAIR inversion and the inversion delay time, some of the fat peaks may be nulled, some may be inverted, but reduced in energy, some may be already positively recovered, but reduced in energy, and some may not be affected at all. Keeping this complex fat signal behavior in mind, the total energy of the fat signal is expected to be smaller than weighted by simple T₁ relaxation. At the echo, the energy of the inverted and the noninverted fat peaks is summed and this can lead to additional fat signal reduction. In the present work, the inversion time between SPAIR and the beginning of the T₂ preparation module was determined experimentally in order to reduce the total fat signal at the beginning of the readout as strongly as possible. The experimental determination of the inversion delay time was optimized in one healthy volunteer by minimizing the energy in the subcutaneous fat when performing the T₂-prepared 3D TSE.

T₂ PREPARATION MODULE. The T₂ preparation module (Fig. 1, II) consists of a modified BIR-4 resonance frequency pulse with varying gaps to obtain T₂ preparation modules with different T₂ weightings.²⁸ Therefore, the T₂ preparation module allows a B₁-insensitive T₂ weighting of the whole water-fat spectral region with at the same time equal T₁ weighting for every T₂ weighting as the T₂ preparation occurs outside of the readout. The T₂ preparation module was designed to have the final magnetization after the T₂ preparation aligned with the main magnetic field. T₁ weighting during the T₂ preparation module can be neglected due to the short duration of the T₂ preparation module.

3D TSE READOUT. The T₂ preparation module was followed by a 3D TSE readout with a flip angle modulation and appropriate start-up echoes (Fig. 1a, III). The flip angle train was designed to achieve a constant signal plateau throughout the TSE shot for

skeletal muscle tissue.¹³ The TSE readout allows a very fast acquisition of the *k*-space center and therefore minimizes the T₁ recovery from the end of the T₂ preparation module until acquisition of the *k*-space center.

SIGNAL CANCELLATION OF FAT PEAKS. In the present work, it was evaluated whether the combination of the T₂-prepared 3D TSE sequence with SPAIR leads to a partial signal cancellation of fat peaks at echo acquisition. It was particularly examined whether the remaining signal of the fat peaks is relatively small compared to the signal of the water peak at the beginning of the 3D TSE readout and whether due to the relatively short maximum duration of the T₂ preparation module only minor changes of the total fat energy occur. Therefore, it was evaluated whether, after the cancellation of the fat peaks, the fat will have a small influence on the T_{2w} determination.

Simulations Based on MRS Data

In order to investigate the performance of the T₂-prepared 3D TSE sequence in combination with SPAIR on T_{2w} determination the following signal model was used:

$$\text{Signal}(T2Prep) = (1 - FF) \cdot W(T2Prep) + FF \cdot c(T2Prep) \cdot F(T2Prep) \quad (1)$$

where *FF* is the fat fraction, *W(T2Prep)* the water signal, and *F(T2Prep)* the fat signal. *F(T2Prep)* represents the combined fat signal of all fat peaks. When the different fat peaks cancel each other out, the ratio of the fat signal contributing to the total signal in Eq. [1] is reduced. A constant *c(T2Prep)* was introduced, representing the energy reduction factor of SPAIR due to T₁ relaxation.

In order to solve the signal model equation, the constant *c(T2Prep)* and the combined fat signal *F(T2Prep)* have to be determined. To accurately investigate the behavior of the different fat peaks during the different components of the SPAIR T₂-prepared 3D TSE sequence, appropriate MRS sequences were designed. In the subcutaneous fat of a healthy volunteer's thigh (female, 24 years old) a T₂-prepared stimulated echo acquisition mode (STEAM), a SPAIR STEAM, and a SPAIR T₂-prepared STEAM according to the pulse sequence diagram in Fig. 1 were performed. Figure 1b

shows the different components of the SPAIR T_2 -prepared STEAM MRS sequence. The sequence parameters for the T_2 -prepared STEAM, the SPAIR STEAM, and the SPAIR T_2 -prepared STEAM are listed in Table 1.

Based on the acquired MRS data from the in vivo experiments in the subcutaneous fat, additional simulations were performed to calculate $c(T_2Prep)$ and $F(T_2Prep)$. Therefore, T_1 and T_2 weightings of the STEAM MRS sequence were removed mathematically based on T_1 and T_2 relaxation times extracted from a STEAM TE- and TM-Series in the subcutaneous fat of the same volunteer. A Bloch simulation of the 3D TSE readout was then performed. The simulation was implemented in MatLab (MathWorks, Natick, MA) and performed a numerical calculation of the magnetization time evolution in discrete time steps based on the well-known Bloch equation.²⁹

Based on the simulated fat peak area the constant c (T_2Prep) and the remaining combined fat signal $F(T_2Prep)$ were calculated.

Using the experimental data from the MRS measurements in the subcutaneous fat of a healthy volunteer's thigh and the signal model presented in Eq. [1], different signal decay curves for the water and fat signal components were determined. The total signal, $Signal(T_2Prep)$, which represents the T_2 signal of the SPAIR T_2 -prepared 3D TSE imaging sequence, was calculated using Eq. [1]. For different fat fractions, different $Signal(T_2Prep)$ values were calculated and T_2 was estimated by fitting $Signal(T_2Prep)$ to a single-exponential T_2 signal expression.

In Vivo MR Measurements in NMD Patients

The study was approved by the local Ethics Commission and written informed consent was obtained from all patients before participation. In order to verify the fatty infiltration independent

determination of T_{2w} using the SPAIR T_2 -prepared 3D TSE, MR measurements were performed in the thigh of 34 patients (64.7% women) with different NMD (Table 2) with a 3 T system (Ingenia, Philips Healthcare, Best, The Netherlands). The whole-body coil, the built-in 12-channel posterior coil, and a 16-channel anterior coil were used. The 16-channel anterior coil was placed on top of the hip and thigh region. Subjects were positioned in a head-first supine position.

Spatially-resolved PDFF mapping was performed for a reference using a six-echo 3D spoiled gradient echo sequence with bipolar readouts. In order to calculate T_2 maps, a 2D MESE with SPAIR fat suppression and a T_2 -prepared 3D TSE with SPAIR fat suppression were acquired in one stack in the mid-thigh. A multi-TE single-voxel STEAM MRS was performed in multiple locations by moving the MRS box within the patients' healthy, edematous, and fatty thigh muscles. The thigh muscles where MRS was applied were selected by qualitative assessment by the scanner operator based on the T_2 -weighted water- and fat-separated images of a T_2 -weighted Dixon TSE sequence and varied depending on the patients' muscle disease pattern.³⁰ The sequence parameters for SPAIR 2D MESE, SPAIR T_2 -prepared 3D TSE, multi-TE single-voxel STEAM MRS, the T_2 -weighted Dixon TSE, and the six-echo 3D spoiled gradient echo sequence are shown in Table 3. The longest duration of the T_2 preparation module in the present work was 60 ms, resulting in an effective T_2 weighting of 56.9 ms and verifying the assumption of neglectable T_1 weighting during the T_2 preparation module.³¹ The parameters of the employed BIR-4 RF pulse were: total pulse duration without gaps of the T_2 preparation module = 10 ms, B_1 amplitude = 13.5 μ T, and frequency sweep = 3700 Hz. The parameters for the employed SPAIR pulse were: pulse duration = 18.4 ms, B_1 amplitude = 7.3 μ T, pulse bandwidth = 680 Hz.

TABLE 1. Sequence Parameters of T_2 -Prepared STEAM MRS, SPAIR STEAM MRS, and SPAIR T_2 -Prepared STEAM MRS Performed in a Healthy Volunteer

	T_2 -prepared STEAM MRS	SPAIR STEAM MRS	SPAIR T_2 -prepared STEAM MRS
VOI (mm ³)	15 x 15 x 15	15 x 15 x 15	15 x 15 x 15
Spectral BW (Hz)	5000	5000	5000
Flip angle (deg)	90	90	90
TR (ms)	2000	2000	2000
TE (ms)	21	20/30/40/50/60	21
TM (ms)	16	16	16
Fat suppression	—	SPAIR, inversion delay 205 ms	SPAIR, inversion delay 205 ms
Startup acquisitions	1	1	1
NSA	24	24	24
Phase cycles	8	8	8
T_2 preparation durations (ms)	20/30/40/50/60	—	20/30/40/50/60
Scan duration (min)	04:10	04:10	04:10

TABLE 2. Patient ID, Age, Gender, and Disease of 34 Patients With NMD

Patient ID	Age	Gender	Disease
P001	63	F	Myotonic dystrophy type 2
P002	54	F	Myotonic dystrophy type 2
P003	47	F	Limb girdle muscular dystrophy type 2A
P004	34	F	Myotonic dystrophy type 2
P005	49	F	Limb girdle muscular dystrophy type 2A
P006	30	F	Limb girdle muscular dystrophy type 2I
P007	26	M	Limb girdle muscular dystrophy type 2A
P008	61	F	Myotonic dystrophy type 2
P009	52	M	Myotonic dystrophy type 2
P010	45	M	Centronuclear myopathy
P011	52	F	Limb girdle muscular dystrophy type 2A
P012	41	M	Amyotrophic lateral sclerosis
P013	61	M	Unclassified myopathy
P014	50	F	Unclassified myopathy
P015	45	F	Limb girdle muscular dystrophy type 2A
P016	19	F	Inflammatory myopathy
P017	20	F	Lamin A/C myopathy
P018	77	M	Inclusion body myositis
P019	22	F	Facioscapulohumeral muscular dystrophy
P020	57	M	Nemaline myopathy 2
P021	66	F	Myotonic dystrophy type 2
P022	36	F	Dermatomyositis
P023	26	F	Rhabdomyolysis
P024	49	F	Bethlem myopathy
P025	55	M	Amyotrophic lateral sclerosis
P026	32	F	Myotonic dystrophy type 1
P027	76	F	Pompe disease
P028	84	M	Pompe disease
P029	70	M	Hypokalemic periodic paralysis

TABLE 2. Continued

Patient ID	Age	Gender	Disease
P030	34	F	Distal myopathy
P031	73	F	Myofibrillar myopathy
P032	69	F	Inclusion body myositis
P033	41	M	Dermatomyositis
P034	48	M	Limb girdle muscular dystrophy type 2L

Data Analysis

PROCESSING OF MRS DATA. The processing of the MRS data was performed with in-house software and included zero-order phasing, Gaussian apodization, and frequency alignment of single acquisitions. For the MRS scan in the health volunteer's subcutaneous fat, the peak area quantification was performed considering six fat peaks and fitting of the fat peak areas was performed independently for each echo time (TE). No more than six fat peaks were considered for the analysis because an accurate determination of T₁ and T₂ relaxation constants as well as peak amplitudes after inversion recovery was only possible when the initial energy of the fat peak was sufficiently high. For the MRS scans performed in the patients with NMD, eight to ten fat peaks (depending on the fat fraction and therefore visibility of smaller fat peaks)³² were considered and the measurement of all four/five TEs was jointly incorporated into a peak-specific T₂ decay signal model.³³ Fitting was constrained with a common fat T₂ (T_{2f}) for all fat peaks. Based on the fat and water T₂ as well as the fat peak amplitudes, the proton density fat fraction (PDFF) was calculated. The MRS quantification was eventually utilized to extract both PDFF and T_{2w}. The MRS-based PDFF values were used in the subsequent statistical analysis.

PROCESSING OF IMAGING DATA. The processing of the multi-echo gradient echo data was performed online using the vendor's routines for PDFF mapping. After phase error correction, water-fat separation was performed based on a complex-based signal formulation employing a multi-peak fat spectrum and single T₂* decay correction.^{34,35} A small flip angle was used to minimize T₁ bias effects.³⁶ The imaging-based PDFF maps were only used for visualizing the spatially heterogeneous muscle fatty infiltration patterns.

Postprocessing of the T₂ maps was performed offline. An exponential fit with linear least-squares was used to fit data. For the MESE data the first echo was excluded to reduce T₂ overestimation due to stimulated echoes.

STATISTICAL ANALYSIS PERFORMED IN NMD PATIENTS.

The statistical analyses were performed using MatLab. Measured T₂ values of the SPAIR 2D MESE sequence and the SPAIR T₂-prepared 3D TSE sequence were correlated with T_{2w} values determined by STEAM MRS using the Pearson correlation coefficient R. Intercept and slope were determined. The relative error of the T₂

TABLE 3. Sequence Parameters of SPAIR 2D MESE, SPAIR T₂-prepared 3D TSE, Multi-TE Single-Voxel STEAM MRS, T₂-weighted Dixon TSE and Six-echo 3D Spoiled Gradient Echo Sequence for PDFF Mapping, Performed in NMD Patients

	SPAIR 2D MESE	SPAIR T ₂ -prepared 3D TSE	Multi-TE single-voxel STEAM MRS	T ₂ W Dixon TSE	Six-echo 3D spoiled gradient echo sequence
TR (ms)	2200	1500	6000	3725	10
TE (ms)	10 echoes with TE ₁ = 20	19	11/15/20/25(/35) with 8 averages	100	1.17
ΔTE (ms)	10	—	—	1.0	0.9
TM (ms)	—	—	16	—	—
Number of slices	30	30	—	26	30
Slice gap (mm)	0	0	—	6	0
Acquisition voxel (mm ³)	2 x 2 x 4	2 x 2 x 8	15 x 15 x 15	2.5 x 2.7 x 6.0	3.2 x 2 x 4
T ₂ preparation durations (ms)	—	20/30/40/50/60	—	—	—
RF-pulses (in readout)	180° refocusing pulses	Flip angle modulated TSE readout (echo spacing: 2.4 ms, 5 start-up echoes)	Slice selective 90° excitation pulses	—	Flip angle of 3°
TSE factor	—	50	—	45	—
Averages	1	Partial averaging (1.4)	8 (4 phase cycles)	2	1
FOV/VOI (mm ³)	420 x 260 x 120	420 x 260 x 120	15 x 15 x 15	330 x 450 x 306	260 x 420 x 120
Scan duration	8:24 min	4:30 min	3:36 (4:30) min	2:07 min	0:20
SENSE	In A/P direction, reduction factor 2	In A/P direction, reduction factor 2	—	—	In L/R direction, reduction factor 2

values of the SPAIR 2D MESE sequence and the SPAIR T₂-prepared 3D TSE sequence compared to the T_{2w} values determined by STEAM MRS was calculated in correlation with MRS-based PDFF.

Results

Healthy Volunteer MRS Results

Figure 2 shows the spectra of the multi-TE single-voxel STEAM MRS performed in the subcutaneous fat of a healthy volunteer's thigh. The spectrum of the T₂-prepared STEAM (Fig. 2a) shows a conventional fat spectrum. The different T₂ weightings that reduce the amplitude of the fat peaks can be observed. In the SPAIR STEAM spectrum (Fig. 2b), the total fat energy is largely reduced. The total fat energy reduction is best visible when referencing the fat peak signals in Fig. 2a and Fig. 2b to the olefinic fat peaks. Furthermore, an

additional energy reduction when all the fat peaks of the spectrum are summed up can be observed. The spectrum of the SPAIR T₂-prepared STEAM (Fig. 2c) adds T₂ weighting to the SPAIR STEAM spectrum. The SPAIR T₂-prepared STEAM represents the fat spectrum present at the acquisition of *k*-space center when the SPAIR T₂-prepared 3D TSE imaging sequence is performed.

Simulation Results

Figure 3a shows the signal decay curves for the water signal (blue), for the fat signal without fat suppression (green), and for the fat signal with SPAIR fat suppression (red) in a theoretical voxel with FF = 50%. The SPAIR T₂-prepared 3D TSE imaging sequence provides the sum of the signal of the water peak and the signal of the fat peak with SPAIR fat suppression. Summing up the water signal decay curve and the

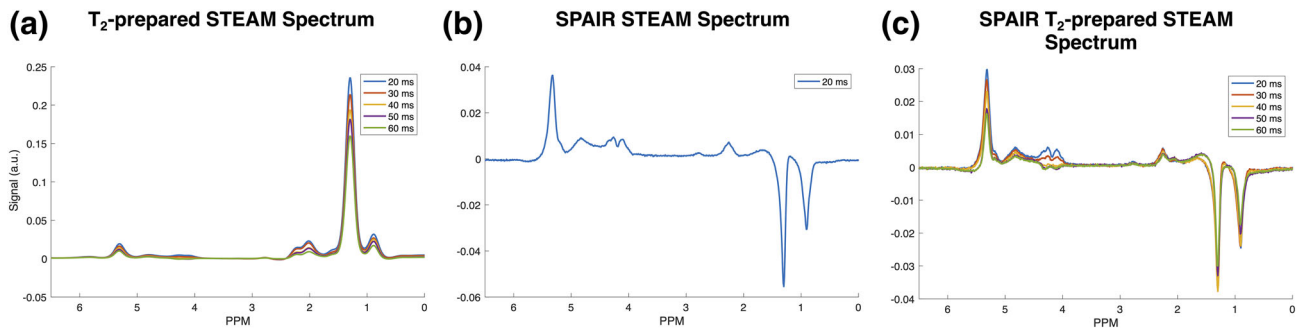


FIGURE 2: Spectra of single-voxel STEAM MRS performed in the subcutaneous fat of a healthy volunteer's thigh: (a) T₂-prepared STEAM spectrum at different echo times, (b) SPAIR STEAM spectrum at TE = 20 ms, and (c) SPAIR T₂-prepared STEAM spectrum at different echo times.

fat signal with SPAIR decay curve, the signal decay is largely dominated by the water signal decay. Even in a theoretical voxel with higher fat fraction, such as FF = 75%, the summed up signal decay of the imaging is largely dominated by the water signal decay and the influence of the fat signal with SPAIR stays small (Fig. 3b).

Based on the results of the MRS measurements in the subcutaneous fat and the Bloch simulations, the following parameters with their dependency on the duration of the T₂ preparation module were determined: $c(T_2Prep) = [0.22 \ 0.21 \ 0.21 \ 0.20 \ 0.19]$ and $F(T_2Prep) = [0.12 \ 0.08 \ 0.04 \ 0.05 \ 0.04]$ for the T₂Prep durations of [20 30 40 50 60] ms. Figure 3c shows the dependence of the simulated T₂ on different fat fractions. The simulated T₂ remains constant within a relative error of not more than 4% up to a fat fraction of 80%. At fat fraction values higher than 80%, deviations from the nominal T₂ values can be observed.

NMD Patients in vivo Results

Representative PDFF maps and T₂ maps based on the SPAIR 2D MESE sequence and the SPAIR T₂-prepared 3D TSE sequence of the thigh of a patient with Pompe disease are shown in Fig. 4. The patient has highly fatty infiltrated muscles, partially fatty infiltrated muscles, and muscles without fatty infiltration. The red arrow indicates T₂ elevations in the SPAIR 2D MESE in contrast to a stable T₂ in the SPAIR T₂-prepared 3D TSE in a region which is typically affected by B₁ errors. In a moderately fatty infiltrated region (PDFF = 25.6 ± 14.5% – circle), the mean T₂ value of the SPAIR 2D MESE was 54.6 ± 11.8 ms, whereas the mean T₂ value of the SPAIR T₂-prepared 3D TSE was 35.4 ± 3.8 ms.

Figure 5 shows the results of the comparison of T_{2w} values determined by STEAM MRS and T₂ mapping data in the scanned 34 NMD patients based on measurements in fatty infiltrated muscle tissue, edematous muscle tissue, and healthy muscle tissue locations. A good agreement between T_{2w} values of STEAM MRS and T₂ values of SPAIR T₂-prepared 3D TSE is reported (R = 0.86; P < 10⁻³; slope = 1.12; intercept = -1.41 ms), whereas the T₂ values of SPAIR 2D MESE show

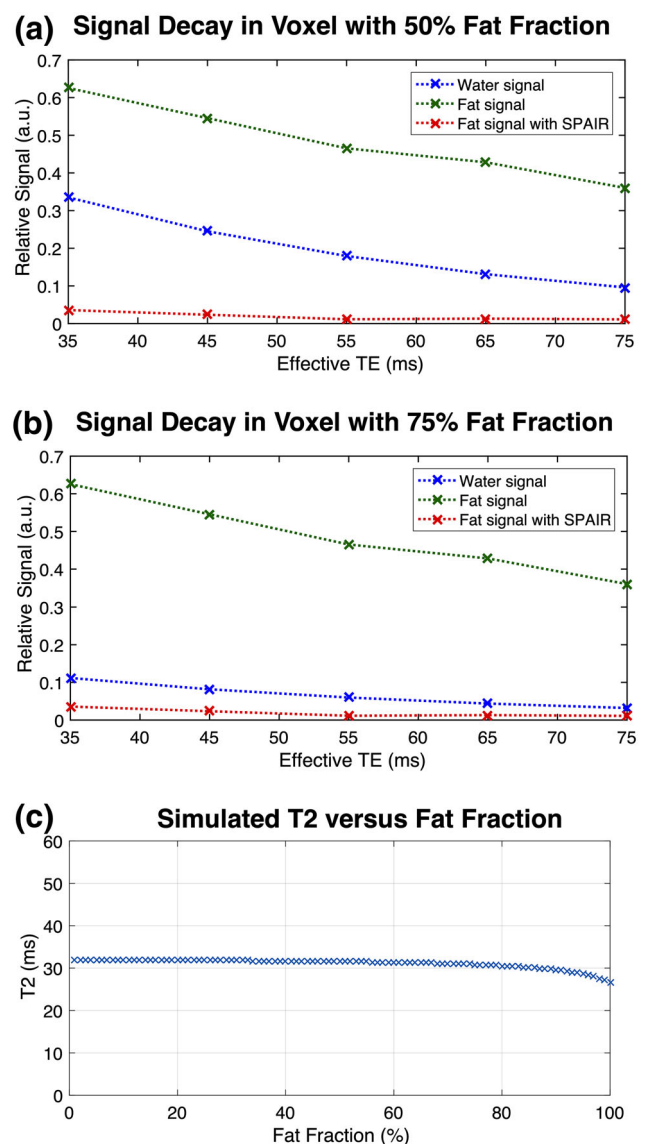


FIGURE 3: (a,b) Simulated SPAIR T₂-prepared T₂-weighted signal decay curves as a function of effective TE for the water signal (blue), the fat signal without fat suppression (green), and the fat signal with SPAIR fat suppression (red) for (a) a voxel with 50% fat fraction and (b) a voxel with 75% fat fraction. (c) Simulated estimated T₂ vs. fat fraction. The simulated T₂ stays rather constant up to a fat fraction of 80%.

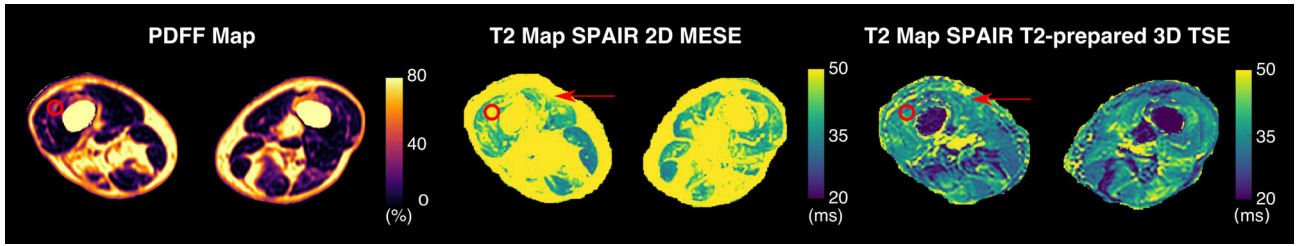


FIGURE 4: Representative PDFF map, T_2 map using SPAIR 2D MESE and T_2 map using SPAIR T_2 -prepared 3D TSE in a patient with Pompe disease. The red arrow indicates a region of typical B_1 inhomogeneity and the red circle indicates a region of moderate fatty infiltration.

large deviations from the T_{2w} values of STEAM MRS ($R = 0.14$; $P < 10^{-3}$; slope = 0.32; intercept = 38.83 ms). The relative error in the T_2 measurement using the SPAIR T_2 -prepared 3D TSE was below 25%, even at PDFF values larger than 60%. The relative error in the T_2 measurement using the SPAIR 2D MESE showed a strong dependence on PDFF and it exceeded 100% at PDFF values larger than 60%.

Discussion

The present work examines how T_{2w} quantification based on the T_2 -prepared 3D TSE sequence with SPAIR fat suppression is affected by the presence of fatty infiltration in skeletal muscle. Therefore, simulations were performed based on MRS measurements in the subcutaneous fat of a healthy volunteer's thigh to theoretically assess the T_2 quantification accuracy of the SPAIR T_2 -prepared 3D TSE in the presence of fat. Additionally, SPAIR T_2 -prepared 3D TSE T_2

measurements were performed in the fatty infiltrated thigh region of 34 patients with various NMD and compared to the routinely used SPAIR 2D MESE T_2 measurements, using single-voxel MRS T_{2w} measurements as the reference standard.

The combination of MESE with fat suppression techniques is known to result in T_2 values in fatty infiltrated skeletal muscles still affected by the presence of fat.³⁷ The reported simulations based on measurements in the subcutaneous fat of a healthy volunteer's thigh confirm the theory that the T_2 -prepared 3D TSE in combination with SPAIR leads to a partial signal cancellation of fat peaks at echo acquisition, enabling a robust determination of T_{2w} values with only a small influence of the remaining fat signal. The relative independence of T_{2w} determination on the underlying fat fraction is mainly due to 1) the partial signal cancellation of the fat peaks caused by the signal reduction of the fat peaks

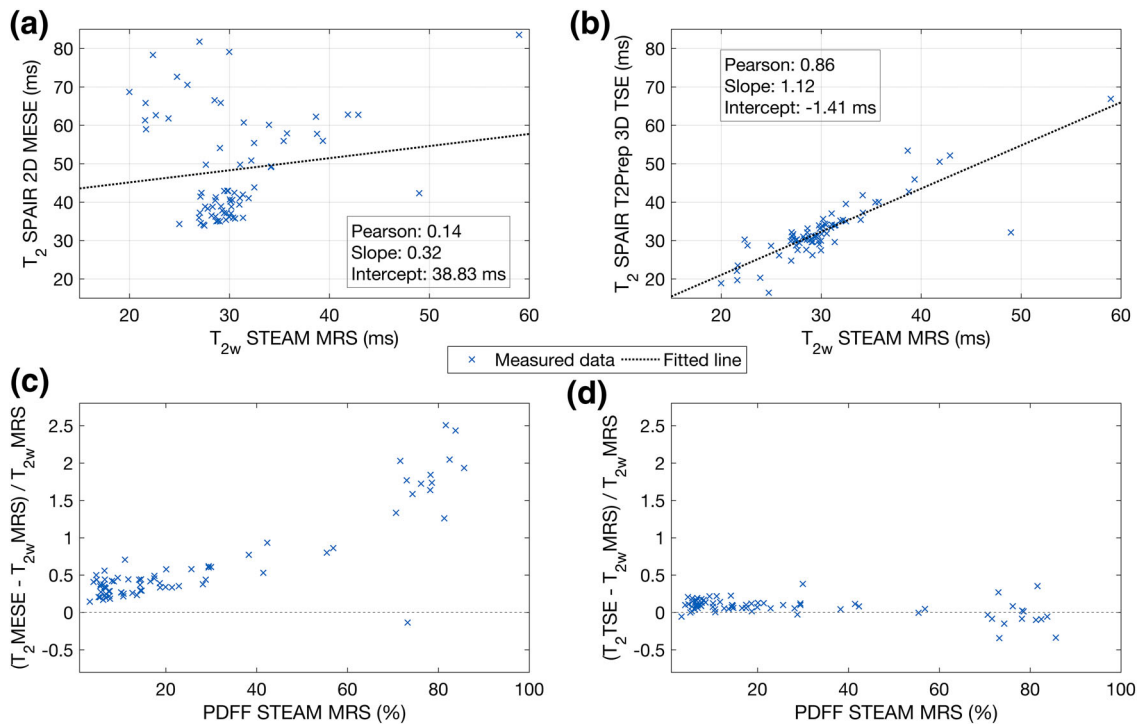


FIGURE 5: (a) T_2 from SPAIR 2D MESE vs. T_{2w} from STEAM MRS and (b) T_2 from SPAIR T_2 -prepared 3D TSE vs. T_{2w} from STEAM MRS. (c) Relative error of SPAIR 2D MESE compared to T_{2w} from STEAM MRS as a function of PDFF and (d) relative error of SPAIR T_2 -prepared 3D TSE compared to T_{2w} from STEAM MRS as a function of PDFF. Results show data from 34 NMD patients.

by the SPAIR inversion pulse; 2) the equal fat T₁ weighting for every T₂ weighting during the T₂ preparation module; and 3) the 3D TSE readout enabling the fast acquisition of the *k*-space center and therefore minimizing any fat T₁ recovery effects.

The reported in vivo results show that T_{2w} mapping based on SPAIR T₂-prepared 3D TSE is minimally sensitive to fatty infiltration even at higher PDF values, and approximately reveals the same T_{2w} values as the reference standard MRS. To the best of the authors' knowledge, the present work is the first to compare quantitative spatially-resolved imaging data based on T₂ maps with MRS in a large number of patients with NMD. Robust T_{2w} mapping, which is comparable to MRS as a reference standard, is essential to get an insight into the spatial distribution of acute and chronic alterations and disease activity in the muscle tissue of patients with NMD.^{3,12} A robust and fat independent determination of the important biomarker T_{2w} is essential, especially in NMD patients, as regions with healthy muscle tissue, edematous muscle tissue, and fatty infiltrated muscle tissue are often simultaneously present in a single muscle of NMD patients.

Previous works have addressed the confounding effects of transmit B₁ sensitivity and fat on T_{2w} quantification in MESE sequences by appropriate signal modeling of the relevant effects, primarily using EPG formulations.^{1,10} T_{2w} mapping based on the T₂-prepared 3D TSE has been previously shown to be insensitive to transmit B₁ inhomogeneity effects in the thigh muscles¹³ and the present work shows that with the addition of SPAIR on the T₂-prepared 3D TSE, the effect of fat on the measured thigh muscle T₂ is also minimized. Therefore, the present SPAIR T₂-prepared 3D TSE sequence effectively and simultaneously addresses the confounding effects of transmit B₁ sensitivity and fat on T_{2w} quantification already on the acquisition side and thus does not rely on modeling of the above two effects on the signal evolution (as performed in MESE acquisitions.^{1,10})

Limitations

The present work has some limitations. First, the present approach for fatty infiltration independent determination of T_{2w} in muscle tissue based on SPAIR is specific to the employed T₂-prepared 3D TSE imaging protocol and cannot be necessarily generalized to other T₂ mapping techniques. Second, the measured T_{2w} using the SPAIR T₂-prepared 3D TSE remains an approximation of the T_{2w} value, as the signal of the different fat peaks is not completely suppressed or separated, and rather the effect of unsuppressed fat is reduced. Third, although the performance of the T₂-prepared 3D TSE is quite independent of transmit B₁ and B₀ field inhomogeneities, the performed SPAIR preparation is prone to B₀ inhomogeneity effects. The sensitivity of SPAIR to B₀ inhomogeneity effects can affect the effectiveness of the inversion of the main fat peaks.²⁷ However, the effect of B₀

inhomogeneities on the SPAIR pulse is estimated to be small, at least for thigh muscle imaging at 3 T. Concerning study design limitations, fourth, the present simulations in order to explain the performance of the combination of SPAIR with the T₂-prepared 3D TSE in regions of fatty infiltrated thigh muscles are based on measurements in the subcutaneous fat of a single healthy volunteer. However, the measurements in the subcutaneous fat are only used to explain the findings of robust T_{2w} mapping with sufficient fat suppression, which is confirmed in 34 patients in the present study. Fifth, the total number of patients per each different disease group in the present study is rather small. However, the present study was performed in patients with rare diseases, and therefore the results in a small cohort number can add significant value to progress in diagnostics and therapy of NMD. Despite the small numbers per disease group, the moderate total number of patients (*n* = 34) shows the effectiveness of the proposed method for effectively measuring T_{2w} across different fatty infiltration patterns in muscle tissue.

Conclusion

T₂-prepared 3D TSE in combination with SPAIR is proposed for T_{2w} mapping in NMD patients. T_{2w} mapping using the proposed SPAIR T₂-prepared 3D TSE is known to have insensitivity to B₁ inhomogeneities and is shown as being minimally affected by the underlying fatty infiltration in thigh muscle imaging at 3 T. Therefore, the SPAIR T₂-prepared 3D TSE enables T_{2w} determination already during acquisition without the need to model the effects of B₁ inhomogeneity and fat presence. The application of the method in NMD patients shows that T_{2w} is spatially heterogeneous and the spatial resolution of T_{2w} mapping needs to be particularly considered in order to potentially monitor disease activity or therapy effectiveness in NMD patients.

References

1. Marty B, Baudin P-Y, Reyngoudt H, et al. Simultaneous muscle water T2 and fat fraction mapping using transverse relaxometry with stimulated echo compensation. *NMR Biomed* 2016;29:431–443.
2. Carlier PG. Global T2 versus water T2 in NMR imaging of fatty infiltrated muscles: Different methodology, different information and different implications. *Neuromuscul Disord* 2014;24:390–392.
3. Carlier PG, Marty B, Scheidegger O, et al. Skeletal muscle quantitative nuclear magnetic resonance imaging and spectroscopy as an outcome measure for clinical trials. *J Neuromuscul Dis* 2016;3:1–28.
4. Arpan I, Forbes SC, Lott DJ, et al. T2 mapping provides multiple approaches for the characterization of muscle involvement in neuromuscular diseases: A cross-sectional study of lower leg muscles in 5–15-year-old boys with Duchenne muscular dystrophy. *NMR Biomed* 2013;26:320–328.
5. Wary C, Azzabou N, Giraudeau C, et al. Quantitative NMRI and NMRS identify augmented disease progression after loss of ambulation in forearms of boys with Duchenne muscular dystrophy. *NMR Biomed* 2015;28:1150–1162.
6. English AE, Joy ML, Henkelman RM. Pulsed NMR relaxometry of striated muscle fibers. *Magn Reson Med* 1991;21:264–281.

7. Kim HK, Laor T, Horn PS, et al. T2 mapping in Duchenne muscular dystrophy: Distribution of disease activity and correlation with clinical assessments. *Radiology* 2010;255:899–908.
8. Carlier PG, Azzabou N, de Sousa PL, et al. Skeletal muscle quantitative nuclear magnetic resonance imaging follow-up of adult Pompe patients. *J Inher Metab Dis* 2015;38:565–572.
9. Hollingsworth KG, de Sousa PL, Straub V, et al. Towards harmonization of protocols for MRI outcome measures in skeletal muscle studies: Consensus recommendations from two TREAT-NMD NMR workshops, 2 May 2010, Stockholm, Sweden, 1-2 October 2009, Paris, France. *Neuromuscul Disord* 2012;22(Suppl 2):S54–67.
10. Azzabou N, Loureiro de Sousa P, Caldas E, et al. Validation of a generic approach to muscle water T2 determination at 3T in fat-infiltrated skeletal muscle. *J Magn Reson Imaging* 2015;41:645–653.
11. Schlaeger S, Weidlich D, Klupp E, et al. Decreased water T2 in fatty infiltrated skeletal muscles of patients with neuromuscular diseases. *NMR Biomed* 2019;32:e4111.
12. Poliachik SL, Friedman SD, Carter GT, et al. Skeletal muscle edema in muscular dystrophy: Clinical and diagnostic implications. *Phys Med Rehabil Clin N Am* 2012;23:107–122, xi.
13. Klupp E, Weidlich D, Schlaeger S, et al. B1-insensitive T2 mapping of healthy thigh muscles using a T2-prepared 3D TSE sequence. *PLoS One* 2017;12:e0171337.
14. Wattjes MP, Kley RA, Fischer D. Neuromuscular imaging in inherited muscle diseases. *Eur Radiol* 2010;20:2447–2460.
15. Mercuri E, Clements E, Offiah A, et al. Muscle magnetic resonance imaging involvement in muscular dystrophies with rigidity of the spine. *Ann Neurol* 2010;67:201–208.
16. Brink HF, Buschmann MD, Rosen BR. NMR chemical shift imaging. *Comput Med Imaging Graph* 1989;13:93–104.
17. Crawley AP, Henkelman RM. Errors in T2 estimation using multislice multiple-echo imaging. *Magn Reson Med* 1987;4:34–47.
18. Majumdar S, Orphanoudakis SC, Gmitro A, et al. Errors in the measurements of T2 using multiple-echo MRI techniques. I. Effects of radio-frequency pulse imperfections. *Magn Reson Med* 1986;3:397–417.
19. Poon CS, Henkelman RM. Practical T2 quantitation for clinical applications. *J Magn Reson Imaging* 1992;2:541–553.
20. Garrod P, Hollingsworth KG, Eagle M, et al. MR imaging in Duchenne muscular dystrophy: Quantification of T1-weighted signal, contrast uptake, and the effects of exercise. *J Magn Reson Imaging* 2009;30:1130–1138.
21. Phoenix J, Betal D, Roberts N, et al. Objective quantification of muscle and fat in human dystrophic muscle by magnetic resonance image analysis. *Muscle Nerve* 1996;19:302–310.
22. Huang Y, Majumdar S, Genant HK, et al. Quantitative MR relaxometry study of muscle composition and function in Duchenne muscular dystrophy. *J Magn Reson Imaging* 1994;4:59–64.
23. Gold GE, Han E, Stainsby J, et al. Musculoskeletal MRI at 3.0 T: Relaxation times and image contrast. *AJR Am J Roentgenol* 2004;183:343–351.
24. Lebel RM, Wilman AH. Transverse relaxometry with stimulated echo compensation. *Magn Reson Med* 2010;64:1005–1014.
25. Janiczek RL, Gambarota G, Sinclair CD, et al. Simultaneous T(2) and lipid quantitation using IDEAL-CPMG. *Magn Reson Med* 2011;66:1293–1302.
26. Weidlich D, Schlaeger S, Kooijman H, et al. T2 mapping with magnetization-prepared 3D TSE based on a modified BIR-4 T2 preparation. *NMR Biomed* 2017;30:e3773.
27. Rosenfeld D, Panfil SL, Zur Y. Design of adiabatic pulses for fat-suppression using analytic solutions of the Bloch equation. *Magn Reson Med* 1997;37:793–801.
28. Haase A. Snapshot FLASH MRI. Applications to T1, T2, and chemical-shift imaging. *Magn Reson Med* 1990;13:77–89.
29. Bloch F. Nuclear induction. *Phys Rev* 1946;70:460–474.
30. Schlaeger S, Klupp E, Weidlich D, et al. T2-weighted Dixon turbo spin echo for accelerated simultaneous grading of whole-body skeletal muscle fat infiltration and edema in patients with neuromuscular diseases. *J Comput Assist Tomogr* 2018;42:574–579.
31. Wang G, El-Sharkawy AM, Edelstein WA, et al. Measuring T2 and T1, and imaging T2 without spin echoes. *J Magn Reson* 2012;214:273–280.
32. Ruschke S, Kienberger H, Baum T, et al. Diffusion-weighted stimulated echo acquisition mode (DW-STEAM) MR spectroscopy to measure fat unsaturation in regions with low proton-density fat fraction. *Magn Reson Med* 2016;75:32–41.
33. Dieckmeyer M, Ruschke S, Cordes C, et al. The need for T(2) correction on MRS-based vertebral bone marrow fat quantification: Implications for bone marrow fat fraction age dependence. *NMR Biomed* 2015;28:432–439.
34. Yu H, Shimakawa A, McKenzie CA, et al. Multiecho water-fat separation and simultaneous R2* estimation with multifrequency fat spectrum modeling. *Magn Reson Med* 2008;60:1122–1134.
35. Yu H, McKenzie CA, Shimakawa A, et al. Multiecho reconstruction for simultaneous water-fat decomposition and T2* estimation. *J Magn Reson Imaging* 2007;26:1153–1161.
36. Karampinos DC, Yu H, Shimakawa A, et al. T(1)-corrected fat quantification using chemical shift-based water/fat separation: Application to skeletal muscle. *Magn Reson Med* 2011;66:1312–1326.
37. Wokke BH, Van Den Bergen JC, Hooijmans MT, et al. T2 relaxation times are increased in skeletal muscle of DMD but not BMD patients. *Muscle Nerve* 2016;53:38–43.

7 Discussion

7.1 Review of the Existing Literature

Oedematous alterations are the MR imaging pendant to increased water content in the muscle tissue and are present in several different circumstances such as injury, tumour, denervation or exercise. In the context of NMD increased water content is seen as a marker for "disease activity" providing information about muscle fibre injury and being a potential predictor for later degenerative changes. Thus, currently skeletal muscles with oedema are preferably chosen for biopsies and oedematous alterations are the pathology of interest for monitoring disease progression and response to treatment. [26, 27, 28, 21, 10, 29, 6, 22, 24, 30, 8, 31]

In the following, first, in section 7.1.1 the existing literature regarding T_{2w} as a quantitative biomarker in the assessment of skeletal muscle health is reviewed. Second, in section 7.1.2 literature about T_{2w} quantification based on MRS is presented. Third, in section 7.1.3 different approaches for T_{2w} mapping with particular focus on the T_2 -prepared 3D TSE with SPAIR fat suppression are introduced.

7.1.1 T_2 Water as a Biomarker in the Context of Skeletal Muscle Health

In the context of T_2 relaxometry measurements in fatty tissue, the two terms global T_2 and T_{2w} have to be distinguished [22, 8]. Muscle global T_2 represents the non chemically specific, mono-exponential T_2 decay of a water-fat tissue mixture, whereas muscle T_{2w} is a measure only of the water component of the tissue [22, 8, 31]. In order to quantify oedematous alterations in the muscle tissue, the biomarker T_{2w} is of interest because it predominately reflects the quality of the muscle fibres [70, 37, 38, 90, 21, 10, 29, 6, 91, 22, 24, 30, 8, 31]. T_{2w} is a measure for the water mobility of the tissue, however it is also influenced by the tissue microenvironment, such as the extracellular matrix, blood, muscle fibres and the presence of fat [22, 41, 8, 31]. Thereby, given the multiple influencing factors, the exact behaviour of T_{2w} in a specific chemical environment is difficult to predict.

If fatty infiltrations are present in the muscle and not accounted for in the MR measurement, global T_2 and not T_{2w} will be measured [8, 22]. As fat has a longer T_2 than water and it is a common pathological change in the skeletal muscles of patients with NMD, a T_{2w} determination without the influence of surrounding fatty infiltration is crucial [22, 41, 8, 31].

However, a complete separation of the water and fat component or a complete suppression of the fat signal is challenging, especially when imaging techniques are employed. These challenges are mainly due to the following characteristics of the complex water-fat

spectrum: (i) in the spectrum the olefinic fat peak is relatively close to the water peak [115], (ii) the different fat peaks have different T_1 and T_2 relaxation times [115], respectively and (iii) in general a complex fat signal behaviour is present because of j-couplings and the overall spectral complexity [116, 117].

7.1.2 T_2 Water Quantification Based on Magnetic Resonance Spectroscopy

MRS offers the possibility to separate different chemical species based on their MR resonance frequency. Therefore, this measurement allows a complete separation of the signal from different fat peaks and the water peak [95, 96, 97, 98, 41, 99]. MRS can be used for an accurate and clean determination of the T_2 decay only in the water peak. This approach provides insights into the behaviour of T_{2w} in different circumstances, e. g. also in regions of moderate to high fatty infiltration. The disadvantage of MRS are the slow acquisition and missing spatial information. The latter is especially unfavourable in patients with NMD because the muscles are sometimes heterogeneously affected [31]. However, MRS can provide a very detailed and accurate view on the investigated tissue of interest [95, 96, 97, 98, 41, 99]. This fact makes the technique valuable in investigating the behaviour of parameters in challenging environments. Particularly, in the context of NMD, it is unknown so far, how the parameter T_{2w} behaves in regions with moderate and high fatty infiltration.

7.1.3 T_2 Water Quantification Based on Magnetic Resonance Imaging

Robust determination of T_{2w} can be provided based on MRS, which allows insights into the molecular composition of the tissue. However, MRS is lacking spatial resolution which is inevitable in order to characterize the pattern of involvement in a single muscle and the whole body. Therefore, quantitative imaging techniques for a robust quantification of T_{2w} are crucial [70, 90, 21, 10, 14, 29, 6, 22, 23, 24, 8, 31]. As chemical-shift imaging (CSI) is very time-consuming, prone to artefacts and additionally limited in spatial resolution [118, 119, 120], T_{2w} mapping is a promising approach for T_{2w} quantification.

T_2 mapping techniques are well established in the MR research nowadays but face particular difficulties when applied in the patients with NMD. Field inhomogeneities [32, 33, 34, 35, 36, 10] and fatty infiltration [37, 38, 39, 40, 41, 22, 8, 31] can be identified as main confounding effects. Transmit B1 and B0 inhomogeneities, present in body MR application, cause an inaccurate application of the applied RF pulses and lead to different, not-desirable signal pathways. These signal pathways eventually lead to measurement errors in the determination of T_{2w} . The presence of unsuppressed fat in the acquired signal leads to an overestimation of the T_{2w} value of the tissue. Therefore, a robust T_{2w} mapping technique has to provide low sensitivity to both field inhomogeneities and surrounding fatty infiltration. Different techniques and postprocessing methods such as Dixon fat separation [114] or a multi-exponential T_2 decay model without/with EPG simulations of MESE data exist [31, 36, 41].

However, the robustness of these techniques decrease with increasing fat content as

the contribution of the water signal to the total signal is decreasing [41]. Klupp et al. reported a different approach of using a BIR-4 RF pulse in the T_2 -preparation model with varying gaps followed by a 3D TSE readout with a varying flip angle train combined with SPAIR fat suppression [42]. This sequence was shown to be rather insensitive to field inhomogeneities [42, 43], whereas its suggestibility to fatty infiltration has not yet been investigated.

7.2 Present Work

Several contributions to the field of quantitative MR measurements in NMD were made within the scope of the present dissertation. The focus was put on the MR biomarker T_{2w} quantifying oedematous alterations of the skeletal muscle tissue. JP-I provides deeper insight into the behaviour of T_{2w} in fatty infiltrated muscles. JP-II evaluates the performance of a novel T_{2w} mapping technique in the presence of fatty infiltration and underlines its value for a clinical implementation. The MR measurements of JP-I and JP-II are based on a large-scale study of patients with various hereditary or acquired NMD, respectively.

7.2.1 Novelty

Both journal publications contribute novelty to the field of quantitative MR measurements in NMD.

Concretely, JP-I shows decreased T_{2w} with increasing fat content of the muscle tissue, when measured by single-voxel ^1H MRS. Due to the spectrally resolved measurements, MRS can reliably determine T_{2w} also in the presence of fat as confounding factor. In the work single-voxel ^1H MRS was used for the first time to determine the behaviour of T_{2w} also in moderately and highly fatty infiltrated muscle tissue.

JP-II evaluates the recently introduced T_{2w} mapping technique T_2 -prepared 3D TSE with SPAIR fat suppression regarding its sensitivity to fatty infiltration. The sequence's robustness regarding transmit B1 and B0 errors has already been investigated [42, 43]. JP-II shows for the first time that the T_2 -prepared 3D TSE sequence with SPAIR is little influenced by fatty infiltration in the investigated muscle tissue. The evaluations performed in JP-II are based on two pillars: on Bloch simulations of the behaviour of T_{2w} with increasing PDFF and on in vivo measurements in patients with NMD compared to the reference standard MRS and to the standard T_2 mapping sequence MESE, respectively.

7.2.2 Impact

The present dissertation advances the future implementation of quantitative MR measurements in the clinical assessment of patients with NMD.

In JP-I the behaviour of T_{2w} in regions of higher fatty infiltration is determined using MRS. Exchange and compartmentalization of the T_2 decay or susceptibility differences between muscle water and fat might contribute to decreased T_{2w} in regions of high

PDFF. The finding that T_{2w} is decreased with increasing PDFF is of great importance when interpreting T_{2w} values in patients with NMD, where fatty infiltration is often simultaneously present in the muscle tissue [31]. Particularly, partial volume effects can lead to a misleading interpretation of mean T_{2w} values of heterogeneously affected muscle tissue. Highly fatty infiltrated muscles with remaining healthy and oedematous muscle tissue showing voxels with oedematous (elevated T_{2w}) and voxels with fatty (reduced T_{2w}) muscle tissue might have a T_2 value similar to healthy muscle tissue. JP-I calls attention to this aspect and hence highlights the need for further development and clinical implementation of robust and high resolution T_{2w} mapping in patients with NMD.

JP-II shows that the T_2 -prepared 3D TSE sequence with SPAIR fat suppression is a good alternative for T_{2w} mapping in patients with NMD. Because of the complex signal behaviour and the non-trivial suppression of fat, fatty infiltration is a main confounding factor for robust T_{2w} mapping in the fatty infiltrated muscles of patients with NMD [37, 38, 39, 40, 41, 22, 8, 31]. The Bloch simulations and in vivo measurements in JP-II show that the combination of SPAIR and the T_2 -preparation module followed by a 3D TSE readout leads to a partial cancellation of the fat signal. Thus, fatty infiltration has a negligible influence on the T_{2w} determination. The rather insensitivity to fatty infiltration in combination with the sequence's robustness towards field inhomogeneities render the T_2 -prepared 3D TSE sequence valuable for a clinical application. Thereby, the reduction of the influence of the fat signal on the T_{2w} determination already at the acquisition side works without post acquisition simulations of signal behaviour.

7.2.3 Limitations

The publications of the present dissertation have the following limitations regarding study cohorts and methodology.

JP-I and JP-II are based on studies that examined patients with various different NMD which are quite rare diseases [45]. Therefore, the total number of patients per each disease group as well as the overall number of examined patients were rather small. In JP-I and JP-II no disease specific or stage specific analyses were performed, respectively. However, such simplifications were reasonable as JP-I tends to give insights about T_{2w} as a general biomarker in NMD and JP-II evaluates the T_2 -prepared 3D TSE sequence with SPAIR regarding its overall performance of T_{2w} determination in NMD patients. Additionally, in JP-I as well as in JP-II up to three MRS voxels were placed in healthy, fatty and oedematous muscle tissue depending on the qualitative presentation of the patients' thigh muscles and corresponding T_{2w} values were extracted. Hence these measurements can not be regarded as completely independent.

Regarding methodological limitations of JP-I, it was not possible to consider a multi-exponential decay of T_{2w} because of the limited amount of four or five TEs. Additionally, the MRS fitting was based on eight to ten fat peaks depending on the amount of fatty infiltration and hence visibility of single fat peaks in order to reduce the residual and therefore enhance the fitting accuracy. As JP-I concentrated on the behaviour of the water peak the assumption of the same fat T_2 for all fat peaks was made for a further

stabilization of the fitting process.

As to limitations of JP-II the presented approach of combining SPAIR with the T_2 -preparation module for a signal reduction of fat is specific for the presented sequence and not generally applicable on other sequences. Additionally, with this approach the fat signal is not completely suppressed or separated rather than its influence on the T_{2w} determination is minimized. Furthermore, in contrast to the T_2 -prepared 3D TSE which is rather insensitive to field errors, the SPAIR pulse is prone to B_0 inhomogeneity effects [72]. However, the effects of B_0 errors on SPAIR should be negligible in the thigh region. The simulations of the T_{2w} behaviour in different PDFFF regimes were based on MRS measurements in the subcutaneous fat of only one healthy volunteer, though the simulation results were confirmed by measurements in 34 patients.

7.3 Perspective

The present dissertation provides new insights about the biomarker T_{2w} in the presence of fat. Based on these findings, a further characterization of T_{2w} as a biomarker in the context of NMD is necessary. Particularly, a further correlation of T_{2w} to biopsy results and an evaluation of the predictive character of T_{2w} in longitudinal studies is needed. Thereby, a correlation of initial T_{2w} alterations to functional impairment and later degenerative fatty infiltration will help to further understand the value of T_{2w} as a biomarker for "disease activity". T_{2w} as a reliable biomarker is highly desirable to accurately track disease progression and therapy effectiveness. As the composition of the NMD patients' skeletal muscles is specifically characterized by a parallel existence of healthy, oedematous and fatty muscle tissue, it is particularly important to respect the influence of fatty infiltration on MR biomarkers. In the future, it might be indicated to perform a voxel-based analysis of quantitative biomarkers rather than a mean value analysis based on the tissue of the whole muscle.

The evaluated T_{2w} mapping technique T_2 -prepared 3D TSE with SPAIR will be considered for future NMD studies. Its implementation in the clinical routine of patients with NMD as a fast and robust quantitative imaging technique should be forwarded. Further studies in patients with NMD are needed to evaluate the reproducibility of T_{2w} values determined by the T_2 -prepared 3D TSE with SPAIR sequence also in the presence of fatty infiltration. An outstanding advantage of the present T_{2w} mapping technique is its insensitivity to field inhomogeneities [42, 43]. This allows T_{2w} mapping also in regions prone to B_1 or B_0 errors such as the shoulder region. Currently, regions prone to field errors are not commonly examined by T_{2w} mapping techniques in NMD patients. However, in NMD such as various limb girdle muscular dystrophies or facioscapulohumeral muscular dystrophy especially the shoulder region is of high interest potentially showing earlier pathological alterations of the muscle tissue than the traditionally examined thigh region. The T_2 -prepared 3D TSE with SPAIR allows examination of these clinically important regions. Furthermore, robust T_{2w} determination in the muscle tissue is not only useful in the context of NMD, but also for an examination of e. g. ageing muscle tissue or muscle injury. Therefore, the T_2 -prepared 3D TSE with SPAIR might

7 Discussion

be used in future studies in patients with sarcopenia or muscle injuries.

Last but not least, the critical part for the extraction of quantitative values from MR measurements is the definition of regions of interest in which the biomarker should be calculated, referred to as segmentation. A time efficient, automated definition of segmentation masks is currently one of the main bottlenecks for further implementation of quantitative techniques in the clinical routine. Large databases providing access to MR images with corresponding segmentation masks have to be allocated such as the MyoSegmentUM databases provided by Schlaeger et al. [121] or Burian et al. [122]. These databases represent the groundwork for the development of automatic segmentation algorithms by providing access to training and test datasets. The development and implementation of such automatic segmentation techniques has to be forwarded in order to allow real impact of quantitative imaging techniques in the clinical workflow [123, 124, 125, 126].

In general, the further evaluation of MR biomarkers allowing to quantify and better understand muscular degeneration non-invasively will take us one step closer to a MR-based characterization of muscle disorders leading to a more personalized patient treatment of these diseases.

Acknowledgements

How to write acknowledgements being in a certain way the most important part of the whole dissertation? The scientific approach would be to browse literature about writing acknowledgements, visit international conferences on the topic, set up your own experimental pipeline, get some results and publish them. Or you simply try your best. . .

Summarizing I would like to thank all the inspiring people I was lucky enough to meet during my research time. I sincerely hope, that I have the possibility to go on working with many of you.

First of all and outstanding I would like to mention Dominik Weidlich. It is absolutely incredible how discussing scientific ideas together with you is creative and beneficial. Your open-mindedness towards medical students never giving up about explaining physical or computer science facts is amazing. During my whole research time, I have never experienced that one single question was too much. Thank you Dominik, it was absolutely fantastic working together with you. I have really enjoyed every minute.

I would like to thank Jan Kirschke for being a real role-model neuroradiologist somehow managing to combine incredibly profound clinical know-how and high impact research. Especially your technical interest and understanding were and are inspiring for me.

Thank you Claus Zimmer for your support and providing the necessary infrastructure as head of an absolutely fantastic and motivating department. Thank you also Ernst J. Rummeny for offering me the opportunity to work with the BMRR group.

Thank you Dimitrios Karampinos for simply being the best group leader one can imagine managing to lead a group with a lot of freedom and at the same time constantly pushing forward to new results, for believing in the technical fascination of a female medical student, for being an inspiring researcher and for grouping so many interesting people in the small Kirchenhof area at the basement of Klinikum rechts der Isar.

I would like to thank Thomas Baum for always having time to talk about not only scientific but also career deciding issues and for constantly having an ear to problems triggering innovative solutions.

Thank you Elisabeth Kottmaier for initiating the whole project, for writing such a nice first e-mail and for being present during my first steps in research.

Thank you Marcus Deschauer, Sarah Bublitz, Benedikt Schoser and Federica Montagenese for being so enthusiastic about setting up the whole study. Without your passion and recruiting of patients, the whole project would never have been possible.

I would like to thank my colleagues and friends of the extended BMRR group: Dominik, Max, Stefan, Barbara, Michael, Jan, Sophia, Chris, Ming, Christoph, Daniela, Andi, Sean, Anh, Stephan and Ronja. Thank you for all the inspiring talks (I still remember one at McDonald's Honolulu International Airport some time at around 3 a. m.

Acknowledgements

waiting for the flight in the morning while talking about some crazy physical theories), for enjoying international conferences together, for hiking in Hawaii, for getting through debilitating abstract deadlines as a team and for building the group spirit based on quite some Whisky.

Thank you Peter Henningsen, for being my mentor in course of the Max Weber-Program, for always offering the possibility to ask questions, for knowing so many interesting and inspiring people and for answering as fast as no one else to urgent e-mails.

Last but not least, the biggest thank goes to my family: my mother, my father and my brother. I know that you know that you are simply the best family on earth (yes Daniel, you've chosen the right one). Thank you for enabling me to study and to do my research work and for always and without exception being there for finding solutions to all urgent problems in life.

I am very happy to have had the possibility of working on this project. It has definitely been so much fun because of all of you.

List of Symbols and Abbreviations

2D	two-dimensional
3D	three-dimensional
^1H	proton
a. u.	arbitrary units
B_0	static main magnetic field [T]
B_1	amplitude of the radio frequency pulses [T]
BIR-4	adiabatic B_1 insensitive rotation-4
CSI	chemical shift imaging
CT	computed tomography
DESS	double-echo-steady-state
EPG	extended phase graph
FID	free induction decay
IDEAL	iterative decomposition of water and fat with echo asymmetry and least-squares estimation
LGMD2A	limb girdle muscular dystrophy type 2A
M_0	net magnetization
MESE	multi echo spin echo
MR	magnetic resonance
MRI	magnetic resonance imaging
MRS	magnetic resonance spectroscopy
ms	milliseconds
NLSD	neutral lipid storage disease
NMD	neuromuscular diseases

List of Symbols and Abbreviations

PDFF	proton density fat fraction
ppm	parts per million
PRESS	point-resolved spectroscopy
QIBA	Quantitative Imaging Biomarkers Alliance
RF	radio frequency (pulse)
RSNA	Radiological Society of North America
SNR	signal-to-noise ratio
SPAIR	spectral adiabatic inversion recovery
STEAM	stimulated echo acquisition mode
STIR	short tau inversion recovery
T	Tesla
t	time
T_1	spin-lattice (longitudinal) relaxation time [s]
T_{2w}	T_2 water, spin-spin (transverse) relaxation time of the water component in the tissue [s]
T_2	spin-spin (transverse) relaxation time [s]
T_2^*	effective transverse relaxation time [s]
TE	echo time
TI	inversion recovery time
TR	repetition time
TSE	turbo spin echo

List of Tables

4.1	T_1 and T_2 relaxation times of skeletal muscle tissue and fat at 1.5 T and 3 T [7].	14
4.2	Semi-quantitative scales for a visual rating of fatty infiltration in affected muscles published by Mercuri et al. [4], Kronblum et al. [16], and Fischer et al. [17].	19
4.3	Semi-quantitative scales for a visual rating of oedematous alterations in affected muscles published by Morrow et al. [18] and Poliachik et al. [14].	20

List of Figures

3.1	A single muscle fibre consists of several myofibrils composed of actin and myosin which are forming a functional unit. Figure according to [64].	8
3.2	Histological assessment of healthy skeletal muscle tissue with nucleoli arranged near the sarcolemma. The typical striated appearance is clearly visible. Hematoxylin and eosin stain. Figure according to Joyce et al. [65].	8
3.3	The three connective tissue layers epimysium, perimysium and endomysium organize skeletal muscles by structuring them in muscle fascicles and muscle fibres. Figure according to [64].	9
3.4	Histopathological assessment of a dermatomyositis patient's muscle biopsy. The disease characteristic atrophy of the muscle fibres at the periphery of fascicles (perifascicular) is prominent. Nicotinamide adenine dinucleotide stain. Figure according to Joyce et al. [65].	10
3.5	Histopathological assessment of an end stage muscle showing an almost complete replacement of muscle fibres by fatty infiltration. Figure according to Joyce et al. [65].	11
3.6	Histopathological assessment of a polymyositis patient's muscle biopsy. Endomysial inflammatory cells (arrow) are prominent. Hematoxylin and eosin stain. Figure according to [71].	12
4.1	Representative whole-body T_1 -weighted and T_2 -weighted sequences with fat suppression in a severely affected patient with limb girdle muscular dystrophy type 2A (LGMD2A). Figure according to Schlaeger et al. [15].	17
4.2	Representative heatmap visualizing the lower limb muscle involvement in patients with neutral lipid storage disease (NLS). For the scheme the five-point Fischer et al. scale for fatty infiltration was used [17]. Figure according to Garibaldi et al. [74].	21
4.3	Representative MR images showing PDFF and T_{2w} values based on maps in a healthy volunteer (a) and a patient with Becker muscular dystrophy (b).	23
4.4	Representative multi-TE single-voxel 1H STEAM spectrum in the highly fatty infiltrated muscle tissue of a patient with distal myopathy.	25
4.5	Voxel location planning based on a T_2 -weighted Dixon TSE fat image (a) and on a T_2 -weighted Dixon TSE water image (b). (c) represents a voxel location in a region with highly fatty infiltrated muscle tissue with the corresponding STEAM spectrum, (d) represents a voxel location in a region with healthy muscle tissue with the corresponding STEAM spectrum. Figure according to JP-I.	26

List of Figures

4.6	Magnitude signal of a healthy lower leg muscle with a gradient echo sequence with out of phase (TE = 3.45 ms and 5.75 ms) and in phase (TE = 4.60 ms) TEs. In the out of phase images, there is no signal at the water-fat boundaries. Figure according to Burakiewicz et al. [49].	27
4.7	Pulse sequence diagram of the T ₂ -prepared 3D TSE with SPAIR sequence. The RF pulses of the T ₂ -preparation module with spacing in between and the flip angle modulation of the 3D TSE readout are illustrated.	30
4.8	Simulation results of the sensitivity of T ₂ quantification based on the T ₂ -prepared 3D TSE to B1 and B0 errors. Figure according to Klupp et al. [42].	31
4.9	Raw T ₂ -weighted images based on the T ₂ -prepared 3D TSE sequence with SPAIR of the thigh region in a patient with Pompe disease. The bottom right corner shows the signal decay for the indicated region of interest in gracilis muscle for different T ₂ -preparation durations of 20, 30, 40, 50 and 60 ms with corresponding mono-exponential fitting.	31

Bibliography

- [1] H. Schedel, C. D. Reimers, M. Nägele, T. N. Witt, D.E. Pongratz, and T. Vogl. “Imaging techniques in myotonic dystrophy. A comparative study of ultrasound, computed tomography and magnetic resonance imaging of skeletal muscles”. In: *European journal of radiology* 15.3 (1992), pp. 230–238.
- [2] Ö. Özsarlak, E. Schepens, P. M. Parizel, J. W. Van Goethem, F. Vanhoenacker, A. M. De Schepper, and J. J. Martin. “Hereditary neuromuscular diseases”. In: *European journal of radiology* 40.3 (2001), pp. 184–197.
- [3] E. Mercuri, H. Jungbluth, and F. Muntoni. “Muscle imaging in clinical practice: diagnostic value of muscle magnetic resonance imaging in inherited neuromuscular disorders”. In: *Current opinion in neurology* 18.5 (2005), pp. 526–537.
- [4] E. Mercuri, A. Pichiecchio, J. Allsop, S. Messina, M. Pane, and F. Muntoni. “Muscle MRI in inherited neuromuscular disorders: past, present, and future”. In: *Journal of Magnetic Resonance Imaging: An Official Journal of the International Society for Magnetic Resonance in Medicine* 25.2 (2007), pp. 433–440.
- [5] M. P. Wattjes, R. A. Kley, and D. Fischer. “Neuromuscular imaging in inherited muscle diseases”. In: *European radiology* 20.10 (2010), pp. 2447–2460.
- [6] M. P. Wattjes and D. Fischer. *Neuromuscular imaging*. Springer, 2013.
- [7] D. W. McRobbie, E. A. Moore, M. J. Graves, and M. R. Prince. *MRI from Picture to Proton*. Cambridge university press, 2017.
- [8] P. G. Carlier, B. Marty, O. Scheidegger, P. Loureiro de Sousa, P.-Y. Baudin, E. Snezhko, and D. Vlodyavets. “Skeletal muscle quantitative nuclear magnetic resonance imaging and spectroscopy as an outcome measure for clinical trials”. In: *Journal of neuromuscular diseases* 3.1 (2016), pp. 1–28.
- [9] *Quantitative Imaging Biomarkers Alliance*. URL: <https://www.rsna.org/research/quantitative-imaging-biomarkers-alliance> (visited on 03/31/2020).
- [10] K. G. Hollingsworth, P. Loureiro de Sousa, V. Straub, and P. G. Carlier. “Towards harmonization of protocols for MRI outcome measures in skeletal muscle studies: consensus recommendations from two TREAT-NMD NMR workshops, 2 May 2010, Stockholm, Sweden, 1–2 October 2009, Paris, France”. In: *Neuromuscular Disorders* 22 (2012), S54–S67.
- [11] D. G. Leung. “Magnetic resonance imaging patterns of muscle involvement in genetic muscle diseases: a systematic review”. In: *Journal of neurology* 264.7 (2017), pp. 1320–1333.

Bibliography

- [12] U. A. Walker. “Imaging tools for the clinical assessment of idiopathic inflammatory myositis”. In: *Current opinion in rheumatology* 20.6 (2008), pp. 656–661.
- [13] A. Degardin, D. Morillon, A. Lacour, A. Cotten, P. Vermersch, and T. Stojkovic. “Morphologic imaging in muscular dystrophies and inflammatory myopathies”. In: *Skeletal radiology* 39.12 (2010), pp. 1219–1227.
- [14] S. L. Poliachik, S. D. Friedman, G. T. Carter, S. E. Parnell, and D. W. Shaw. “Skeletal muscle edema in muscular dystrophy: clinical and diagnostic implications”. In: *Physical Medicine and Rehabilitation Clinics* 23.1 (2012), pp. 107–122.
- [15] S. Schlaeger, E. Klupp, D. Weidlich, B. Cervantes, S. C. Foreman, M. Deschauer, B. Schoser, C. Katemann, H. Kooijman, E. J. Rummeny, C. Zimmer, J. S. Kirschke, and D. C. Karampinos. “T2-weighted dixon turbo spin echo for accelerated simultaneous grading of whole-body skeletal muscle fat infiltration and edema in patients with neuromuscular diseases”. In: *Journal of computer assisted tomography* 42.4 (2018), pp. 574–579.
- [16] C. Kornblum, G. Lutterbey, M. Bogdanow, K. Kesper, H. Schild, R. Schröder, and M. P. Wattjes. “Distinct neuromuscular phenotypes in myotonic dystrophy types 1 and 2”. In: *Journal of neurology* 253.6 (2006), pp. 753–761.
- [17] D. Fischer, R. A. Kley, K. Strach, C. Meyer, T. Sommer, K. Eger, A. Rolfs, W. Meyer, A. Pou, J. Pradas, C. M. Heyer, A. Grossmann, A. Huebner, W. Kress, J. Reimann, R. Schröder, B. Eymard, Fardeau M., B. Udd, L. Goldfarb, Vorgerd M., and M. Olivé. “Distinct muscle imaging patterns in myofibrillar myopathies”. In: *Neurology* 71.10 (2008), pp. 758–765.
- [18] J. M. Morrow, E. Matthews, D. L. R. Rayan, A. Fischmann, C. D. J. Sinclair, M. M. Reilly, J. S. Thornton, M. G. Hanna, and T. A. Yousry. “Muscle MRI reveals distinct abnormalities in genetically proven non-dystrophic myotonias”. In: *Neuromuscular Disorders* 23.8 (2013), pp. 637–646.
- [19] D. C. Karampinos, H. Yu, A. Shimakawa, T. M. Link, and S. Majumdar. “T1-corrected fat quantification using chemical shift-based water/fat separation: application to skeletal muscle”. In: *Magnetic resonance in medicine* 66.5 (2011), pp. 1312–1326.
- [20] S. B. Reeder, H. H. Hu, and C. B. Sirlin. “Proton density fat-fraction: a standardized MR-based biomarker of tissue fat concentration”. In: *Journal of magnetic resonance imaging* 36.5 (2012), pp. 1011–1014.
- [21] H. K. Kim, T. Laor, P. S. Horn, J. M. Racadio, B. Wong, and B. J. Dardzinski. “T2 mapping in Duchenne muscular dystrophy: distribution of disease activity and correlation with clinical assessments”. In: *Radiology* 255.3 (2010), pp. 899–908.

Bibliography

- [22] P. G. Carlier. “Global T2 versus water T2 in NMR imaging of fatty infiltrated muscles: different methodology, different information and different implications”. In: *Neuromuscular Disorders* 24.5 (2014), pp. 390–392.
- [23] S. C. Forbes, R. J. Willcocks, W. T. Triplett, W. D. Rooney, D. J. Lott, D. Wang, J. Pollaro, C. R. Senesac, M. J. Daniels, R. S. Finkel, B. S. Russman, B. J. Byrne, E. L. Finanger, G. I. Tennekoon, G. A. Walter, H. L. Sweeney, and K. Vandenborne. “Magnetic resonance imaging and spectroscopy assessment of lower extremity skeletal muscles in boys with Duchenne muscular dystrophy: a multicenter cross sectional study”. In: *PloS one* 9.9 (2014), e106435.
- [24] P. G. Carlier, N. Azzabou, P. Loureiro de Sousa, A. Hicks, J.-M. Boisserie, A. Amadon, R.-Y. Carlier, C. Wary, D. Orlikowski, and P. Laforêt. “Skeletal muscle quantitative nuclear magnetic resonance imaging follow-up of adult Pompe patients”. In: *Journal of inherited metabolic disease* 38.3 (2015), pp. 565–572.
- [25] H. H. Hu, Y. Li, T. R. Nagy, M. I. Goran, and K. S. Nayak. “Quantification of absolute fat mass by magnetic resonance imaging: a validation study against chemical analysis”. In: *International journal of body composition research* 9.3 (2011), p. 111.
- [26] G. Walter, L. Cordier, D. Bloy, and H L. Sweeney. “Noninvasive monitoring of gene correction in dystrophic muscle”. In: *Magnetic resonance in medicine* 54.6 (2005), pp. 1369–1376.
- [27] C. A. Pacak, G. A. Walter, G. Gaidosh, N. Bryant, M. A. Lewis, S. Germain, C. S. Mah, K. P. Campbell, and B. J. Byrne. “Long-term skeletal muscle protection after gene transfer in a mouse model of LGMD-2D”. In: *Molecular Therapy* 15.10 (2007), pp. 1775–1781.
- [28] T. Yokota, Q. Lu, T. Partridge, M. Kobayashi, A. Nakamura, S. Takeda, and E. Hoffman. “Efficacy of systemic morpholino exon-skipping in Duchenne dystrophy dogs”. In: *Annals of Neurology: Official Journal of the American Neurological Association and the Child Neurology Society* 65.6 (2009), pp. 667–676.
- [29] I. Arpan, S. C. Forbes, D. J. Lott, C. R. Senesac, M. J. Daniels, W. T. Triplett, J. K. Deol, H. L. Sweeney, G. A. Walter, and K. Vandenborne. “T2 mapping provides multiple approaches for the characterization of muscle involvement in neuromuscular diseases: a cross-sectional study of lower leg muscles in 5–15-year-old boys with Duchenne muscular dystrophy”. In: *NMR in biomedicine* 26.3 (2013), pp. 320–328.
- [30] C. Wary, N. Azzabou, C. Giraudeau, J. Le Louër, M. Montus, T. Voit, L. Servais, and P. G. Carlier. “Quantitative NMRI and NMRS identify augmented disease progression after loss of ambulation in forearms of boys with Duchenne muscular dystrophy”. In: *NMR in biomedicine* 28.9 (2015), pp. 1150–1162.

Bibliography

- [31] B. Marty, P.-Y. Baudin, H. Reyngoudt, N. Azzabou, E. C. Araujo, P. G. Carlier, and P. Loureiro de Sousa. “Simultaneous muscle water T2 and fat fraction mapping using transverse relaxometry with stimulated echo compensation”. In: *NMR in biomedicine* 29.4 (2016), pp. 431–443.
- [32] S. Majumdar, S. C. Orphanoudakis, A. Gmitro, M. O’donnell, and J. C. Gore. “Errors in the measurements of T2 using multiple-echo MRI techniques. I. Effects of radiofrequency pulse imperfections”. In: *Magnetic resonance in medicine* 3.3 (1986), pp. 397–417.
- [33] A. P. Crawley and R. M. Henkelman. “Errors in T2 estimation using multislice multiple-echo imaging”. In: *Magnetic resonance in medicine* 4.1 (1987), pp. 34–47.
- [34] C. S. Poon and R. M. Henkelman. “Practical T2 quantitation for clinical applications”. In: *Journal of Magnetic Resonance Imaging* 2.5 (1992), pp. 541–553.
- [35] O. Dietrich, M. F. Reiser, and S. O. Schoenberg. “Artifacts in 3-T MRI: physical background and reduction strategies”. In: *European journal of radiology* 65.1 (2008), pp. 29–35.
- [36] R. M. Lebel and A. H. Wilman. “Transverse relaxometry with stimulated echo compensation”. In: *Magnetic resonance in medicine* 64.4 (2010), pp. 1005–1014.
- [37] Y. Huang, S. Majumdar, H. K. Genant, W. P. Chan, K. R. Sharma, P. Yu, M. Mynhier, and R. G. Miller. “Quantitative MR relaxometry study of muscle composition and function in Duchenne muscular dystrophy”. In: *Journal of Magnetic Resonance Imaging* 4.1 (1994), pp. 59–64.
- [38] J. Phoenix, D. Betal, N. Roberts, T. R. Helliwell, and R. H. T. Edwards. “Objective quantification of muscle and fat in human dystrophic muscle by magnetic resonance image analysis”. In: *Muscle & Nerve: Official Journal of the American Association of Electrodiagnostic Medicine* 19.3 (1996), pp. 302–310.
- [39] G. E. Gold, E. Han, J. Stainsby, G. Wright, J. Brittain, and C. Beaulieu. “Musculoskeletal MRI at 3.0 T: relaxation times and image contrast”. In: *American Journal of Roentgenology* 183.2 (2004), pp. 343–351.
- [40] P. Garrod, K. G. Hollingsworth, M. Eagle, B. S. Aribisala, D. Birchall, K. Bushby, and V. Straub. “MR imaging in Duchenne muscular dystrophy: quantification of T1-weighted signal, contrast uptake, and the effects of exercise”. In: *Journal of Magnetic Resonance Imaging: An Official Journal of the International Society for Magnetic Resonance in Medicine* 30.5 (2009), pp. 1130–1138.
- [41] N. Azzabou, P. Loureiro de Sousa, E. Caldas, and P. G. Carlier. “Validation of a generic approach to muscle water T2 determination at 3T in fat-infiltrated skeletal muscle”. In: *Journal of Magnetic Resonance Imaging* 41.3 (2015), pp. 645–653.

Bibliography

- [42] E. Klupp, D. Weidlich, S. Schlaeger, T. Baum, B. Cervantes, M. Deschauer, H. Kooijman, E. J. Rummeny, C. Zimmer, J. S. Kirschke, and D. C. Karampinos. “B1-insensitive T2 mapping of healthy thigh muscles using a T2-prepared 3D TSE sequence”. In: *PloS one* 12.2 (2017), e0171337.
- [43] D. Weidlich, S. Schlaeger, H. Kooijman, P. Börnert, J. S. Kirschke, E. J. Rummeny, A. Haase, and D. C. Karampinos. “T2 mapping with magnetization-prepared 3D TSE based on a modified BIR-4 T2 preparation”. In: *NMR in Biomedicine* 30.11 (2017), e3773.
- [44] A. E. H. Emery. “The muscular dystrophies”. In: *Bmj* 317.7164 (1998), pp. 991–995.
- [45] J. M. Bhatt. “The epidemiology of neuromuscular diseases”. In: *Neurologic clinics* 34.4 (2016), pp. 999–1021.
- [46] B. M. Morrison. “Neuromuscular diseases”. In: *Seminars in neurology*. Vol. 36. 05. Thieme Medical Publishers. 2016, pp. 409–418.
- [47] J. Walton and P. K. Thomas. “Classification of neuromuscular diseases”. In: *Journal of the Neurological Sciences* 86.2 (1988), pp. 333–360.
- [48] S. Zierz. *Muskelerkrankungen*. Georg Thieme Verlag, 2014.
- [49] J. Burakiewicz, C. D. J. Sinclair, D. Fischer, G. A. Walter, H. E. Kan, and K. G. Hollingsworth. “Quantifying fat replacement of muscle by quantitative MRI in muscular dystrophy”. In: *Journal of neurology* 264.10 (2017), pp. 2053–2067.
- [50] *Muskelerkrankungen*. URL: <https://www.dgm.org/muskelerkrankungen> (visited on 03/31/2020).
- [51] S. Cirak, V. Arechavala-Gomez, M. Guglieri, L. Feng, S. Torelli, K. Anthony, S. Abbs, M. E. Garralda, J. Bourke, D. J. Wells, G. Dickson, M. J. Wood, S. D. Wilton, V. Straub, R. Kole, S. B. Shrewsbury, C. Sewry, J. E. Morgan, K. Bushby, and F. Muntoni. “Exon skipping and dystrophin restoration in patients with Duchenne muscular dystrophy after systemic phosphorodiamidate morpholino oligomer treatment: an open-label, phase 2, dose-escalation study”. In: *The Lancet* 378.9791 (2011), pp. 595–605.
- [52] F. Muntoni and M. J. A. Wood. “Targeting RNA to treat neuromuscular disease”. In: *Nature reviews Drug discovery* 10.8 (2011), pp. 621–637.
- [53] V. Arechavala-Gomez, K. Anthony, J. Morgan, and F. Muntoni. “Antisense oligonucleotide-mediated exon skipping for Duchenne muscular dystrophy: progress and challenges”. In: *Current gene therapy* 12.3 (2012), pp. 152–160.
- [54] A. G. L. Douglas and M. J. A. Wood. “Splicing therapy for neuromuscular disease”. In: *Molecular and Cellular Neuroscience* 56 (2013), pp. 169–185.
- [55] D. Erriquez, G. Perini, and A. Ferlini. “Non-coding RNAs in muscle dystrophies”. In: *International journal of molecular sciences* 14.10 (2013), pp. 19681–19704.

Bibliography

- [56] E. Mercuri and F. Muntoni. “Muscular dystrophy: new challenges and review of the current clinical trials”. In: *Current opinion in pediatrics* 25.6 (2013), pp. 701–707.
- [57] E. L. Scotter and C. E. Shaw. “Neuromuscular disease: New insights and avenues for therapy”. In: *The Lancet Neurology* 12.1 (2013), pp. 13–15.
- [58] A. Toscano and B. Schoser. “Enzyme replacement therapy in late-onset Pompe disease: a systematic literature review”. In: *Journal of neurology* 260.4 (2013), pp. 951–959.
- [59] K. Bushby, R. Finkel, B. Wong, R. Barohn, C. Campbell, G. P. Comi, A. M. Connolly, J. W. Day, K. M. Flanigan, N. Goemans, K. J. Jones, E. Mercuri, R. Quinlivan, J. B. Renfroe, B. Russman, M. M. Ryan, M. Tulinius, T. Voit, S. A. Moore, H. L. Sweeney, R. T. Abresch, K. L. Coleman, M. Eagle, J. Florence, E. Gappmaier, Al. M. Glanzman, E. Henricson, J. Barth, G. L. Elfring, A. Reha, R. Spiegel, M. W. O’donnell, S. W. Peltz, and C. M. McDonald. “Ataluren treatment of patients with nonsense mutation dystrophinopathy”. In: *Muscle & nerve* 50.4 (2014), pp. 477–487.
- [60] A. Touznik, J. J. A. Lee, and T. Yokota. “New developments in exon skipping and splice modulation therapies for neuromuscular diseases”. In: *Expert opinion on biological therapy* 14.6 (2014), pp. 809–819.
- [61] T. Voit, H. Topaloglu, V. Straub, F. Muntoni, N. Deconinck, G. Champion, S. J. De Kimpe, M. Eagle, M. Guglieri, S. Hood, L. Liefwaard, A. Loubakos, A. Morgan, J. Nakielny, N. Quarcoo, V. R. Ricotti, K. Rolfe, L. Servais, C. W. Wardell, R. Wilson, P. W. Wright, and J. E. Kraus. “Safety and efficacy of drisapersen for the treatment of Duchenne muscular dystrophy (DEMAND II): an exploratory, randomised, placebo-controlled phase 2 study”. In: *The Lancet Neurology* 13.10 (2014), pp. 987–996.
- [62] Y. Blat and S. Blat. “Drug discovery of therapies for duchenne muscular dystrophy”. In: *Journal of biomolecular screening* 20.10 (2015), pp. 1189–1203.
- [63] G. M. Buyse, T. Voit, U. Schara, C. S. M. Straathof, M. G. D’Angelo, G. Bernert, J.-M. Cuisset, R. S. Finkel, N. Goemans, C. M. McDonald, C. Rummey, and T. Meier. “Efficacy of idebenone on respiratory function in patients with Duchenne muscular dystrophy not using glucocorticoids (DELOS): a double-blind randomised placebo-controlled phase 3 trial”. In: *The Lancet* 385.9979 (2015), pp. 1748–1757.
- [64] *Anatomy & Physiology*. URL: <http://cnx.org/contents/14fb4ad7-39a1-4eee-ab6e-3ef2482e3e22@8.24> (visited on 04/20/2020).
- [65] N. C. Joyce, B. Oskarsson, and L.-W. Jin. “Muscle biopsy evaluation in neuromuscular disorders”. In: *Physical Medicine and Rehabilitation Clinics* 23.3 (2012), pp. 609–631.
- [66] J. L. Fleckenstein, V. John III, and C. D. Reimers. *Muscle imaging in health and disease*. Springer Science & Business Media, 2012.

Bibliography

- [67] S. Inhuber, N. Sollmann, S. Schlaeger, M. Dieckmeyer, E. Burian, C. Kohlmeyer, D. C. Karampinos, J. S. Kirschke, T. Baum, F. Kreuzpointner, and A. Schwirtz. “Associations of thigh muscle fat infiltration with isometric strength measurements based on chemical shift encoding-based water-fat magnetic resonance imaging”. In: *European radiology experimental* 3.1 (2019), pp. 1–10.
- [68] S. Schlaeger, S. Inhuber, A. Rohrmeier, M. Dieckmeyer, F. Freitag, E. Klupp, D. Weidlich, G. Feuerriegel, F. Kreuzpointner, A. Schwirtz, E. J. Rummeny, C. Zimmer, J. S. K., D. C. Karampinos, and T. Baum. “Association of paraspinal muscle water–fat MRI-based measurements with isometric strength measurements”. In: *European radiology* 29.2 (2019), pp. 599–608.
- [69] B. H. Wokke, J. C. Van Den Bergen, M. J. Versluis, E. H. Niks, J. Milles, A. G. Webb, E. W. van Zwet, A. Aartsma-Rus, J. J. Verschuuren, and H. E. Kan. “Quantitative MRI and strength measurements in the assessment of muscle quality in Duchenne muscular dystrophy”. In: *Neuromuscular Disorders* 24.5 (2014), pp. 409–416.
- [70] A. E. English, M. L. G. Joy, and R. M. Henkelman. “Pulsed NMR relaxometry of striated muscle fibers”. In: *Magnetic resonance in medicine* 21.2 (1991), pp. 264–281.
- [71] A. Malik, G. Hayat, J. S. Kalia, and M. A. Guzman. “Idiopathic inflammatory myopathies: clinical approach and management”. In: *Frontiers in neurology* 7 (2016), p. 64.
- [72] D. Rosenfeld, S. L. Panfil, and Y. Zur. “Design of adiabatic pulses for fat-suppression using analytic solutions of the Bloch equation”. In: *Magnetic resonance in medicine* 37.5 (1997), pp. 793–801.
- [73] W. T. Dixon. “Simple proton spectroscopic imaging.” In: *Radiology* 153.1 (1984), pp. 189–194.
- [74] M. Garibaldi, G. Tasca, J. Diaz-Manera, P. Ottaviani, F. Laschena, D. Pantoli, S. Gerevini, C. Fiorillo, L. Maggi, E. Tasca, A. D’Amico, O. Musumeci, A. Toscano, C. Bruno, R. Massa, C. Angelini, E. Bertini, G. Antonini, and E. M. Pennisi. “Muscle MRI in neutral lipid storage disease (NLSL)”. In: *Journal of neurology* 264.7 (2017), pp. 1334–1342.
- [75] A. M. Heemskerk, G. J. Strijkers, A. Vilanova, M. R. Drost, and K. Nicolay. “Determination of mouse skeletal muscle architecture using three-dimensional diffusion tensor imaging”. In: *Magnetic Resonance in Medicine: An Official Journal of the International Society for Magnetic Resonance in Medicine* 53.6 (2005), pp. 1333–1340.
- [76] M. A. Weber, S. Nielles-Vallespin, M. Essig, K. Jurkat-Rott, H. U. Kauczor, and F. Lehmann-Horn. “Muscle Na⁺ channelopathies: MRI detects intracellular ²³Na accumulation during episodic weakness”. In: *Neurology* 67.7 (2006), pp. 1151–1158.

Bibliography

- [77] T. Hsieh, C.-K. Wang, H.-Y. Chuang, Y. Jong, C.-W. Li, and G.-C. Liu. “In vivo proton magnetic resonance spectroscopy assessment for muscle metabolism in neuromuscular diseases”. In: *The Journal of pediatrics* 151.3 (2007), pp. 319–321.
- [78] C. D. J. Sinclair, J. M. Morrow, T. A. Yousry, M. M. Reilly, M. G. Hanna, X. Golay, and J. S. Thornton. “P86 Inter-scan reproducibility of quantitative neuromuscular MRI”. In: *Neuromuscular Disorders* 20 (2010), S28.
- [79] M. Gloor, S. Fasler, A. Fischmann, T. Haas, O. Bieri, K. Heinimann, S. G. Wetzel, K. Scheffler, and D. Fischer. “Quantification of fat infiltration in oculopharyngeal muscular dystrophy: comparison of three MR imaging methods”. In: *Journal of magnetic resonance imaging* 33.1 (2011), pp. 203–210.
- [80] A. Fischmann, P. Hafner, S. Fasler, M. Gloor, O. Bieri, U. Studler, and D. Fischer. “Quantitative MRI can detect subclinical disease progression in muscular dystrophy”. In: *Journal of neurology* 259.8 (2012), pp. 1648–1654.
- [81] B. H. Wokke, C. Bos, M. Reijnierse, C. S. van Rijswijk, H. Eggers, A. Webb, J. J. Verschuuren, and H. E. Kan. “Comparison of dixon and T1-weighted MR methods to assess the degree of fat infiltration in duchenne muscular dystrophy patients”. In: *Journal of Magnetic Resonance Imaging* 38.3 (2013), pp. 619–624.
- [82] T. A. Willis, K. G. Hollingsworth, A. Coombs, M.-L. Sveen, S. Andersen, T. Stojkovic, M. Eagle, A. Mayhew, P. Loureiro de Sousa, L. Dewar, J. M. Morrow, C. D. J. Sinclair, J. S. Thornton, K. Bushby, H. Lochmüller, M. G. Hanna, J.-Y. Hogrel, P. G. Carlier, J. Vissing, and V. Straub. “Quantitative muscle MRI as an assessment tool for monitoring disease progression in LGMD2I: a multicentre longitudinal study”. In: *PloS one* 8.8 (2013).
- [83] J.-Y. Hogrel, C. Wary, A. Moraux, N. Azzabou, V. Decostre, G. Ollivier, A. Canal, C. Lilien, I. Ledoux, M. Annoussamy, N. Reguiba, T. Gidaro, A. G. Le Moing, R. Cardas, T. Voit, P. G. Carlier, and L. Servais. “Longitudinal functional and NMR assessment of upper limbs in Duchenne muscular dystrophy”. In: *Neurology* 86.11 (2016), pp. 1022–1030.
- [84] J. M. Morrow, C. D. J. Sinclair, A. Fischmann, P. M. Machado, M. M. Reilly, T. A. Yousry, J. S. Thornton, and M. G. Hanna. “MRI biomarker assessment of neuromuscular disease progression: a prospective observational cohort study”. In: *The Lancet Neurology* 15.1 (2016), pp. 65–77.
- [85] R. J. Willcocks, W. D. Rooney, W. T. Triplett, S. C. Forbes, D. J. Lott, C. R. Senesac, M. J. Daniels, D. Wang, A. T. Harrington, G. I. Tennekoon, B. S. Russman, E. L. Finanger, B. J. Byrne, R. S. Finkel, G. A. Walter, H. L. Sweeney, and K. Vandeborne. “Multicenter prospective longitudinal study of magnetic resonance biomarkers in a large duchenne muscular dystrophy cohort”. In: *Annals of neurology* 79.4 (2016), pp. 535–547.

Bibliography

- [86] T. Yokoo, M. Bydder, G. Hamilton, M. S. Middleton, A. C. Gamst, T. Wolfson, T. Hassanein, H. M. Patton, J. E. Lavine, J. B. Schwimmer, and C. B. Sirlin. “Nonalcoholic fatty liver disease: diagnostic and fat-grading accuracy of low-flip-angle multiecho gradient-recalled-echo MR imaging at 1.5 T”. In: *Radiology* 251.1 (2009), pp. 67–76.
- [87] C. D. G. Hines, A. Frydrychowicz, G. Hamilton, D. L. Tudorascu, K. K. Vigen, H. Yu, C. A. McKenzie, C. B. Sirlin, J. H. Brittain, and S. B. Reeder. “T1 independent, T2* corrected chemical shift based fat–water separation with multi-peak fat spectral modeling is an accurate and precise measure of hepatic steatosis”. In: *Journal of magnetic resonance imaging* 33.4 (2011), pp. 873–881.
- [88] S. Meisamy, C. D. G. Hines, G. Hamilton, C. B. Sirlin, C. A. McKenzie, H. Yu, J. H. Brittain, and S. B. Reeder. “Quantification of hepatic steatosis with T1-independent, T2*-corrected MR imaging with spectral modeling of fat: blinded comparison with MR spectroscopy”. In: *Radiology* 258.3 (2011), pp. 767–775.
- [89] T. Yokoo, M. Shiehorteza, G. Hamilton, T. Wolfson, M. E. Schroeder, M. S. Middleton, M. Bydder, A. C. Gamst, Y. Kono, A. Kuo, H. M. Patton, S. H. Horgan, J. E. Lavine, J. B. Schwimmer, and C. B. S. Sirlin. “Estimation of hepatic proton-density fat fraction by using MR imaging at 3.0 T”. In: *Radiology* 258.3 (2011), pp. 749–759.
- [90] S. M. Maillard, R. Jones, C. Owens, C. Pilkington, P. Woo, L. R. Wedderburn, and K. J. Murray. “Quantitative assessment of MRI T 2 relaxation time of thigh muscles in juvenile dermatomyositis”. In: *Rheumatology* 43.5 (2004), pp. 603–608.
- [91] I. Arpan, R. J. Willcocks, S. C. Forbes, R. S. Finkel, D. J. Lott, W. D. Rooney, W. T. Triplett, C. R. Senesac, M. J. Daniels, B. J. Byrne, E. L. Finanger, B. S. Russman, D. Wang, G. I. Tennekoon, G. A. Walter, H. L. Sweeney, and K. Vandenborne. “Examination of effects of corticosteroids on skeletal muscles of boys with DMD using MRI and MRS”. In: *Neurology* 83.11 (2014), pp. 974–980.
- [92] S. D. Friedman, S. L. Poliachik, R. K. Otto, G. T. Carter, C. B. Budech, T. D. Bird, D. G. Miller, and D. W. W. Shaw. “Longitudinal features of stir bright signal in FSHD1”. In: *Muscle & nerve* 49.2 (2014), pp. 257–260.
- [93] B. H. Janssen, N. B. M. Voet, C. I. Nabuurs, H. E. Kan, J. W. J. de Rooy, A. C. Geurts, G. W. Padberg, B. G. M. van Engelen, and A. Heerschap. “Distinct disease phases in muscles of facioscapulohumeral dystrophy patients identified by MR detected fat infiltration”. In: *PloS one* 9.1 (2014), e85416.
- [94] S. Ponrartana, L. Ramos-Platt, T. A. L. Wren, H. H. Hu, T. G. Perkins, J. M. Chia, and V. Gilsanz. “Effectiveness of diffusion tensor imaging in assessing disease severity in Duchenne muscular dystrophy: preliminary study”. In: *Pediatric radiology* 45.4 (2015), pp. 582–589.

Bibliography

- [95] P. A. Bottomley, Y. Lee, and R. G. Weiss. “Total creatine in muscle: imaging and quantification with proton MR spectroscopy.” In: *Radiology* 204.2 (1997), pp. 403–410.
- [96] C. Boesch. “Musculoskeletal spectroscopy”. In: *Journal of Magnetic Resonance Imaging: An Official Journal of the International Society for Magnetic Resonance in Medicine* 25.2 (2007), pp. 321–338.
- [97] S. B. Reeder, I. Cruite, G. Hamilton, and C. B. Sirlin. “Quantitative assessment of liver fat with magnetic resonance imaging and spectroscopy”. In: *Journal of magnetic resonance imaging* 34.4 (2011), pp. 729–749.
- [98] C. H. Cullen, G. J. Ray, and C. M. Szabo. “A comparison of quantitative nuclear magnetic resonance methods: internal, external, and electronic referencing”. In: *Magnetic Resonance in Chemistry* 51.11 (2013), pp. 705–713.
- [99] H. K. Kim, S. Serai, D. Lindquist, A. C. Mellow, P. S. Horn, D. H. Kim, and B. L. Wong. “Quantitative skeletal muscle MRI: part 2, MR spectroscopy and T2 relaxation time mapping—comparison between boys with Duchenne muscular dystrophy and healthy boys”. In: *American Journal of Roentgenology* 205.2 (2015), W216–W223.
- [100] K. G. Hollingsworth, P. Garrood, M. Eagle, K. Bushby, and V. Straub. “Magnetic resonance imaging in Duchenne muscular dystrophy: longitudinal assessment of natural history over 18 months”. In: *Muscle & nerve* 48.4 (2013), pp. 586–588.
- [101] G. H. Glover and E. Schneider. “Three-point Dixon technique for true water/fat decomposition with B₀ inhomogeneity correction”. In: *Magnetic resonance in medicine* 18.2 (1991), pp. 371–383.
- [102] S. B. Reeder, A. R. Pineda, Z. Wen, A. Shimakawa, H. Yu, J. H. Brittain, G. E. Gold, C. H. Beaulieu, and N. J. Pelc. “Iterative decomposition of water and fat with echo asymmetry and least-squares estimation (IDEAL): application with fast spin-echo imaging”. In: *Magnetic Resonance in Medicine: An Official Journal of the International Society for Magnetic Resonance in Medicine* 54.3 (2005), pp. 636–644.
- [103] S. B. Reeder, Z. Wen, H. Yu, A. R. Pineda, G. E. Gold, M. Markl, and N. J. Pelc. “Multicoil Dixon chemical species separation with an iterative least-squares estimation method”. In: *Magnetic Resonance in Medicine: An Official Journal of the International Society for Magnetic Resonance in Medicine* 51.1 (2004), pp. 35–45.
- [104] P. G. Carlier, N. Azzabou, P. Loureiro de Sousa, B. Florkin, E. Deprez, N. B. Romero, S. Denis, V. Decostre, and L. Servais. “P. 14.4 Diagnostic role of quantitative NMR imaging exemplified by 3 cases of juvenile dermatomyositis”. In: *Neuromuscular Disorders* 23.9 (2013), p. 814.
- [105] A. Haase. “Snapshot FLASH MRI. Applications to T₁, T₂, and chemical-shift imaging”. In: *Magnetic Resonance in Medicine* 13.1 (1990), pp. 77–89.

Bibliography

- [106] E. L. Hahn. “Spin echoes”. In: *Physical review* 80.4 (1950), p. 580.
- [107] V. L. Yarnykh. “Actual flip-angle imaging in the pulsed steady state: a method for rapid three-dimensional mapping of the transmitted radiofrequency field”. In: *Magnetic Resonance in Medicine: An Official Journal of the International Society for Magnetic Resonance in Medicine* 57.1 (2007), pp. 192–200.
- [108] N. Ben-Eliezer, D. K. Sodickson, and K. T. Block. “Rapid and accurate T2 mapping from multi-spin-echo data using Bloch-simulation-based reconstruction”. In: *Magnetic resonance in medicine* 73.2 (2015), pp. 809–817.
- [109] W. D. Rooney, J. Pollaro, S. C. Forbes, D. J. Wang, K. Vandenborne, and G. A. Walter. “Application of the extended phase graph technique to improve T2 quantitation across sites”. In: *Proc Intl Soc Mag Reson Med*. Vol. 19. 2011, p. 138.
- [110] G. H. Welsch, K. Scheffler, T. C. Mamisch, T. Hughes, S. Millington, M. Deimling, and S. Trattnig. “Rapid estimation of cartilage T2 based on double echo at steady state (DESS) with 3 Tesla”. In: *Magnetic Resonance in Medicine: An Official Journal of the International Society for Magnetic Resonance in Medicine* 62.2 (2009), pp. 544–549.
- [111] T.-Y. Huang, Y. Liu, A. Stemmer, and B. P. Poncelet. “T2 measurement of the human myocardium using a T2-prepared transient-state TrueFISP sequence”. In: *Magnetic Resonance in Medicine: An Official Journal of the International Society for Magnetic Resonance in Medicine* 57.5 (2007), pp. 960–966.
- [112] C. L. Hoad, E. F. Cox, and P. A. Gowland. “Quantification of T2 in the abdomen at 3.0 T using a T2-prepared balanced turbo field echo sequence”. In: *Magnetic Resonance in Medicine: An Official Journal of the International Society for Magnetic Resonance in Medicine* 63.2 (2010), pp. 356–364.
- [113] J. Oh, E. T. Han, D. Pelletier, and S. J. Nelson. “Measurement of in vivo multi-component T2 relaxation times for brain tissue using multi-slice T2 prep at 1.5 and 3 T”. In: *Magnetic resonance imaging* 24.1 (2006), pp. 33–43.
- [114] R. L. Janiczek, G. Gambarota, C. D. J. Sinclair, T. A. Yousry, J. S. Thornton, X. Golay, and R. D. Newbould. “Simultaneous T2 and lipid quantitation using IDEAL-CPMG”. In: *Magnetic resonance in medicine* 66.5 (2011), pp. 1293–1302.
- [115] G. Hamilton, D. L. Smith Jr, M. Bydder, K. S. Nayak, and H. H. Hu. “MR properties of brown and white adipose tissues”. In: *Journal of Magnetic Resonance Imaging* 34.2 (2011), pp. 468–473.
- [116] M. Oostendorp, U. F. H. Engelke, M. Willemsen, and R. A. Wevers. “Diagnosing inborn errors of lipid metabolism with proton nuclear magnetic resonance spectroscopy”. In: *Clinical chemistry* 52.7 (2006), pp. 1395–1405.

Bibliography

- [117] G. Hamilton, M. S. Middleton, M. Bydder, T. Yokoo, J. B. Schwimmer, Y. Kono, H. M. Patton, J. E. Lavine, and C. B. Sirlin. “Effect of PRESS and STEAM sequences on magnetic resonance spectroscopic liver fat quantification”. In: *Journal of Magnetic Resonance Imaging: An Official Journal of the International Society for Magnetic Resonance in Medicine* 30.1 (2009), pp. 145–152.
- [118] H. F. Brink, M. D. Buschmann, and B. R. Rosen. “NMR chemical shift imaging”. In: *Computerized medical imaging and graphics* 13.1 (1989), pp. 93–104.
- [119] T. Kirchner, A. Fillmer, J. Tsao, K. P. Pruessmann, and A. Henning. “Reduction of voxel bleeding in highly accelerated parallel 1H MRSI by direct control of the spatial response function”. In: *Magnetic resonance in medicine* 73.2 (2015), pp. 469–480.
- [120] N. E. Wilson, B. L. Burns, Z. Iqbal, and M. A. Thomas. “Correlated spectroscopic imaging of calf muscle in three spatial dimensions using group sparse reconstruction of undersampled single and multichannel data”. In: *Magnetic resonance in medicine* 74.5 (2015), pp. 1199–1208.
- [121] S. Schlaeger, F. Freitag, E. Klupp, M. Dieckmeyer, D. Weidlich, S. Inhuber, M. Deschauer, B. Schoser, S. Bublitz, F. Montagnese, C. Zimmer, E. J. Rummeny, D. C. Karampinos, J. S. Kirschke, and T. Baum. “Thigh muscle segmentation of chemical shift encoding-based water-fat magnetic resonance images: the reference database MyoSegmenTUM”. In: *PloS one* 13.6 (2018), e0198200.
- [122] E. Burian, A. Rohrmeier, S. Schlaeger, M. Dieckmeyer, M. N. Diefenbach, J. Syväri, E. Klupp, D. Weidlich, C. Zimmer, E. J. Rummeny, D. C. Karampinos, J. S. Kirschke, and T. Baum. “Lumbar muscle and vertebral bodies segmentation of chemical shift encoding-based water-fat MRI: the reference database MyoSegmenTUM spine”. In: *BMC musculoskeletal disorders* 20.1 (2019), p. 152.
- [123] R. J. Willcocks, W. T. Triplett, S. C. Forbes, H. Arora, C. R. Senesac, D. J. Lott, T. R. Nicholson, W. D. Rooney, G. A. Walter, and K. Vandenborne. “Magnetic resonance imaging of the proximal upper extremity musculature in boys with Duchenne muscular dystrophy”. In: *Journal of neurology* 264.1 (2017), pp. 64–71.
- [124] E. Lareau-Trudel, A. Le Troter, B. Ghattas, J. Pouget, S. Attarian, D. Bendahan, and E. Salort-Campana. “Muscle quantitative MR imaging and clustering analysis in patients with facioscapulohumeral muscular dystrophy type 1”. In: *PLoS One* 10.7 (2015), e0132717.
- [125] S. Makrogiannis, S. Serai, K. W. Fishbein, C. Schreiber, L. Ferrucci, and R. G. Spencer. “Automated quantification of muscle and fat in the thigh from water-, fat-, and nonsuppressed MR images”. In: *Journal of Magnetic Resonance Imaging* 35.5 (2012), pp. 1152–1161.

Bibliography

- [126] V. Positano, T. Christiansen, M. F. Santarelli, S. Ringgaard, L. Landini, and A. Gastaldelli. “Accurate segmentation of subcutaneous and intermuscular adipose tissue from MR images of the thigh”. In: *Journal of Magnetic Resonance Imaging: An Official Journal of the International Society for Magnetic Resonance in Medicine* 29.3 (2009), pp. 677–684.